Table 5.1.11B-1

Disengager Test Results - GEESI

Test No.	Test Duration, Min	Disengager Inlet Velocity, ft/s	Solids Feed Rate, lb/hr	Solids Loss Rate, lb/hr	Solids/ Gas Ratio	Collection Efficiency, Percent
1	2.0	26.0	19,440	345	6.4	98.2
2	1.5	26.0	21,000	100	6.9	99.5
3	1.78	45.2	16,183	707	3.05	95.6
4	0.62	45.2	46,878	632	8.85	98.7
5	0.108	45.2	387,969	1,385	73.2	95.6
6	2.24	45.2	18,543	750	3.5	95.96
7	1.85	26.0	6,858	2,562	2.3	48.0
8	3.17	26.0	2,170	1,184	0.71	45.4
9	2.15	35.5	10,788	363	2.6	96.6
10	1.37	35.5	16,002	154	3.9	99.0

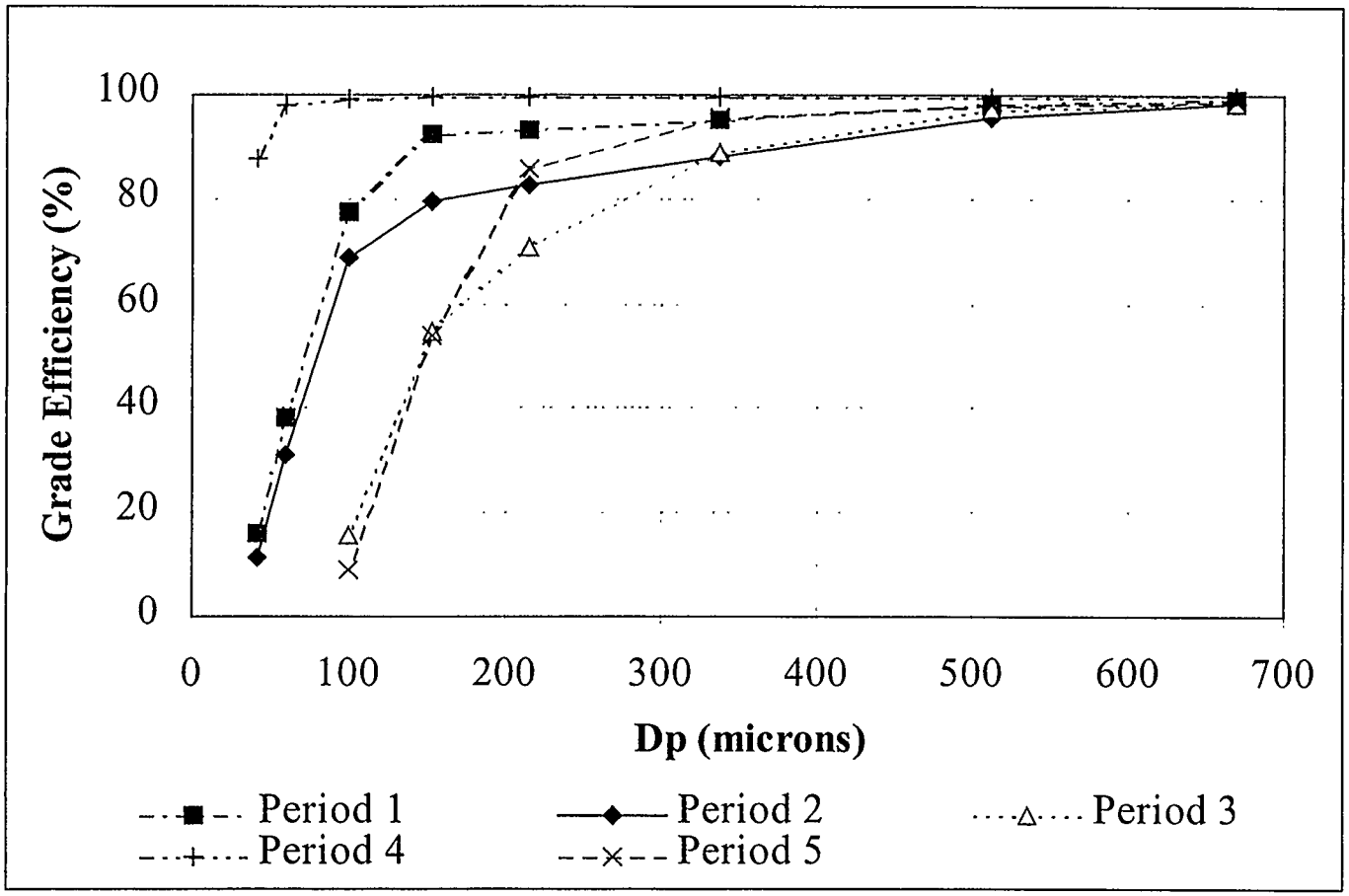

Figure 5.1.11A-1 Disengager Grade Efficiency Curve

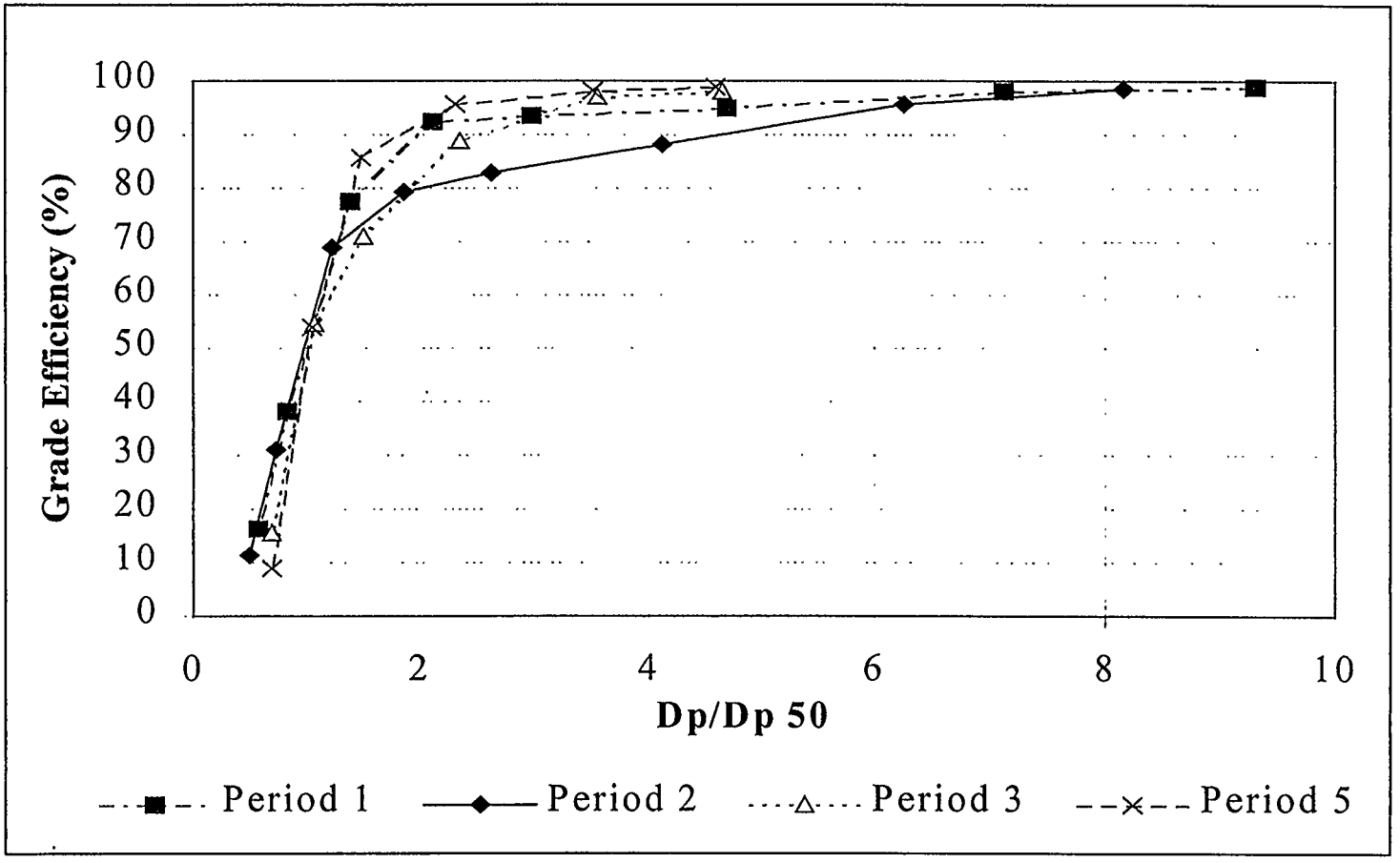

Figure 5.1.11A-2 Disengager Grade Efficiency Curve

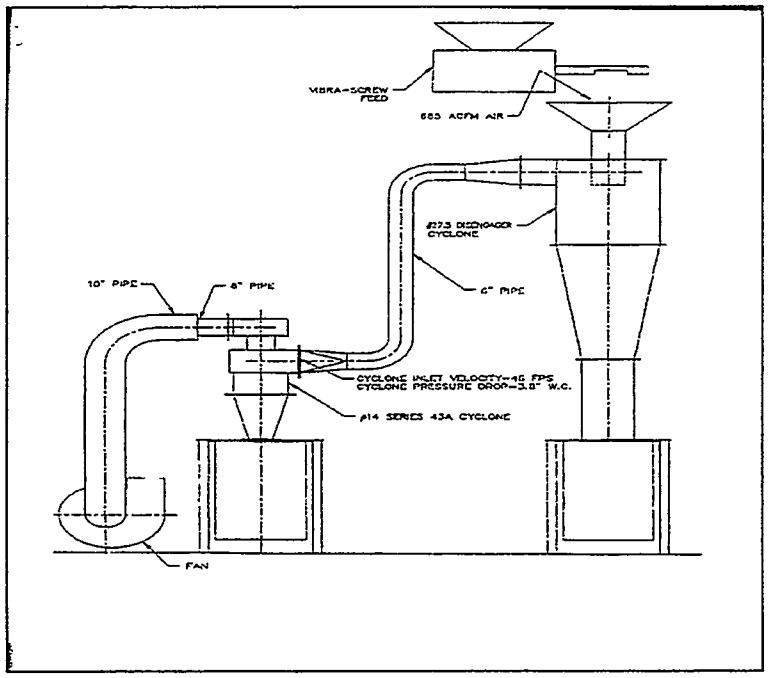

Figure 5.1.11B-1 Schematic Diagram of Experimental Setup at GEESI

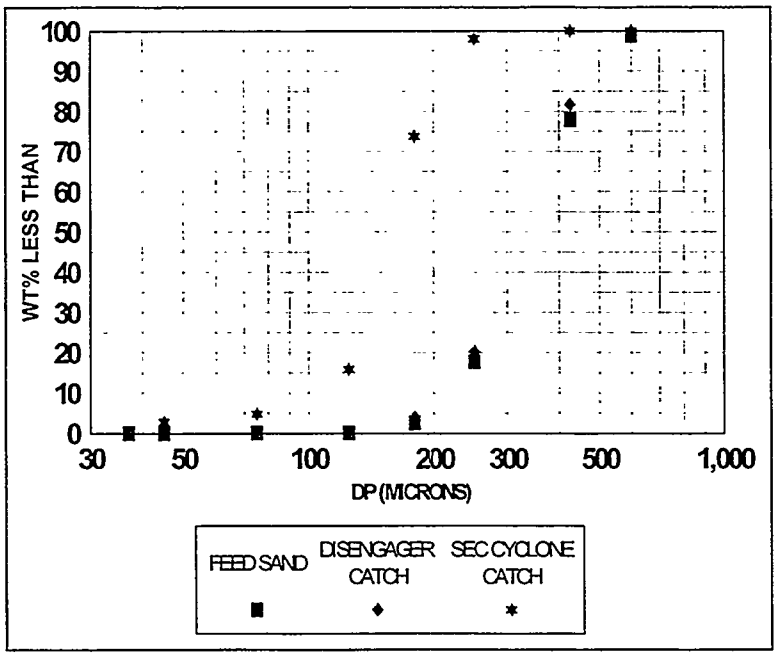

Figure 5.1.11B-2 GEESI Disengager Cold Flow Test Results

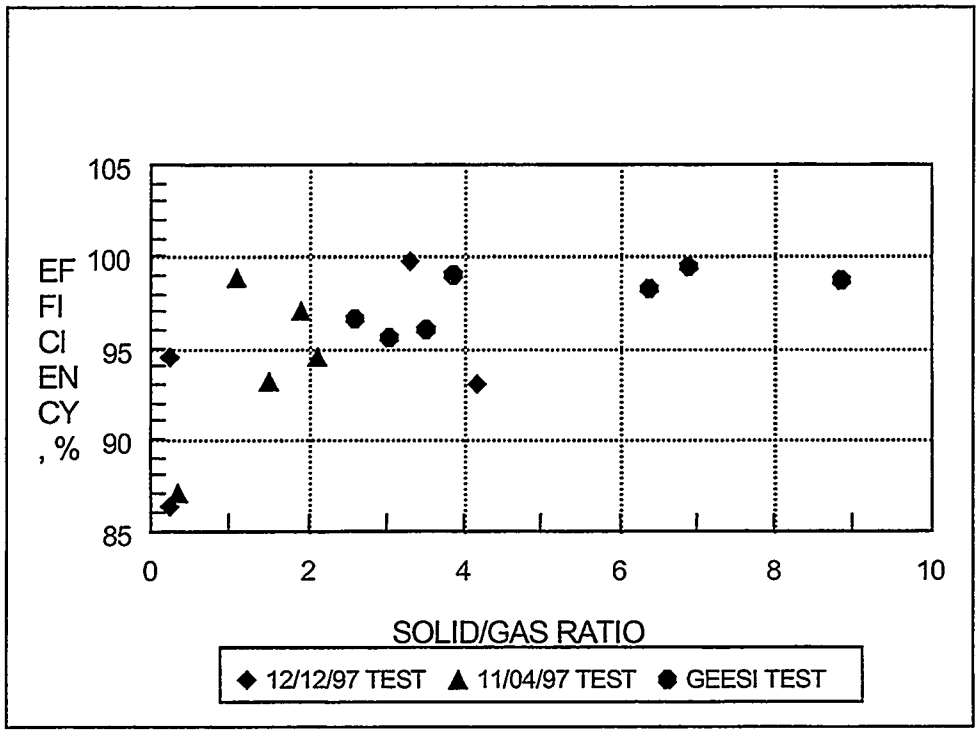

Figure 5.1.11B-3 Comparison of Disengager Performances (PSDF Vs GEESI)

PSDF\1996\5_1_11.doc

5.1.12 Solids Conveying System

5.1.12.1 Introduction

This section provides operational background and history of various solids conveying systems in the process. All solid conveying systems were provided by Clyde Pneumatics. During the initial testing (when alumina was used), several problems developed with the Clyde Pneumatics conveying equipment. The rotofeeders on FD0210 (coal), FD0220 (sorbent), and FD0530 (spent solids) tended to bind and the motors had to be manually turned. For FD0210 and FD0530, spacers were installed to allow more clearance between the rotor and the internal plates. When FD0530 was taken apart for this operation, the plate on top of the rotor was extensively scored. There was an area near the center part of the driving shaft where the scoring was more severe. The metal rolled up causing the rotor to bind. The other problem was associated with the Spheri valves. The valves tended to bind between the valve hemisphere and the pressure seal. Additional spacing was added to the FD0520 (PCD fines) and the FD0510 (standpipe ash) bottom Spheri valves, the FD0210 (coal feeder) bottom and middle Spheri valves, and the FD0220 (sorbent feeder) middle Spheri valve so that the hemisphere part would not bind but the inflated seal would still provide sealing. The FD0140 (used for initial reactor filling) and FD0820 (baghouse ash) dense-phase pumps worked well, although the FD0820 had not transported as many solids as the FD0140 system. As of this time FD0810 (sulfator ash) and FD0610 (sulfator sorbent addition) had not been put in service.

5.1.12.2 Coal Feeder (FD0210)

Based on the binding problem experience with FD0530, a spacer was placed in the FD0210 rotofeeder. The bottom of the rotofeeder would not operate properly due to the presence of moisture. The rotofeeder was taken apart and cleaned out. Water had been introduced into the system through a vent line on the coal feeder that did not have a rain hat. A rain hat was installed to prevent this from occurring again. When alumina was added the rotofeeder bound frequently. Sometimes the rotofeeder could be freed by rotating the motor by hand. Pieces of grating were found plugging the 1-inch discharge line from FD0140. A screen was placed in the FD0140 silo to prevent the transfer of oversized material.

Solids carryover from the FD0210 and FD0220 vent lines to the process line upstream of the reactor pressure letdown valve (PV287) was found to be the cause of the PV287 erosion. These vents valves were intended to allow a flow through the dispense vessel while maintaining the dispense vessel at a pressure a few psig above the conveying line pressure. Valves were installed in these lines and were closed to prevent the erosion from occurring. A design was completed to route the vents to the silos above the feeders; however, it was found in CCT1C that the rotofeeders would operate without the vents. Differential pressure (between the dispense vessel and the nitrogen supply to the purge valves) controllers were added to reduce the flow rate through the dispense vessels when

operating at low pressures. This was done so that when operating at 50 psig there will not be too much air flow forced through the flow orifices that are supplied air at 315 psig. By controlling the upstream pressure, the amount of flow was reduced.

Other problems developed with the FD0210 feeder when it would not transfer solids. When the bottom was removed, epoxy paint chips were found. The inside of the vessels had been previously coated with epoxy (some of which had lost adhesion). Most of the loose epoxy was removed from the inside of the vessels. Also during CCT1C, the FD0210 tripped due to the top lock vessel Spheri valve failing to fully close. By enabling and disabling the fill cycle, the Spheri valve closed and the feeder was started. After coal was added to FD0210, the operation became smoother. Due to the plugging that occurred between the rotofeeder outlet and where the solids entered a smaller pipe, the bottom line was modified by adding a valve at the elbow to allow the rodding out of plugs or blowing out the line.

During CCT2C the coal flow into the feeder became erratic. The cycles became very short with the coal blowing back into the silo. Coal could be drained out of the drain chute very easily which indicated that the bottom of the coal bin was not plugged. The erratic feeding continued which resulted in the plant operation shutting down. Four drums of coal were drained from the feeder, and the feeder was inspected with a boroscope. The lock vessel was clean and the dispense vessel was clean except for missing patches of epoxy and a small amount of coal on the feeder plate. By using a boroscope for inspection, an area was found that appeared to be raised on the dispense vessel Spheri valve seal; however, when the vessel was taken apart, the raised area was determined to be corrosion on the outer plate. A Clyde representative indicated that when the level probe in the lock hopper was not working, it caused the vessel to overfill thereby causing the coal to pack in the lock vessel and on the walls during pressurization which can cause it to hang-up.

The feeder was taken apart to check the Spheri valves and the connection valve (XV8457). The connection valve was partially blocked by an off-center piece of gasket. The dispense vessel Spheri valve seal was found to be okay. Gaskets were installed to increase the spacing (to 0.020-inch clearance). The valve was very hard to turn so it was further inspected. It was found that the grease seals were too tight and the valve could not be turned by hand like other valves. The lock vessel Spheri valve was found to have a roughed surface on the Spheri valve seal. The seal was replaced and gaskets were added to space the seal further apart. A bridge of wet coal was found above the upper Spheri valve. The wet coal was removed. The upper valve of the three Spheri valves was not modified.

5.1.12.3 Sorbent Feeder (FD0220)

The FD0220 rotofeeder has a history similar to the FD0210 rotofeeder. The line from the rotofeeder is smaller and plugs easily. When the fines were recycled in August, the

pressure drop in the transfer line was erratic. As with the FD0210 feeder, a valve was added at the elbow to allow the rodding out of plugs or blowing out the line.

On several occasions the level probe in the dispense vessel would not function. The probe was adjusted and later readjusted with alumina in a bucket. On August 16 the pressure tubing within the purge control cabinet ruptured. Fortunately the cabinet relief valves were adequate for the flow. Most of the tube fittings were changed to Swagelock.

In October the lock vessel Spheri valve seal was found to be leaking because the O-ring was pinched. The O-ring and the seal were both replaced. After this repair, the nitrogen flow rate used for the Spheri valve seals became small as indicated by the FV490 valve position. At one point in November, the middle Spheri valve would not close. The shaft was oiled and has worked properly since that time.

5.1.12.4 Sorbent Material Transporter (FD0510)

When alumina was transferred from the reactor standpipe, both Spheri valves would not rotate. The gap for the bottom Spheri valve was increased to add clearance, and the pressure seal was replaced. The upper Spheri valve was loosened by increasing the pressure on the actuator piston. On another occasion, the top Spheri valve would not rotate. The air lines to one side of the actuator were removed and the valve rotated freely.

In August the top Spheri valve on FD0510 would not close. After adjusting the pressure to the cylinder that rotates the valve, the valve would close. The FD0206 and FD0510 were run for a few minutes each hour to avoid condensation. In October the dispense vessel level probe would not function. Water and a loose connector in the wiring was found and repaired. The dispense vessel Spheri valve seal was found to be leaking and was replaced.

5.1.12.5 PCD Fine Ash Transporter (FD0520)

In July the bottom Spheri valve would not completely close and had to be removed. Some chunks of refractory were found on top of the hemisphere and the top of the hemisphere was scored. The pressure seal was replaced, the spacing was increased, and the top of the hemisphere was polished with sand paper. Later the discharge clogged several times with refractory pieces. It was cleared by rodding into the discharge line. Due to the reduction in cross section between the vessel and 2-inch discharge line, there is little tolerance for larger particles.

In November the vent valve was found to be leaking a large amount of gas. (There is a 4.7-mm orifice downstream of the valve. The FD0530 baghouse was running 5 to 10 inches of water.) When inspected this valve was found to be severely scored. FD0520 also had to be tapped to get the solids to flow due to a leaking vent valve. Also, the Spheri valve was not closing within the delay timer's range due to a stuck shuttle valve. The piston and shuttle

valves on FD0210, FD0220, FD0510, and FD0520 (two per feeder) were greased with O-ring grease.

5.1.12.6 Standpipe to FD0510 Screw Conveyor (FD0206)

During initial pressure testing of the reactor, the screw cooler leaked and the packing glands were tightened to prevent additional leakage. During initial operation and testing the glands were loosened to prevent stalling the motor. After operating the motor, the packing was tightened again but the packing continued to leak as indicated by the purge flow. The original packing was replaced with rope packing and tightened. This has proved to be a satisfactory solution to the problem.

5.1.12.7 Sulfator Sorbent Feeder (FD0610)

Functional checks were written for FD0610 (limestone/sorbent to the sulfator) and completed.

5.1.12.8 Sulfator Overflow to Ash Silo Screw Conveyor (FD0602)

Functional checks were written for FD0602 (screw cooler on sulfator ash to FD0810) and completed October 31.

5.1.12.9 Standpipe and PCD Ash Transport to Ash Silo (FD0530)

FD0530 Logic: During the preliminary run through, the whole program remained locked in the first cycle. The PLC programs are geared to completion of every condition in order to continue to the next. If any condition is not satisfied the program does not continue.

The first step did not complete because the differential pressure switch (PDS8562) between the lock hopper and the storage bin would not indicate that the pressure had dropped when the lock vessel vent valve was opened. It was determined that the problem was that the high leg of the switch had water on the process side. The PDS8562 switch setting was increased from 0 to 15 millibar, i.e., at less then 15 millibar the lock vessel will be considered to be depressured. Should solids accumulate in the lock vessel vent the switch may not work in the future since 15 millibar is only about 6 inches of water (the maximum setting on the switch is 60 millibar). Thus, the vent line will need a purge to prevent water from entering the unit. During later operation, it was found that this pressure switch was wired to the normally open contacts whereas it should have been wired to the normally closed contacts.

The DCS showed that out-of-range was a condition as part of the interlock; however, there were no steps in the program that used the out-of-range condition. An out-of-range condition was put into the program so that when any instrument becomes out of range the program will stop on the next cycle.

One reading that was not present on the system was the storage bin temperature (TE8562 and TT8562). A resistor was installed on the PLC to take the place of the temperature switch until the temperature instruments can be installed.

After the above repairs, FD0530 would cycle completely through the rotofeed fill cycle. At the start of the rotofeed fill (which is started by a low level reading in the rotofeed vessel), the vent valve on the lock vessel is vented. When the pressure switch (PDS8562) is satisfied, the isolation Spheri valve is opened followed by the lock vessel Spheri valve. These valves remain open for 30 seconds or until the level switch in the lock vessel indicates level. Then the lock vessel vent valve is closed followed by the isolation Spheri valve and the lock vessel Spheri valve. The lock vessel pressure is then equalized with the rotofeed vessel. When the pressure has equalized the rotofeed vessel Spheri valve opens for 25 seconds. The rotofeed vessel Spheri valve then closes. At this point the cycle restarts if the level in the rotofeed vessel is still low. During this test the rotofeeder motor was running.

A DCS representation is needed for the level switches in the storage bin. Currently there is no method to know where the levels are.

FD0530 Operation: When first tested on alumina in March, the rotofeeder bound tight and the motor could not be rotated by hand. The rotofeeder was inspected and the plate on top of the rotor was found to be scored. The area near the shaft indicated metal-to-metal galling which could cause the binding. As a solution to the problem shims were used to increase the gap between the rotor and the top plate.

When alumina was transferred from the FD0530 bin to the ash silo, the motor would stop continuously. The motor could be turned by hand with some difficulty and could eventually be freed by rotating the motor forward and backward by hand. The rotofeeder would not operate continuously until the feeder was almost empty. The level probe in the dispense vessel indicated the vessel was full when it was not. In November the rotofeeder plugged. The rotorfeeder was cleaned and the shaft was greased. It worked for only a short time. Moisture contained in the blow through from the FD0520 vent valve leak was suspected as the cause of the problems.

5.1.12.10 Feedstock and Start-up Bed Material Transporters

The BOP dense phase was completed in April 1996. Functional check lists were prepared and used for the FD0140, FD0154, and FD0104 systems. For the FD0140 system, the three-way valves were not set up the same as the logic. The valves were therefore taken apart and reassembled so that the switch and the panel matched the valves actual function. Also, one of the proximity switches on the three-way valve was found to be broken. For the FD0154 and FD0104 systems, the high high-level switches on the FD0210 and FD0220 wiring was changed to make it function properly. Also the logic for the level switch on FD0104 had to be reversed. The FD0140 (used for initial reactor filling), the FD0154

(sorbent transport from pulverized silo to MWK silo), and the FD0104 (coal transport from the pulverized silo to the MWK silo) have worked well.

5.1.12.11 Summary

All of the balance of plant dense phase transports have performed well (FD0104, FD0105, FD0140, and FD0820). The instrumentation on FD0810 and FD0610 have been checked, but have not been operated with solids.

The five feeders in the structure had a number of problems (FD0210, FD0220, FD0510, FD0520, and FD0530). The current status of these feeders is unsatisfactory. With hind sight these feeders might have worked fine if they had not been operated with alumina which flows well and has created scoured parts since it is a hard substance.

Since the rotofeeders will not tolerate any large particles, any foreign material that falls into them of a slightly larger size will plug them. The rotofeeders were coated on the inside with epoxy paint which specifically should not have been done per the MWK purchase order. The slow peeling of the epoxy requires that the epoxy be completely removed from the FD0210 and FD0220 vessels to prevent future outages.

Due to the undersized line on FD0220 (3/4-inch diameter, XX strong), the plan is to replace the line with a larger line.

The FD0510 and FD0520 vessels have a major problem with the reduction at the exit from 4 to 2 inches which creates a natural choke point. Since larger lines would consume much more nitrogen, a number of ports have been added to blow backward and forward and to rod out the lumps.

5.1.13 Pressure Letdown Valve

5.1.13.1 Chronology and Modifications

This section is a discussion of the modifications made to the trim of the MWK reactor pressure letdown valve PV-287 and the results these modifications have on the flow characteristics of the valve.

Per MWK specifications, PV-287 was originally supplied with a modified Whisper III trim. However, it was soon discovered that the valve did not have the flow capacity required for start-up (50 psi inlet). Instead the valve was sized for normal operating conditions only (320 psi inlet). To remedy this, the valve trim was replaced with an equal percentage trim that provided the required flow capacity for start-up.

Upon replacing the Whisper III trim with the equal percentage trim, it was necessary to rotate the valve 180° horizontally in the pipe line so that flow was from top to bottom (as opposed to from bottom to top as with the Whisper III cage). The equal percentage cage performed well in allowing the desired flow capacity; however, due to solids in the line three sets of trim were soon eroded to the point of failure/inoperability (as well as three valve bodies). As the air/solids passed through the trim, this flow was divided into eight streams, each near sonic velocity and traveling directly downward toward the bottom of the body. This resulted in extreme wear problems. Therefore the third time that the valve/body deteriorated, it was decided to modify the original Whisper III cage to provide more flow capacity and place this modified trim back in the valve body. The theory was that cage flow in the Whisper III would enter the valve at the bottom of the trim, flow up through the cage where it would be dispersed into many small flow streams (816 with the valve 100-percent open), then flow out of the top of the trim. This upward flow path coupled with the multiple (816) small streams would be less erosive than the downward flow path with the eight large streams.

To determine the required modifications to the Whisper III cage, the holes in the cage were counted and the hole pattern mapped. An estimation was then made of how many holes would be exposed versus valve plug position. Each hole was one-sixteenth-inch diameter on the inlet side with a step to one-eighth-inch diameter on the outlet side. A simple orifice calculation was performed for a one-sixteenth-inch diameter orifice to determine the amount of flow each hole could pass. This calculation uncovered a discrepancy between the calculated valve flow coefficients (Cgs) and the ones on the MWK valve data sheet. The valve data sheet indicates that the flow characteristic is basically linear, while the orifice calculation indicated that the flow was similar to an equal percentage characteristic for the first 50 percent of travel, then linear for the remaining 50 percent of travel. To resolve this, Fisher Valves sent the actual Cg vs percent open data for the original valve trim that was provided. This data confirmed that the data sheets did not match what was actually provided. The maximum Cg was correct, but the flow characteristic was not.

To modify the Whisper III cage, all of the holes in the cage were drilled to seven-sixty-fourths of an inch (0.109) diameter on the inlet side. The outlet side remained at one-eighth-inch (0.125) diameter. Figure 5.1.13-1 compares the flow characteristic of the original cage vs the modified cage. As is shown, the original cage was extremely inadequate to provide the required flow during start-up, while the modified cage was sufficient.

During operation, when the valve is opened less than 50 percent, one method to detect wear in the valve trim is to compare the actual position of the valve with the predicted position based on calculations. If the valve is open considerably more than calculations predict, then wear may be a problem. Figures 5.1.13-2 through -7 show the flow capacity vs percent valve open for various inlet pressures. The outlet pressures have also been varied slightly to account for different operating parameters, but this has a minimal effect on the calculations. The main component is inlet pressure. For all calculations, 500°F was used as the operating temperature. This is conservative in that the higher the temperature, the higher the specific volume of the fluid and therefore the less flow capacity of the valve at a given position. Therefore, if the operating temperature is less, the flows shown will be greater. These curves will be helpful in monitoring the operability of valve PV-287 and determining the condition of the valve trim.

5.1.13.2 Summary

An anomalous venting operation from the feed system caused the high erosion of the back pressure control valve. The high erosion resulted in a valve failure which affected the control of the back pressure.

The original valve size was in error and has been corrected. The original Whisper III trim was changed to equal percentage trim, which allowed desired flow control at low air pressures during start-up. The Whisper III cage was modified to provide better control during start-up. It will be tested at a later date.

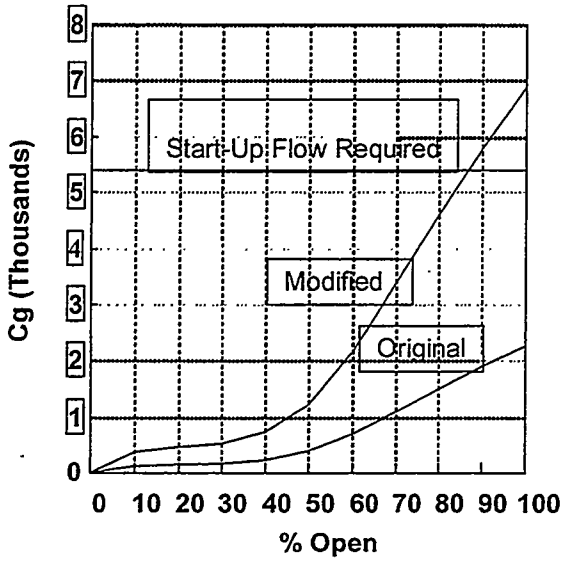

Figure 5.1.13- 1
PV-287 Whisper III Trim

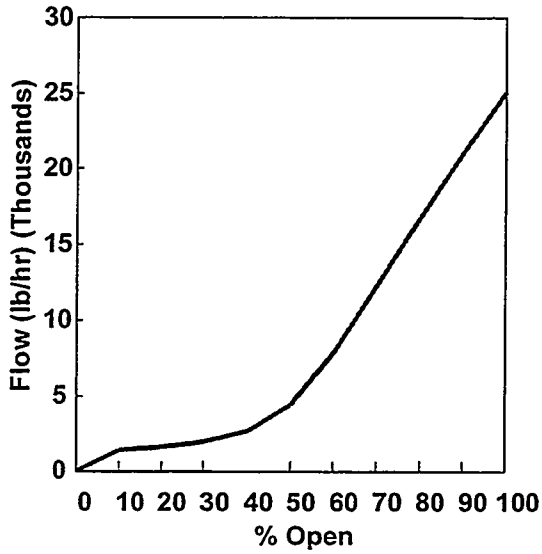

Figure 5.1.13-2
PV-287 P1=50 psi, P2=2 psi, T=500 °F

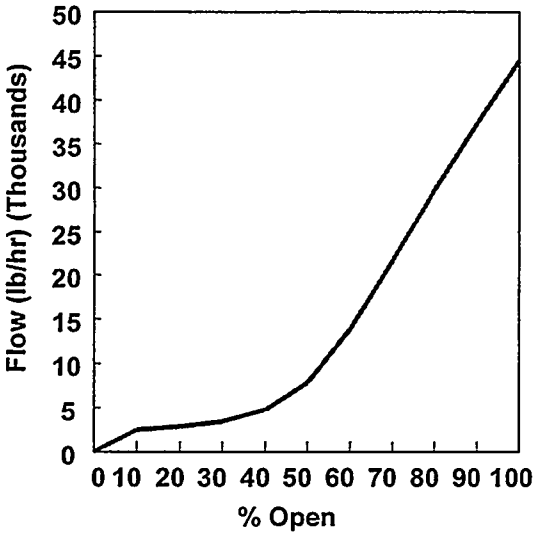

Figure 5.1.13-3
PV-287 P1=100 psi, P2=10 psi, T=500°F

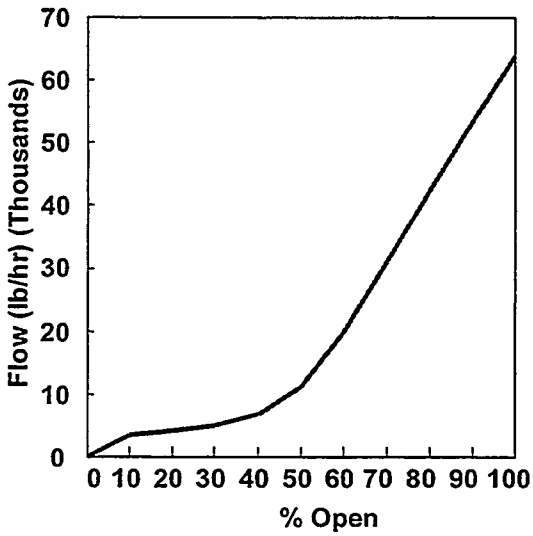

Figure 5.1.13-4
PV-287 P1=150 psi, P2=20 psi, T=500°F

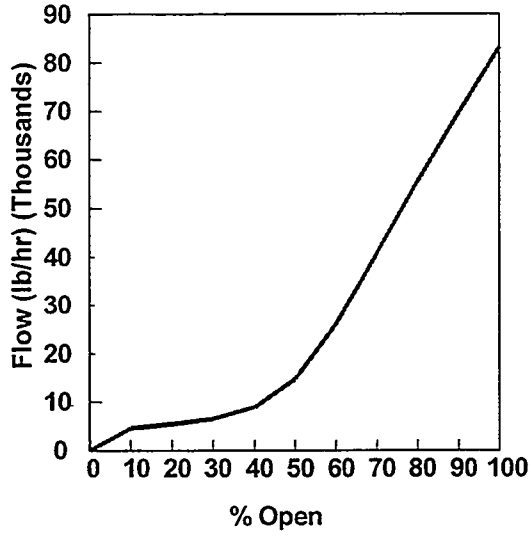

Figure 5.1.13-5
PV-287 P1=200 psi, P2=30 psi, T=500°F

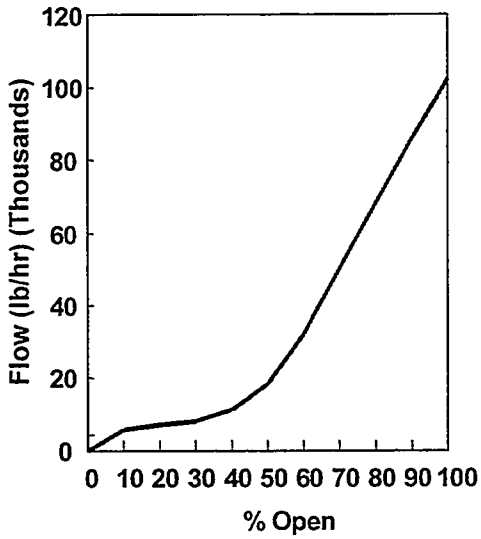

Figure 5.1.13-6
PV-287 P1=250 psi, P2=40 psi, T=500°F

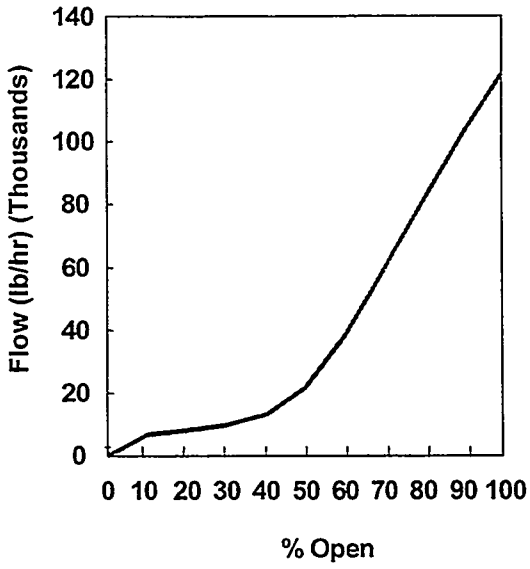

Figure 5.1.13-7
PV-287 P1=300 psi, P2=50 psi, T=500°F

S:\PSDF\5_1_13.doc

5.2 OPERABILITY ANALYSIS OF COMMISSIONING TESTS

The purpose of this section is to analyze some of the operational data in order to achieve a better understanding of the reactor system and to provide a guideline for future operation and design. In the past two combustion tests during August (CCT1C test run) and November (CCT2C test run) of 1996 a large amount of data was collected. It is very difficult to cover all aspects of test data analysis. This section of analysis covers some of the operation data that will illustrate some important observations and give some insights for future operations and design.

5.2.1 Analysis of the Reactor Coal Feed Rate and Comparison With Other Processes

The coal feed rate for a given reactor size is an important index in assessing the pilot plant reactor's commercial potential because a higher coal feed rate means a smaller reactor for a given thermal output. This lowers not only the capital cost of the reactor system associated with procurement but also lower costs due to smaller footprint, less structural requirements, and faster installation. In the following, the coal feed rates that have been achieved during the reactor test runs are first presented and then these throughputs are compared with that in other combustion processes.

Ideally, the coal feed rate can be directly measured through weight cell in the coal feed system. In reality the coal feed rate is not very easy to measure due to the fluctuation of the weight cell readings. In order to achieve a better estimation, the coal feed rate is also calculated from the oxygen balance.

Figures 5.2-1 through 5.2-4 give comparisons of coal feed rate calculated from the oxygen balance and weigh cell. (All figures for section 5.2 are found as an exhibit following section 5.2.5.) The agreement between the coal feed rate calculated from the oxygen balance and that from weigh cell is acceptable considering the scatter in data. The coal feed rate comparison for the August 19 through 21 test period is better than that for November 19 through 21. The fluctuations in the weight cell readings during the August tests are less severe than that in November tests. Due to the FD0210 coal feeder problems in the November tests, FD0220 was used as a backup feeder and coal feed was switched between these two feeders quite often. Overall, it seems that the results of the coal feed rate calculated from oxygen balance are quite reasonable. For future tests, carbon balance will also be used as another method to calculate the coal feed rate.

These comparisons bring out an important issue for large pilot plant coal combustion processes. In general, the perception is that the direct measurement is always more reliable than indirect measurement. Taking the coal feed as an example, common preference is to measure the coal flow rate directly by many researchers. Unfortunately, the direct and instantaneous measurement of coal flow rate is difficult although one does not see it in formal publications. The weigh cell weight fluctuations and accuracy problems over a wide range are well known. Oxygen or carbon balance generally gives reliable results

because the gas flow rate and composition can be measured accurately. Figures 5.2-1 through 5.2-4 seem to indicate that the coal feed rate from the oxygen balance is, at least, if not more reliable than weight cell measurements.

It should be pointed out that the coal feed rates given in figures 5.2-1 through 5.2-4 are slightly lower than the coal feed rates expected at operating pressures. The coal feed rates can be increased further by operating the combustor heat exchanger with higher level of solids, which will increase the circulation of cold solids through the riser. However, the coal feed rates achieved during the reactor test runs are still quite high compared to other existing combustion processes. Table 5.2-1 gives a comparison of heat release rates among different combustion processes.

From table 5.2-1, one can see that even if the coal feed rate is 500 lb/hr the heat release rate for this reactor is still comparable with the pressurized circulating fluidized combustor. At the feed rate 700 lb/hr, which is roughly the feed rate that the reactor was operated for the November test run, the heat release rate is already about 30 percent higher than the pressurized circulating combustion processes. For the coal feed rate of 1,000 lb/hr, which corresponds to the feed rate of August 20 to 21 (CCT1C) test run, the reactor heat release rate is already double that of pressurized CFB.

The transport reactor operates with much smaller particle sizes. Therefore, the combustion process should be kinetically controlled and should not be diffusion limited. The main reasons for the higher heat release rate in transport reactor are the smaller coal particle size and the higher gas-phase velocity necessary for the reactor operation. Both factors are in favor of increasing the coal combustion reaction rate. The smaller particle means a higher reaction area is available. The higher gas flow rate means faster mass transfer rate between the gas and the solid phase. Under most circumstances the combustion process is diffusion controlled. Both factors (smaller particles and higher gas velocity) will increase the diffusion rate. The effect of the gas flow rate on the reactor heat release rate can be further illustrated from examples suggested by some researchers (e.g., Waters, 1975) that the reactor (or grate) heat release rate can be estimated for the circulating fluidized bed combustors using:

$$R_E \propto \frac{U_o}{E_x}, \qquad (5.2.1)$$

where R_E, U_O, and E_X are the grate heat release rate, the superficial gas velocity, and air flow factor relative to the stoichiometric air flow rate, respectively. The superficial gas velocity should be calculated based on 300°K temperature. Equation 5.2.1 indicates that the heat release rate will increase linearly with the superficial gas velocity. Since the transport reactor operates at a much higher gas velocity, the heat release rate will be higher. For the normal operating conditions, the CFB generally has a superficial gas velocity of 5 to 7 m/s while the transport reactor operates at 10 to 14 m/s. For the same

coal particle size, the heat release rate in transport reactor compared to CFB should be double based on equation 5.2.1. This extrapolation of equation 5.2.1 from CFB to the transport reactor probably goes too far since equation 5.2.1 is a pure empirical correlation which should be carefully applied to conditions that are beyond the experimental data from which the correlation is obtained. However, all the mass transfer studies in the fluidized bed reactors seem to indicate that the mass transfer rate should be proportional to the superficial velocity to a power of 0.5 to 1.0. Taking the lowest limit, the heat release rate should be roughly 1.5 times higher when the gas velocity increases by a factor of 2.

The smaller particle size gives a much higher diffusion rate which in-turn increases the combustion rate. For a spherical particle under steady state, the diffusion rate of oxygen to a single particle can be estimated:

$$R_d = D\left.\frac{dC}{dr}\right|_{r=R} \propto \frac{1}{R}, \qquad (5.2.2)$$

where R_d, D, R, and r, are the oxygen diffusion rate to the particle, diffusivity, particle diameter, and coordinate, respectively. The particle size used in the transport reactor is generally about half the size of a pressurized CFB. This means that the combustion rate in the transport reactor should be twice as much in lieu of equation 5.2.2, if the combustion process is diffusion controlled. The combination of the smaller particle and higher gas velocity makes it possible that the heat release rate in the transport reactor can be three times as high as the CFB. The above arguments show that the observed heat release rates as shown in table 5.2-1 are potentially achievable.

Table 5.2-1

Comparison of Heat Release Rates From Different Combustion Processes*

	Heat Release Rate (MW/m^2)	Heat Release Rate ($MBtu/hr\ ft^2$)	Operating Pressure (psig)
PC boiler	2.0	0.63	0
Atmosphere CFB	6.8	2.2	0
Pressurized bubbling bed	15.0	4.8	160
Pressurized CFB	50.0	15.8	160
MWK PSDF transport reactor at 500 lb/hr** coal feed rate	47.0	14.8	160
MWK PSDF transport reactor at 700 lb/hr** coal feed rate	65.0	20.7	160
MWK PSDF transport reactor at 1,000 lb/hr** coal feed rate	93.0	29.6	160
MWK PSDF transport reactor at 1,600 lb/hr** designed coal feed rate	149.0	47.0	280

* Data for other processes from: Basu, P. and Fraser, S. A., *Circulating Fluidized Bed Boiler, Design and Operations*, Butterworth-Heinemann, Boston, 1991.

** Assuming 13,000 Btu/lb for the heating value of coal.

5.2.2 The Relationship Between the Coal Feed Rate and Solid Circulation Rate

It has been mentioned that circulation of the solid from the combustion heat exchanger can control the temperature in the reactor. In the last section, the upper limitation on the solid circulation rate is explored from reactor riser choking and standpipe free settling velocity considerations. In this section, the relationship between the solid circulation rate and the coal feed rate will be addressed.

The energy balance around the reactor can provide information about the amount of solid circulating through the combustion heat exchanger. A heat balance control volume can be drawn as follows:

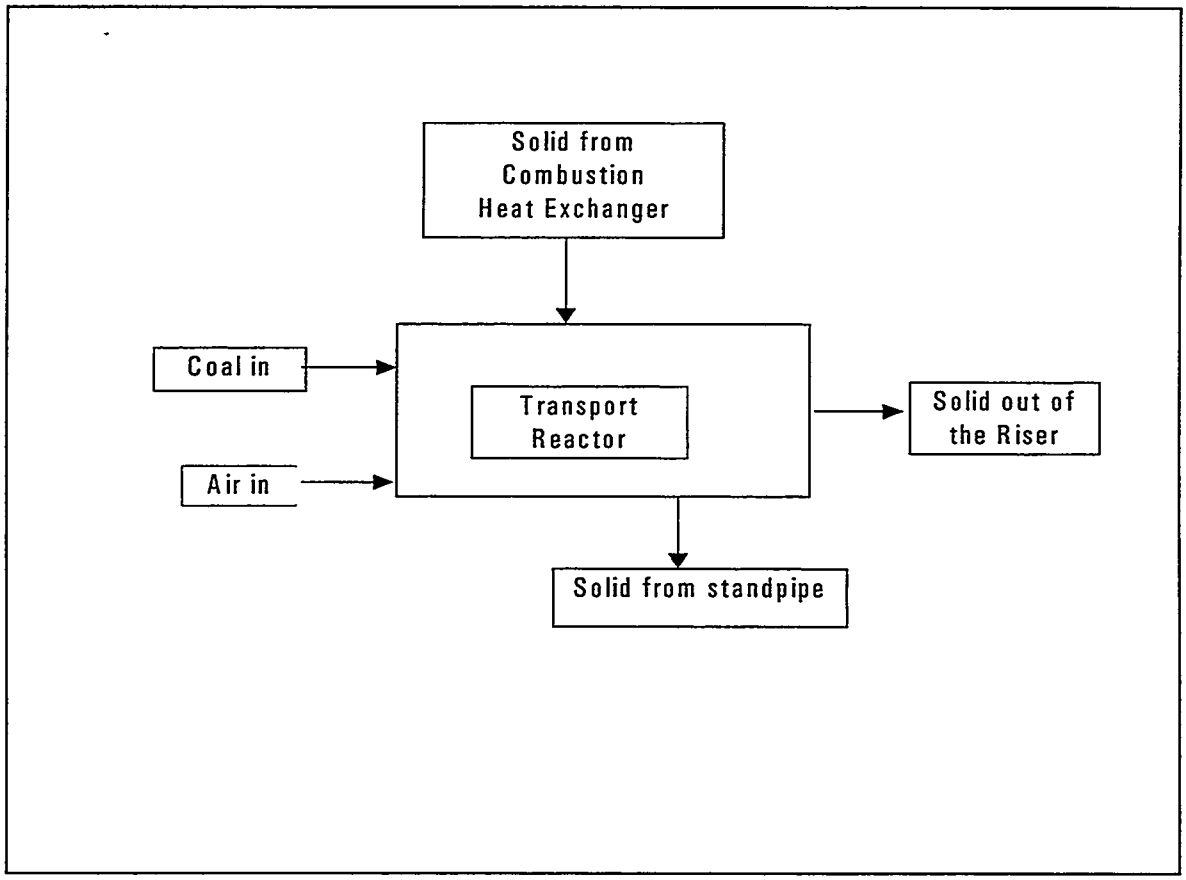

The energy balance around the control volume can be written as:

$$W_c(\Delta H_c + T_c C_c) + W_a T_a C_a + (1-x) W_s T_{Hs} C_s + x W s T_{Js} C_s = W_T C_T T_T \qquad (5.2.3)$$

where,

C_a = heat capacity of air, Btu/(lb °F);
C_c = heat capacity of coal, Btu/(lb °F);
C_s = heat capacity of circulating solids, Btu/(lb °F);
C_T = mean heat capacity of fluid and solids at the exit conditions, Btu/(lb °F);
T = exit temperature of gas and solids;
T_a = inlet temperature of air;
T_c = inlet temperature of coal;
T_{Hs} = inlet temperature of solids from combustion heat exchanger;
T_{Js} = inlet temperature of solids from the reactor standpipe;
W_c = mass flow rate of coal, lb/hr;
W_a = mass flow rate of air, lb/hr;
W_s = mass flow rate of circulating solids, lb/hr; and
x = mass fraction of solids from the reactor standpipe.

The solid circulation rate can be simplified by the fact that the heat capacity of the materials flowing in the reactor is roughly the same. Then equation 5.2.3 can be rewritten as:

$$W_s = \frac{W_c \Delta H_c / C - W_c(T - T_c) - W_a(T - T_a)}{T - (1-x)T_{Hs} - xT_{Js}} \qquad (5.2.4)$$

For a given feed rate and feed stream temperatures, equation 5.2.4 can be used to calculate the solid circulation rate. Figure 5.2-5 gives the results of the calculated solid circulation rate versus the coal feed rate at different mass fraction of solids circulating through the reactor standpipe with the mixture heat capacity of 0.25 Btu/(lb °F). To calculate the solid circulation rate using equation 5.2.4, the mass fraction of circulating solids from the reactor standpipe (which is unknown) is required. Another equation is needed to solve for the mass fraction from the reactor standpipe. However, the calculation becomes quite difficult because the temperature difference between the standpipe solids and those solids in the mixing zone is too small. This small temperature difference may cause larger calculation errors.

This problem can be avoided if the total solid circulation rate is calculated by selecting the top portion of the mixing zone and riser as the control volume. From such a control volume, the total solid circulation rate can be expressed as:

$$W_s = \frac{W_c \Delta H / C - W_a(T_o - T_i) - W_c(T_o - T_i)}{T_o - T_i} \qquad (5.2.5)$$

where T_i and T_o are the temperatures at the top of the riser and bottom of the control volume, respectively.

Equation 5.2.5 is remarkably simple. However, there is another pitfall in the application of equation 5.2.5 to calculate the circulation rate, the selection of the inlet temperature to control volume. Because it is possible that coal combustion may occur in the mixing zone, the inlet temperature estimated would be higher, which in turn will give an overestimated solid circulation rate. The reason for this situation is that in writing equation 5.2.5 it was assumed that all combustion reactions will be completed inside the control volume. It is almost unavoidable that some of the combustion reactions will occur outside the control volume selected. Our hope is that the amount of coal combustion in the selected region of the mixing zone can be minimized. Further, since the core temperature of a solid particle is lower than the surface temperature, it will partially compensate for the overestimated inlet temperature. The calculated solid circulation rate will be closer to the actual circulation rate.

The following will attempt to further explain why circulating solids may not be completely heated up to the fluid temperature in a short time and need some elaboration. Figure 5.2-6 gives the results of the heat up rate of a spherical particle. This figure shows the dimensionless temperature profile inside a spherical particle varying with dimensionless time. The dimensionless variables are defined as:

$$\tau = \frac{\alpha t}{R^2}, \quad \text{dimensionless time} \qquad (5.2.6)$$

$$\Theta = \frac{T - T_0}{T_f - T_0}, \quad \text{dimensionless temperature} \qquad (5.2.7)$$

where α is the thermal diffusivity of the solid particle and T, T_f, and T_o are temperatures inside of a particle, fluid, and solid inlet, respectively.

If a 400μ particle has a thermal conductivity of 0.025 Btu/hr ft °F, heat capacity of 0.25 and density of 160 lb/ft^3, the volume weighted average temperature of the particle is about 80 percent of the fluid temperature for a 1-second residence time. This is roughly the time period needed for a particle traveling from the bottom of the mixing zone to the bottom of the riser. Therefore, the solid may not completely heat up to the fluid temperature.

From the above reasoning, we may hope that equation 5.2.5 gives reasonable results for the solid circulation rate. Using equation 5.2.5, figure 5.2-7 gives the calculated solid circulation rate for a 24-hour operation period August 19 to 20, 1996. The corresponding coal feed rate is given in figure 5.2-1 for this operation period. Comparing figures 5.2-1 and 5.2-7, one can clearly see that there is a certain degree of correlation between coal feed rate and solid circulation rate in the first 12-hour period. The trend is that an increase in solid circulation rate corresponds to an increase in coal feed rate. This is not the case for the last 12-hour period in which the solid circulation rate is higher and the coal feed rate is

lower than the previous 12 hours. Equation 5.2.4 or figure 5.2-5 can better explain the phenomena. As shown in figure 5.2-5, if 40 percent of circulating solids comes from the combustion heat exchanger, the required total solid circulation rate is only 100,000 lb/hr to have a coal feed rate of 1,000 lb/hr. The solid circulation rate has to be 225,000 lb/hr for 10-percent circulating solids from combustion heat exchanger to obtain the same coal feed rate. That is why in the last 12-hour operation period the solid circulation rate is higher as shown in figure 5.2-7, and the coal feed rate is lower as shown in figure 5.2-1. In order to illustrate this point further, figure 5.2-8 gives the measured standpipe pressure difference, which is an indication of the solid column height in the standpipe. Comparing figure 5.2-7 with figure 5.2-8, one can see that an increase in the standpipe level results in an increase in the overall solid circulation rate as expected. Figure 5.2-9 gives the relationship between the solid circulation rate and the standpipe pressure difference. The solid line is a best-fit line using a polynomial of second degree. Notwithstanding the scatter of the data, a certain degree of correlation can be observed.

All data in figures 5.2-7 through 5.2-9 indicate that the majority of the solids circulating in the reactor are coming from the standpipe instead of from the combustion heat exchanger. That is why the solid circulation rate corresponds to the solid column height in the standpipe quite well. This also means that solids circulating in the reactor do not have the best cooling effect in the riser. Therefore, an increase in the solid circulation rate through reactor J-leg may not result in an increase in coal feed rate at constant reactor temperature.

Figure 5.2-10 shows a plot of coal feed rate vs. the solid circulation rate for the same operation period as in figure 5.2-1. On the surface, the coal feed rate does not appear to correlate with the solid circulation rate. However, if one examines the data carefully, one would find that the data in figure 5.2-10 have two branches. The upper branch covers the coal feed rate in the first 12-hour operation period. The lower branch covers the data from last 12-hour period. In this last 12-hour period the standpipe level is high and most of solids are circulating through the standpipe. As has been mentioned, solids from the standpipe do not have a good cooling effect. Therefore, the coal feed rate can not be increased with an increase in the solid circulation rate from standpipe while keeping the reactor temperature constant. Figure 5.2-11 shows the plot of coal feed rate vs. solid circulation rate in the first 12-hour period. It shows that with the increase in the solid circulation rate the coal feed rate increased. Even for this 12-hour period, the data on the plot is still quite scattered. The reason is that the mass fraction of circulating solids from the combustion heat exchanger was not constant due to problems in its operation. It was observed in the November test that solid circulation from combustion heat exchanger was quite unsteady. Solids in the combustion heat exchanger kept bridging and arching in the bottom of the combustion heat exchanger, and as a result, the pressure difference in the bottom of the combustion heat exchanger varied widely.

Figure 5.2-12 is another example of the coal feed rate varying with the solid circulation rate for the operation period of August 20 to 21. Comparing figure 5.2-12 with figures 5.2-10 and 5.2-11, one may notice that for the data in figure 5.2-12, the coal feed rate increases more rapidly with an increase in solid circulation rate. Furthermore, the overall circulation rate is lower in figure 5.2-12 than in figure 5.2-11 and coal feed rate is higher in figure 5.2-12 than in figure 5.2-11. One of the reasons is that the standpipe level was lower in the August 20 to 21 operation period compared with that in the November operation period. Figure 5.2-13 gives the standpipe pressure difference for the August 20 to 21 operation period. Comparing figure 5.2-13 with figure 5.2-8, it can be noted that the standpipe pressure difference was not only lower but also more stable during the August test. A lower standpipe solid column height means a relatively lower solid circulation rate from the standpipe. A low solid circulation rate and high coal feed rate means that the solid circulation rate from the combustion heat exchanger was relatively high. Other reasons the August 20 to 21operation coal feed rate correlate with the solid circulation rate better are (1) the smaller particle size and (2) different start-up bed material.

Still another example of the coal feed rate varying with the solid circulation rate is given in figure 5.2-14, in which the test data of November 20 to 21 are plotted. Again the coal feed rate does not correlate well with the solid circulation rate.

From figures 5.2-10 through 5.2-12 and 5.2-14, one can clearly see that an increase in the standpipe level will result in an increase in the solid circulation rate. However, from the viewpoint of combustion operations, the solids circulating from the standpipe is quite ineffective in controlling reactor temperature. That is why an increase in the solid circulation rate does not always increase the coal feed rate as shown in figures 5.2-10 and 5.2-14. Only those solids circulating through the combustion heat exchanger can effectively control the reactor temperature.

5.2.3 The Relationship Between the Reactor Temperature and the Coal Feed Rate

At constant coal feed to the reactor with solids circulation and heat removal from the system through the external heat exchanger not changing with time and the external heat loss is constant, the reactor temperature will be constant also. During the current runs being analyzed, some difficulties were experienced in establishing smooth solids circulation through the combustor heat exchanger. This resulted in the heat removal from the system to vary, decreasing as solids circulation through the heat exchanger drops and vice versa. An increase in coal feed rate when the combustor heat exchanger was circulating poorly resulted in an increase in reactor temperature.

Figures 5.2-15 and 5.2-16 give the relationship between the reactor temperature and the coal feed rate for a total of 48 hours of operations during November 19 through 21, 1996. The trend is quite clear that an increase in coal feed rate will increase the reactor temperature. This means that the amount of solids circulating through the combustion heat exchanger was quite limited and almost constant during this time period. This also means that the overall solid circulation rate will not correlate with the reactor temperature very well because the solids circulating through the reactor standpipe cannot be used as a cooling medium as has been mentioned in the previous section. This point can be borne out by figure 5.2-17, in which the solid circulation rate is plotted against the riser temperature. The increased solid circulation rate may not control the reactor temperature properly if those solids come from the reactor standpipe.

In order to control and maintain a constant reactor temperature, while increasing the coal feed rate, one can increase the solid circulation rate through the combustion heat exchanger and reduce the solid circulation rate from the reactor standpipe. The easiest way to realize a minimum solid circulation rate through the standpipe and a maximum solid circulation rate through the combustion heat exchanger is to lower the aeration rate in the standpipe and in the reactor J-leg.

5.2.4 Solid Carryover and Cyclone Separation Efficiency

One of the anomalous problems that has been troublesome during operations is the high solid carryover rate. The high solid carryover rate results in losing solids to the PCD faster than that generated through ash from coal combustion. In order to keep roughly a constant solid inventory, inert materials have to be added. Various causes for the high solid carryover rate have been speculated. In this section, the possible causes for the high solid carryover rate will be explored.

The estimated solid carryover rates for two 24-hour operations are given in figures 5.2-18 and 5.2-19. The average solid carryover rate in this 48-hour period is 600 lb/hr. The ash generation rate is about 100 lb/hr. This means that roughly 500 lb/hr of inert materials were fed to the reactor in order to keep a constant reactor inventory.

In order to diagnose the high solid carryover rate problem, the overall combined separation efficiency of the disengager and the primary cyclone is estimated as shown in figures 5.2-20 and 5.2-21. In preparing figures 5.2-20 and 5.2-21, the average solid carryover rate was used to calculate the separation efficiencies. Because of the operational instabilities experienced, the method used to calculate the separation efficiency is not accurate because the solid carryover rate in a 48-hour operation period is not a constant. In addition without a direct measurement, the solid carryover rate is very difficult to estimate. However, the average carryover rate still gives a reasonable estimation of the total separation efficiency. It is surprising that the correlation between the total collection efficiency and the solids-to-gas loading ratio is generally good considering the wide range of the solids-to-gas loading ratio that was used during the total 48-hour operation period. As a comparison, the collection efficiency of the disengager alone from the cold flow tests at GEESI is also given in figure 5.2-20. Considering the short test duration (a few minutes) of each test performed at GEESI, the data in figure 5.2-20 can be deemed as comparable with the tests at PSDF. It is very difficult to distinguish the exact amount of contribution from the disengager or from the cyclone to the total collection efficiency. Comparing the cold flow test data with PSDF operation data in December, it seems certain that the major gas-solid separation is from the disengager not the cyclone. One obvious reason is that the disengager is collecting larger particles. If it is assumed that the disengager efficiency is 1.0 to 2.0 percent lower than the total collection efficiency, the collection efficiency of the cyclone can be estimated. For a given total efficiency and disengager efficiency, the cyclone efficiency can be calculated as follows:

$$\eta_2 = 1 - \frac{1-\eta}{1-\eta_1}, \qquad (5.2.8)$$

where η, η_1, and η_2 are the total collection efficiency, disengager efficiency, and cyclone efficiency, respectively.

Figure 5.2-22 gives the estimated cyclone collection efficiency from the assumed disengager collection efficiency. It may be quite surprising that in order to increase the total collection efficiency by 1.0 percent, the cyclone collection must vary from 60 to 75 percent and for a 2.0 percent contribution to the total collection efficiency it must vary from 73 to 85 percent. For the particle size used in the test this efficiency may deemed to be low.

Figure 5.2-18 indicates the required efficiency to balance the solid carryover rate with the ash generation rate. The solid/gas loading ratio is taken from the same operation period as in figure 5.2-20. The required total collection efficiency must be greater than 99.8 percent to balance the ash production rate and ash generation rate. If we still assume that the disengager efficiency is 2.0 percent lower than the total efficiency, the cyclone efficiency will vary from about 91 to 96 percent as shown in figure 5.2-24. It is a difficult task to achieve such high total collection efficiencies. First, a certain amount of fines generally exists due to attrition, break up by high heat-up rate, and fines in the feed materials. These smaller particles will pass through both the disengager and cyclone uncollected.

Second, the overall collection efficiency is lower for a circulation system. Suppose that a cyclone has a constant cut size dp_{50}. The particle with a size corresponding to dp_{50} will have a 50-percent probability to be collected in one pass. For the same size particles, the second passing through the cyclones will have the same probability to be collected. From this reasoning, all the particles with a size of dp_{50} will be lost to the down stream. Furthermore, if the particle size is not extremely coarse, there are always some particles passing through the cyclone due to fluid entrainment. For each pass through, the amount of the particle carryover may not be very large. The collected amount of solid passing through the cyclone may be substantial after many cycles. It should be mentioned that the designed cyclone efficiency is much higher than the efficiency given in figure 5.2-24 required to balance the data.

It should be emphasized that the above argument does not mean that the current cyclone efficiency is already high enough. Certainly the cyclone has room for improvement. One indication that the cyclone efficiency can be improved is that the pressure drop across the cyclone is quite low. Figure 5.2-25 gives the pressure drop across the cyclone in terms of the inlet head, which is calculated from the following formula:

$$H_i = 0.003\overline{\rho}U_i^2$$

where,

H_i = the inlet pressure head, inH_2O
$\overline{\rho}$ = inlet mean density, lb/ft^3
U_i = Inlet gas velocity, ft/s

From figure 5.2-25, one can see that the pressure drop across the cyclone in terms of the number of the inlet velocity head is about 2. This is in the lower range of the pressure

drop through a cyclone. The low-pressure drop generally indicates the low efficiency within certain operation range.

The question is why the pressure drop across the cyclone is low. The main reason for the low-pressure drop is the lower inlet velocity. Figure 5.2-26 gives the plot of the cyclone inlet gas velocity vs. the pressure drop. Notwithstanding the scatter in the data, the increase in the cyclone inlet gas velocity will increase the overall pressure drop. The operation range of the inlet velocity should be deemed low for the particle size used in the operation.

Although both the cyclone pressure drop and inlet velocity are low, this does not explain why the cyclone cannot collect the particle size as large as 400μ This anomaly has not been resolved. The fact that large particle sizes can pass through the cyclone system is the phenomenon that was observed throughout operations thus far. It was also repeatedly observed that the solid carryover rate would increase whenever solids were fed to the reactor through the feeder systems. This provides further evidence that the cyclone can only collect larger size particles because the feed materials always contain some particles smaller than the average size of the circulating materials.

There are two interacting factors that prevent us from pinpointing the exact reason that the cyclone cannot collect the particle size as large as 400 μ. Both are related to the solid circulating through the combustion heat exchanger. The first factor is the gas short-circuit resulting in a reverse upward flow in the dipleg of the cyclone. It is not necessary that the reverse flowing gas velocity should be greater than the particle terminal velocity to interfere with the cyclone collection efficiency, but the reverse flowing gas provides some energy to help entrain the particle to the vortex tube.

Another important interaction that should be discussed is the relationship between the solid circulation rate and the rate of the solid carryover. Obviously, at a given cyclone efficiency (note that we have pointed out that an increase in the solid/gas loading ratio will increase the efficiency) the higher the solid circulation rate, the higher the solid carryover rate. Figures 5.2-27 and 5.2-28 give the relationship between the solid carryover rate and the solid circulation rate for a 48-hour operation period. Although data are quite scattered, the overall trend is that an increase in the solid circulation rate will result in an increase in the solid carryover rate. The point is that the overall efficiency of the whole cyclone system may not be as low as it appears. Comparing figures 5.2-20 and 5.2-40 for the same operation period, one can see that although the cyclone system has an efficiency above 99 percent, the solid carryover rate may still be quite high compared with the ash generation rate from coal combustion.

In summary, the high solid carryover rate may be caused by several reasons. The higher solid circulation rate will give a high carryover rate. Since the cyclone efficiency will improve with an increase in the solid gas load ratio, the carryover rate should reduce by a

decrease in the reactor gas velocity. However, the lower limit of the gas velocity is the choking velocity.

5.2.5 Riser Pressure Drop and Solid Circulation Rate

There are two pressure drop measurements in the riser. One measures the pressure drop for the entire riser. The other measures the pressure drop in the top section of the riser. The pressure drop in the top of the riser also gives the riser density from which the solid circulation rate can be estimated.

One problem that was noticed was that the measured pressure drop across the entire riser may be low. Figure 5.2-.29 gives the measured pressure drop vs. the gas velocity in the riser for a 24-hour operation period. For the purposes of comparison, the pressure drops calculated from gas flow only and gas flow with solids that were fed (no solid circulation) are also given figure 5.2-29. The measured average pressure drop for the riser in this 24-hour operation is about 6.5 inH_2O. If the measured pressure drop is representative to the actual pressure drop across the riser, it means that the solid circulation rate is extremely low.

The true reasons for this low measured pressure drop are not known. The speculation is that the leg that measures high static pressure in the pressure difference measurement is located in the fluid acceleration zone. In the acceleration zone, the higher the fluid acceleration rate, the lower the static pressure. If the higher pressure measurement leg measures the higher static pressure, the overall measured pressure drop will be lower.

There is another pressure drop measurement in the top of the riser. This pressure drop measurement seems reasonable (although still lower for the reasons given later). Figure 5.2-30 gives a comparison between the measured pressure drop and calculated pressure drop by the correlation of Konno and Saito. The calculated pressure drop is higher than the measured one for this period of the operation. Two obvious reasons are either the calculated pressure drop is too high or the measured pressure drop too low or both. It is possible that the calculated pressure drop is higher than the actual value because the solid circulation rate (calculated based on the energy balance) may be higher than the actual circulation rate. As mentioned previously, some of the coal may be combusted outside the control volume and will result in a higher inlet temperature of fluid entering the control volume, which affects the solid circulation rate calculations. It is possible that the measured pressure drop is lower than the actual one due to the location of the low leg of the static pressure measurement. The low-pressure measurement leg is located at the top of the riser very close to the crossover. At the very top of the riser, there is an extended dead leg to minimize the erosion of the bend. When the gas phase carrying the solids is flowing upwards, both phases are subject to reverse flow at the dead end. Some of the solids may flow downwards. According to the Bernoulli equation, this is a deceleration zone wherein the static pressure is higher. The low leg of the differential pressure measurement reads a higher static pressure. This will result in a differential pressure between the high leg and low leg, which is lower than the actual value. If one examines figure 5.2-30, one can see that the data between the measured pressure drop and calculated one are systematically biased. The higher the measured pressure drop, the bigger the

difference between the measured and calculated pressure drop. This result is consistent with the above reasoning. When the solid circulation rate is increasing, the probability of solid downward flow becomes larger. The static pressure in this deceleration zone will get higher.

Figures 5.2-31 and 5.2-32 give comparisons between the solid circulation rate calculated from the energy balance and from the measured pressure drop in the top of the riser. The solid circulation rate calculated from the riser pressure drop is based on no-slip between gas and solid phase. The data presented in figure 5.2-31 show that the solid circulation rates calculated from both methods agree reasonably well when the solid circulation rate is below 120,000 lb/hr. When the solid circulation rate is above 120,000 lb/hr, the solid circulation rate calculated from the measured pressure drop is much lower than that calculated from the energy balance. One of the reasons is due to the solids downward flow from the dead zone as mentioned above. The data presented in figure 5.2-32 are somehow different from those in figure 5.2-31. In figure 5.2-32, the solid circulation rate calculated from energy balance is much higher than that calculated from the pressure drop measurement. It is noted that the solid circulation rates calculated from the riser pressure drop are the maximum values because of the assumption of no-slip between the phases.

From figures 5.2-31 and 5.2-32, one is inclined to conclude that the calculated solid circulation rate from energy balance is always higher than that from the measured pressure drop. It also means that the calculated pressure drop based on the solid circulation rate is higher than measured pressure drop because the major factor that influences the pressure drop calculation is the solid circulation rate. In other words, the estimated solid circulation rate from energy balance is too high. In fact, further evidence shows that it is not the case. Figure 5.2-33 gives the solid circulation rate calculated from the riser pressure drop measurement and from the energy balance for the test period of August 20 to 21. One can see that the former is much higher than the latter. The same is true for figure 5.2-34, which represents data from the operation period of August 19 to 20. Figures 5.2-31 through 5.2-34 seem to indicate that the calculated solid circulation rate based on energy balance may be more reasonable than that based on the riser pressure difference. The data in figures 5.2-33 and 5.2-34 also indicate that a slip between the gas and solid phases exist. Figures 5.2-33 and 5.2-34 also seem to confirm the speculation that the solid downward flow at the top of the riser causes the measured pressure drop to be lower than the actual value during the test run in November. One major difference between August and November operations is the particle size. For the August operation, the particle size is about one-third to one-quarter the size used in the November operation. The smaller particle is easier to be entrained by the gas phase, and as a result, has less opportunity to flow downward near the top of the riser. Therefore, the lower leg of the pressure drop measurement may give results, which closely reflects the actual pressure.

Exhibit

Figures for

Section 5.2

Operability Analysis of Commissioning Tests

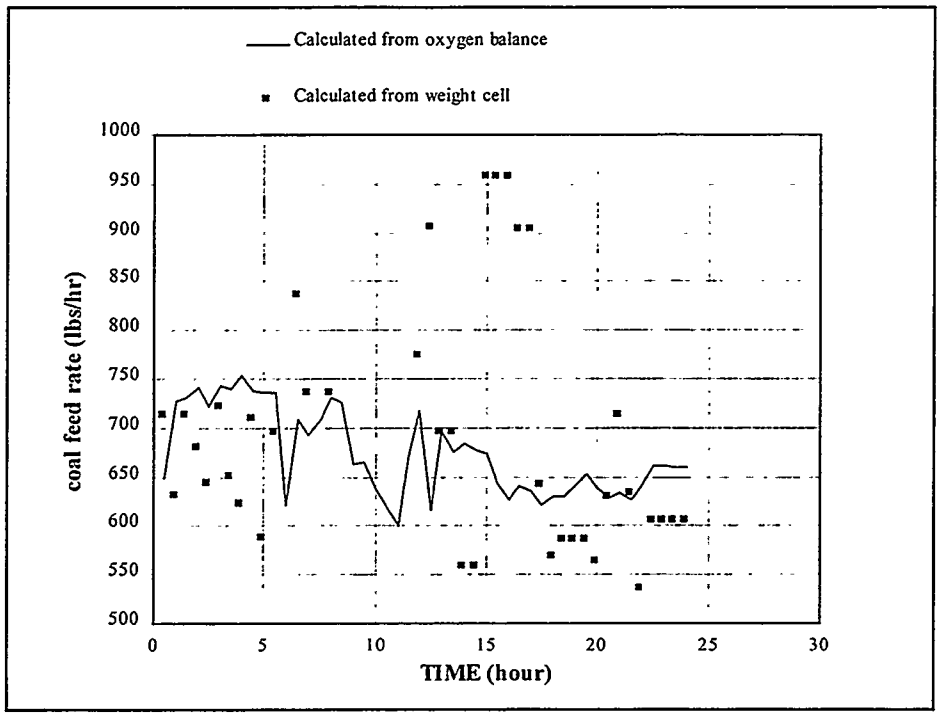

Figure 5.2-1 Comparison of Coal Feed Rates Calculated From Oxygen Balance and From Weight Cell Measurements for Test Period November 19 to 20, 1996

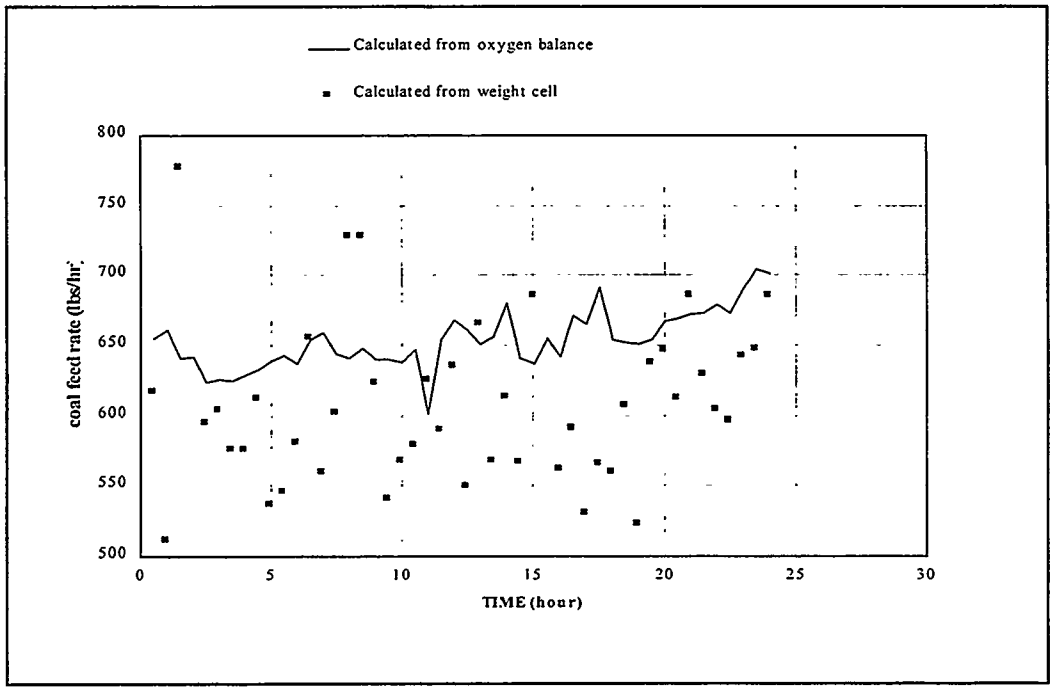

Figure 5.2-2 Comparison of Coal Feed Rates Calculated From Oxygen Balance and From Weight Cell Measurements for Test Period November 19 to 20, 1996

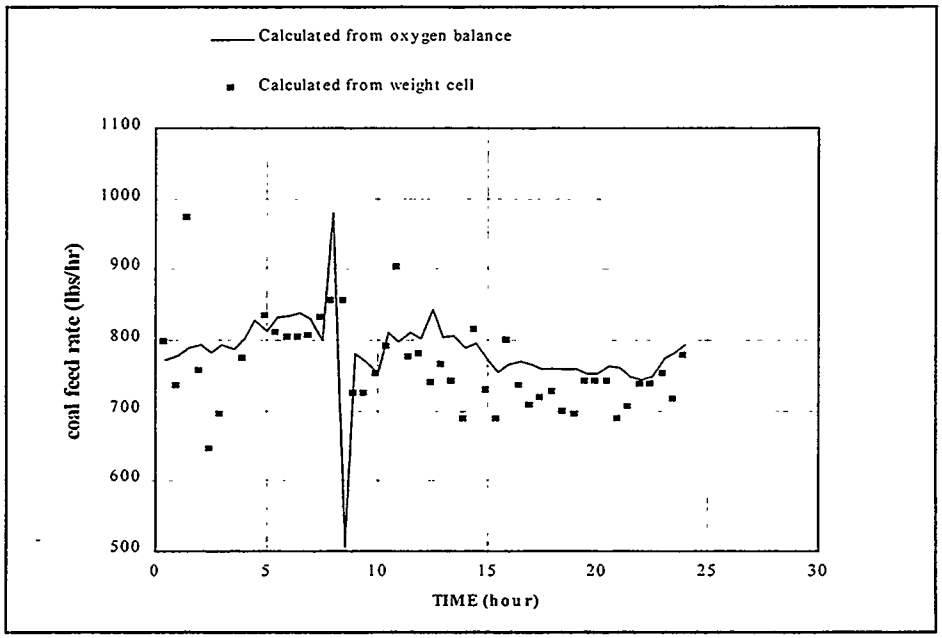

Figure 5.2-3 Comparison of Coal Feed Rates Calculated From Oxygen Balance and From Weight Cell Measurements for Test Period August 19 to 20, 1996

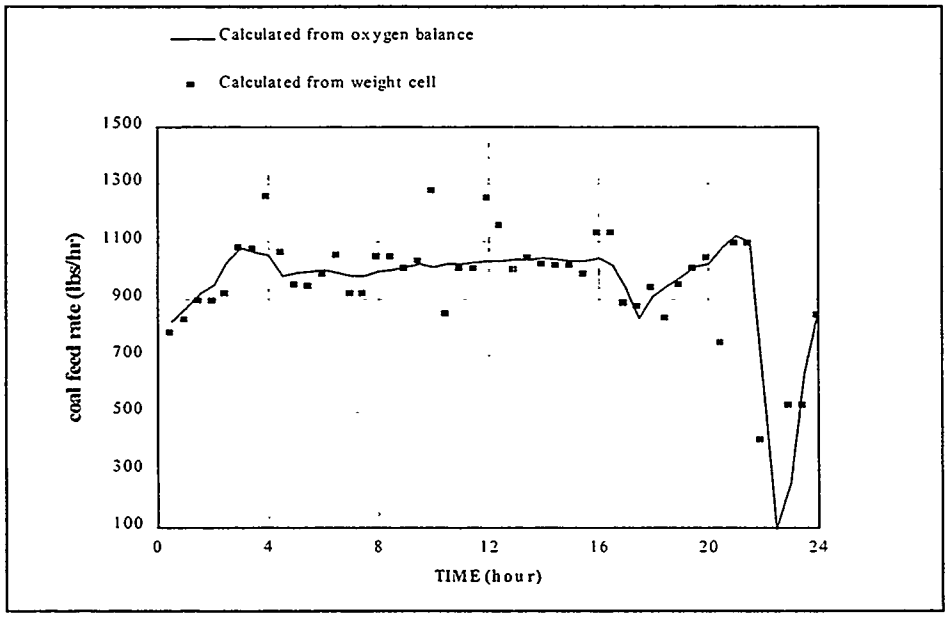

Figure 5.2-4 Comparison of Coal Feed Rates Calculated From Oxygen Balance and From Weight Cell Measurements for Test Period August 20 to 21, 1996

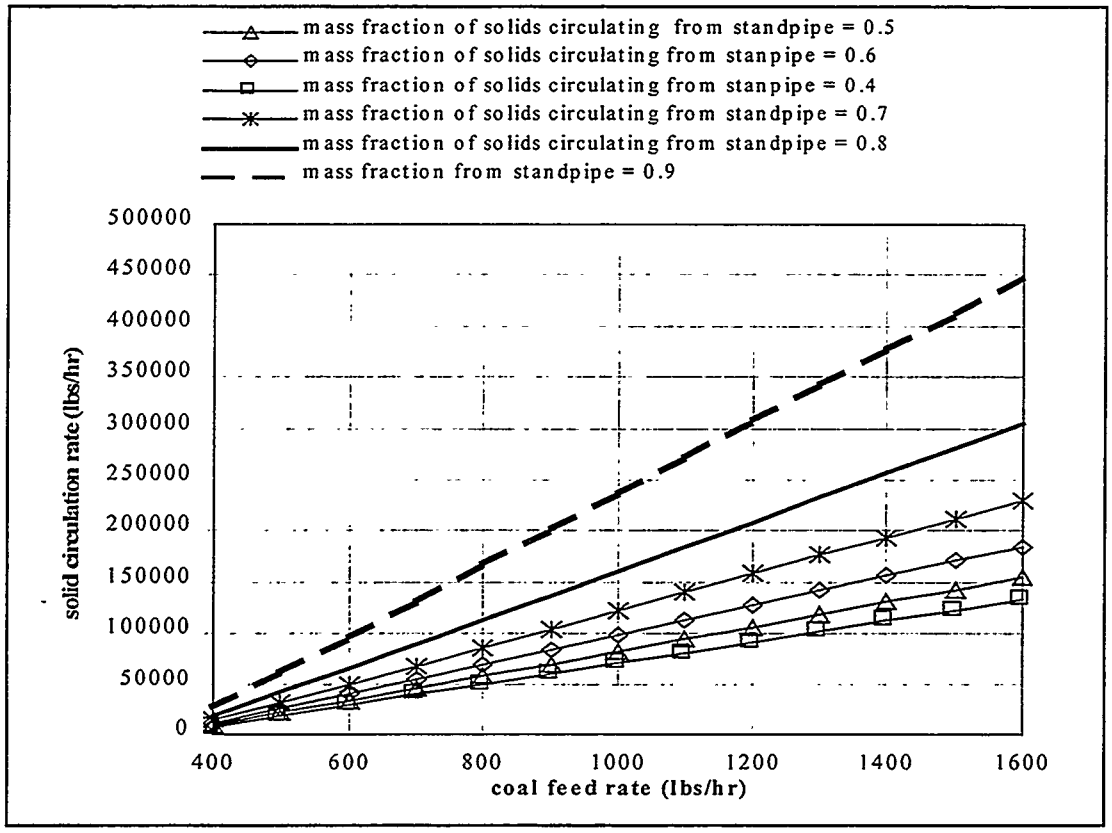

Figure 5.2-5 Variation of Required Solid Circulation Rate With Coal Feed Rate at Different Mass Fraction of Solid Circulating Through Reactor Standpipe (Assumes That the Solids Exit Combustion Heat Exchanger at 600°F)

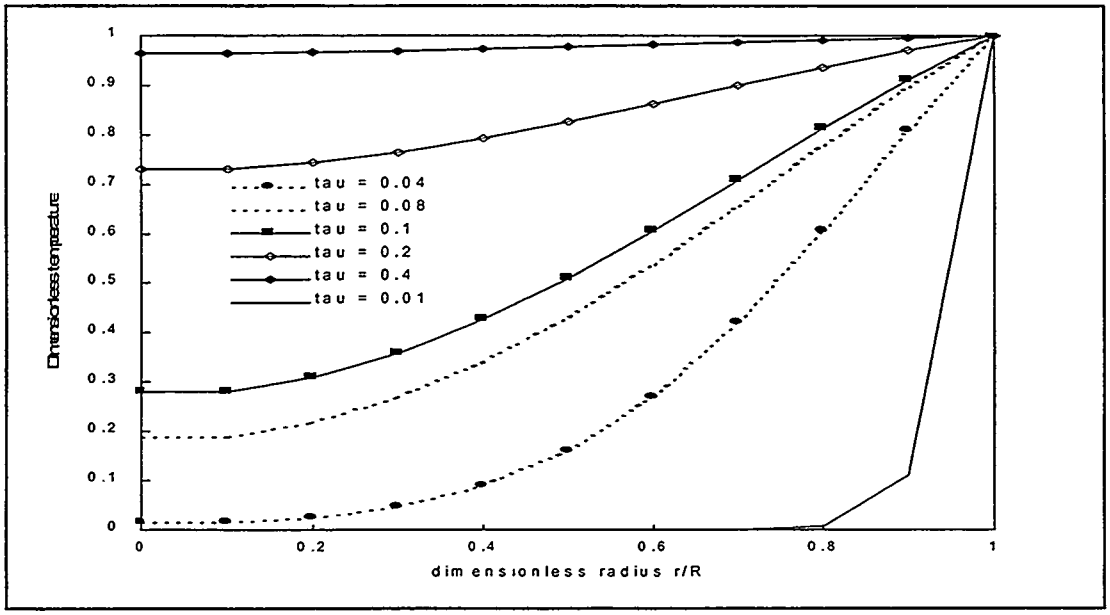

Figure 5.2-6 Heat-up Rate of a Single Particle vs Dimensionless Radius

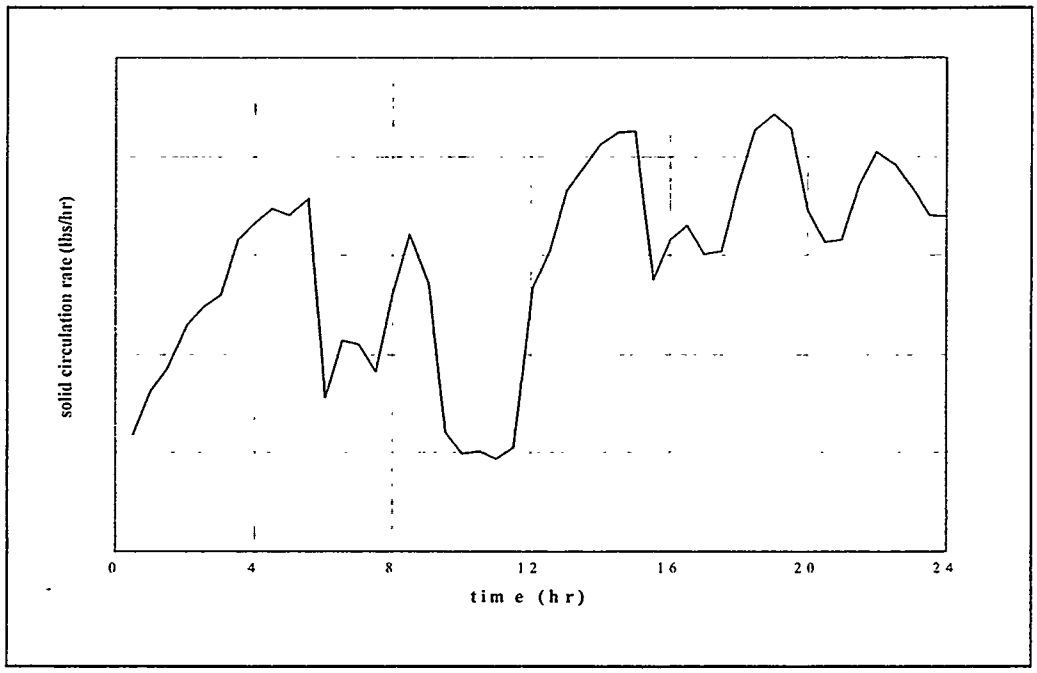

Figure 5.2-7 Variation of Required Solid Circulation Rate With Time for Test Period November 19 to 20, 1996 (Same Test Period as shown in Figure 5.2-1. Average coal Feed Rate for This Test Period was About 670 lb/hr)

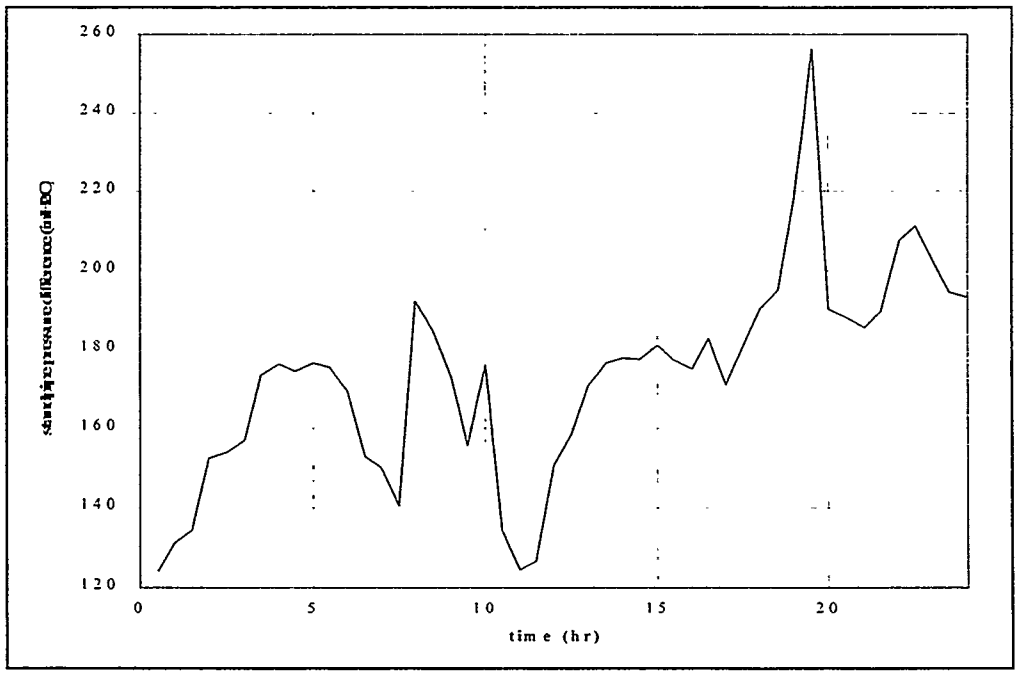

Figure 5.2-8 Variation of Measured Standpipe Pressure Difference (Which is an Indication of the Standpipe Level) With Time. Same Time Period as Shown in Figure 5.2-7)

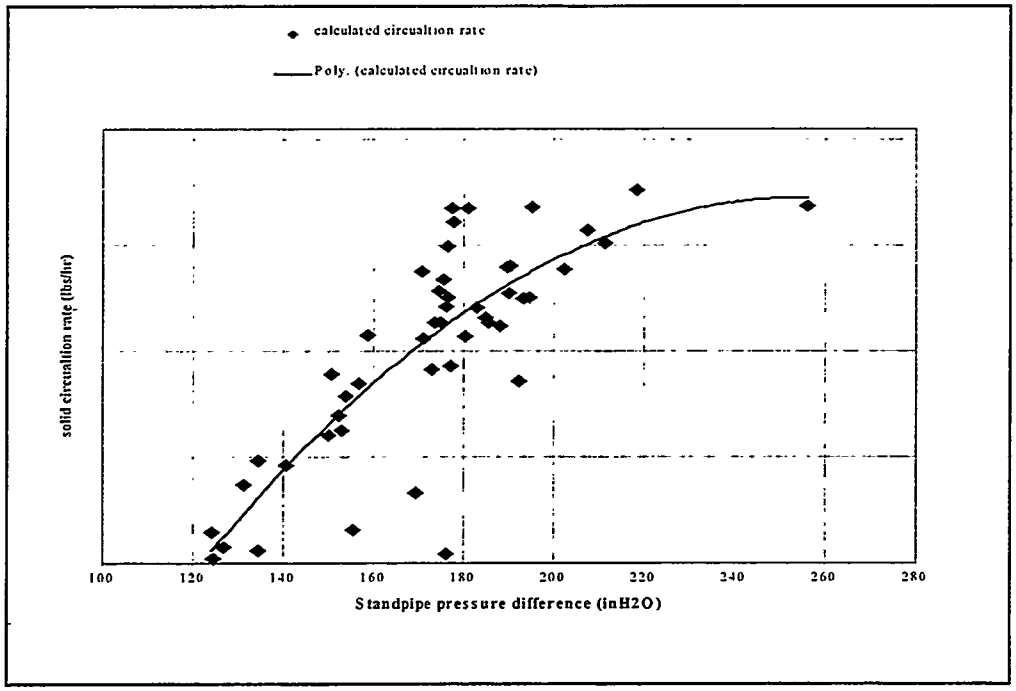

Figure 5.2-9 Variation of Solid Circulation Rate With Standpipe Pressure Difference (Solid Line is a Second-Degree Polynomial Fit of the Data)

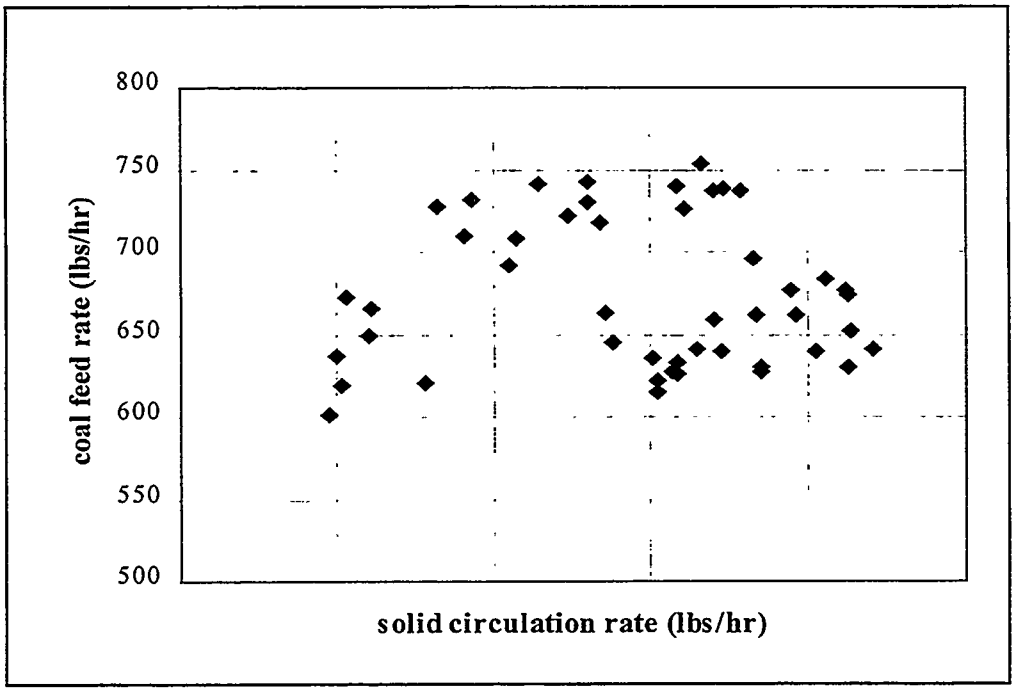

Figure 5.2-10 The Relationship Between the Coal Feed Rate and Solid Circulation Rate for Test Period November 19 to 20, 1996.

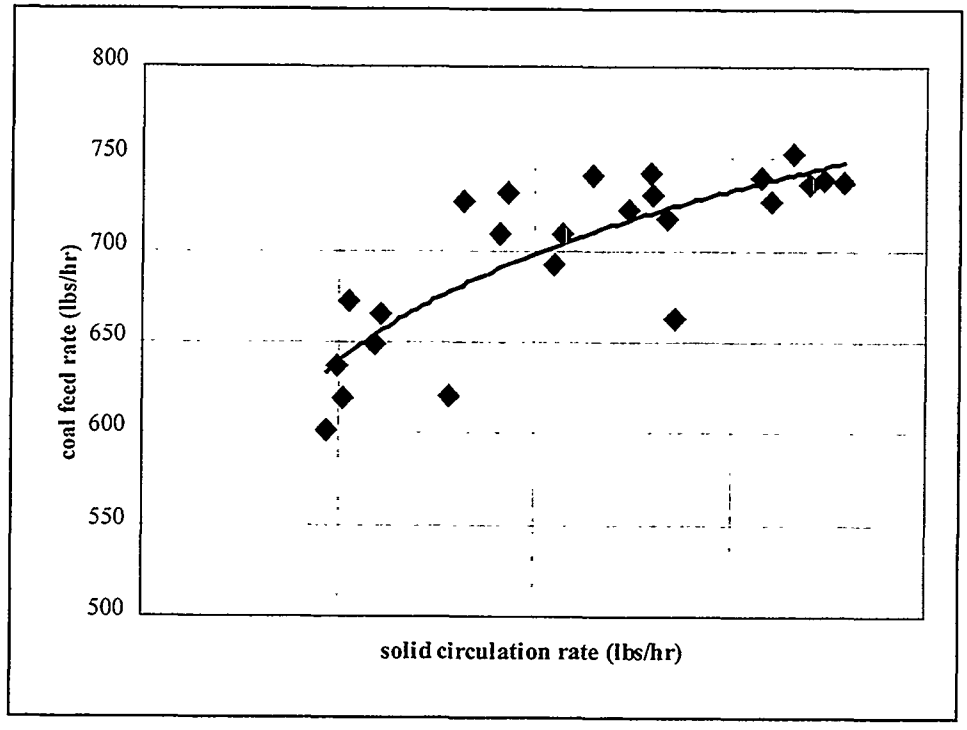

Figure 5.2-11 The Variation of Coal Feed Rate With Solid Circulation Rate for First 12 Hours of Operation on November 19 to 20, 1996

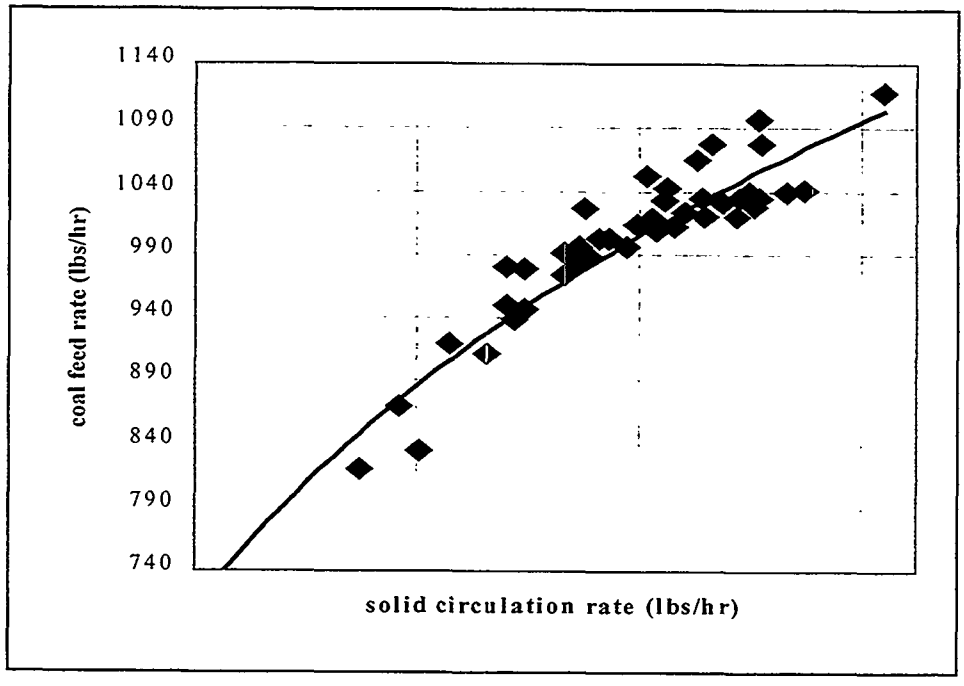

Figure 5.2-12 The Variation of Coal Feed Rate With Solid Circulation Rate for Test Period of August 20 to 21, 1996

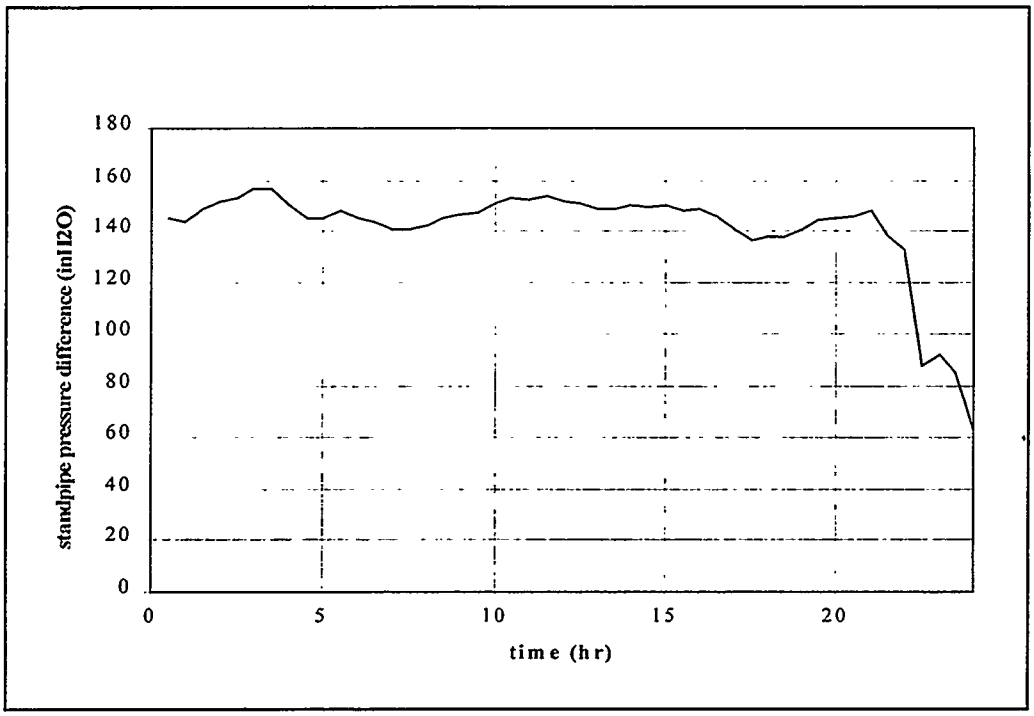

Figure 5.2-13 Variation of Solids Level in the Standpipe With Time for Test Period of August 20 to 21, 1996.

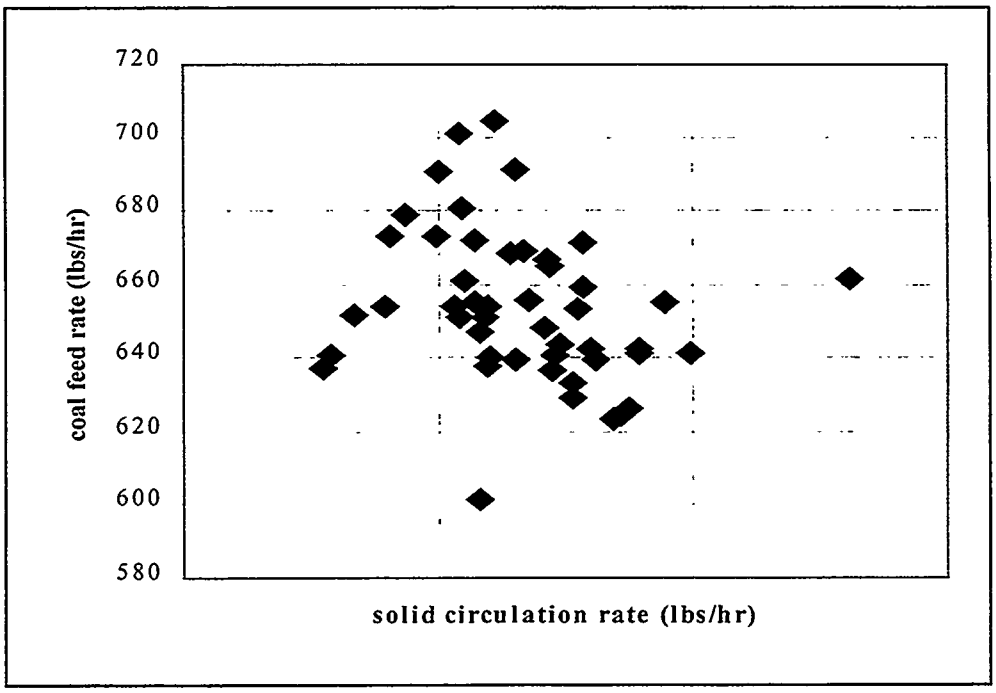

Figure 5.2-14 Variation of Coal Feed Rate With Solid Circulation Rate for Test Period of November 20 to 21, 1996.

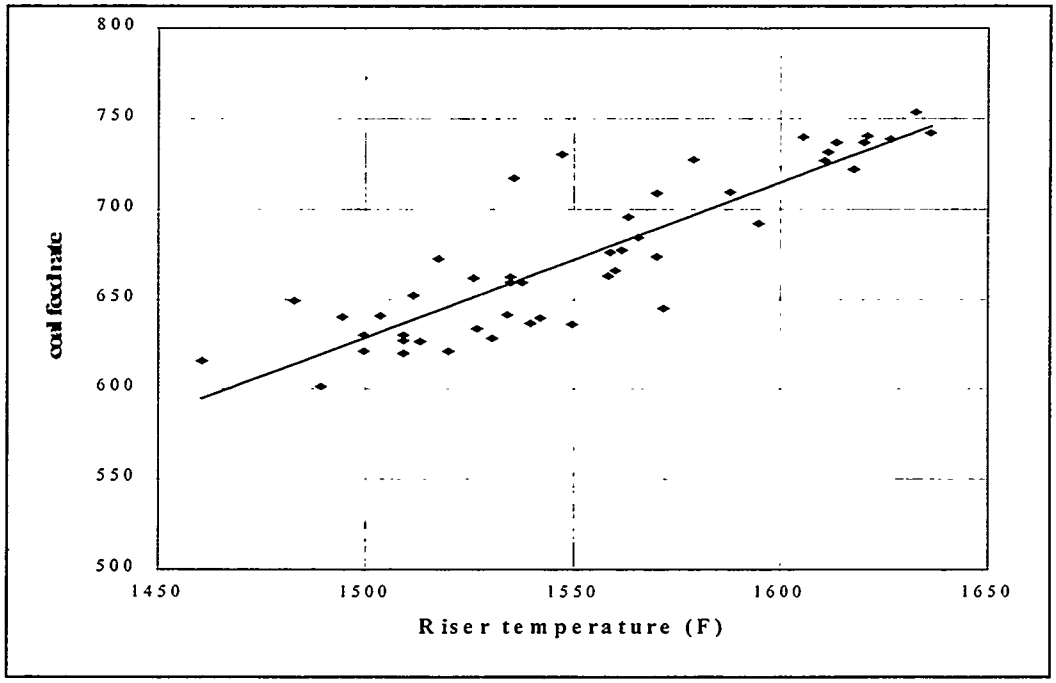

Figure 5.2-15 Coal Feed Rate vs Riser Temperature for Test Period of November 19 to 20, 1996

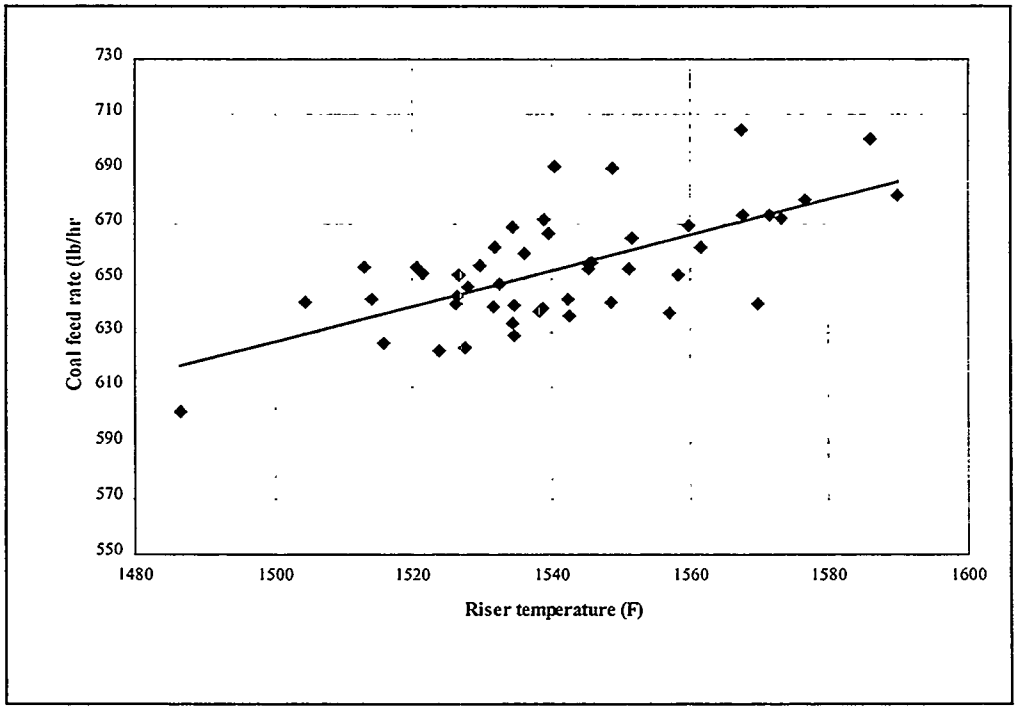

Figure 5.2-16 Coal Feed Rate vs Riser Temperature for Test Period November 20 to 21, 1996

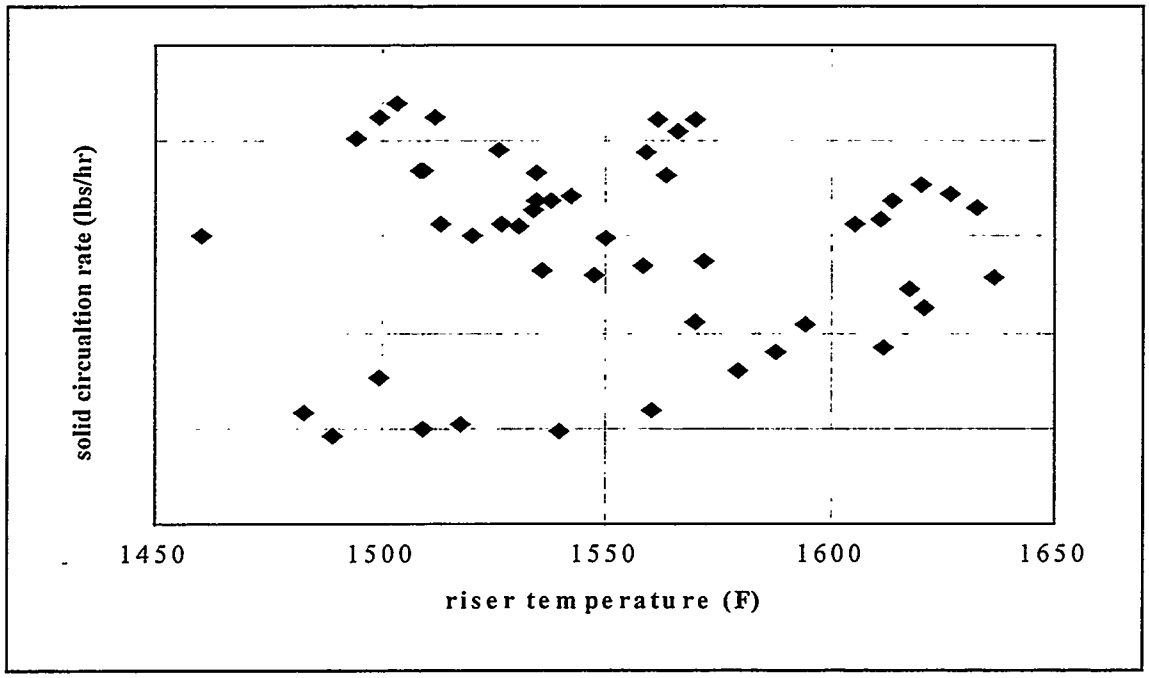

Figure 5.2-17 Solid Circulation Rate vs Riser Temperature for Operation Period of November 19 to 20,1996.

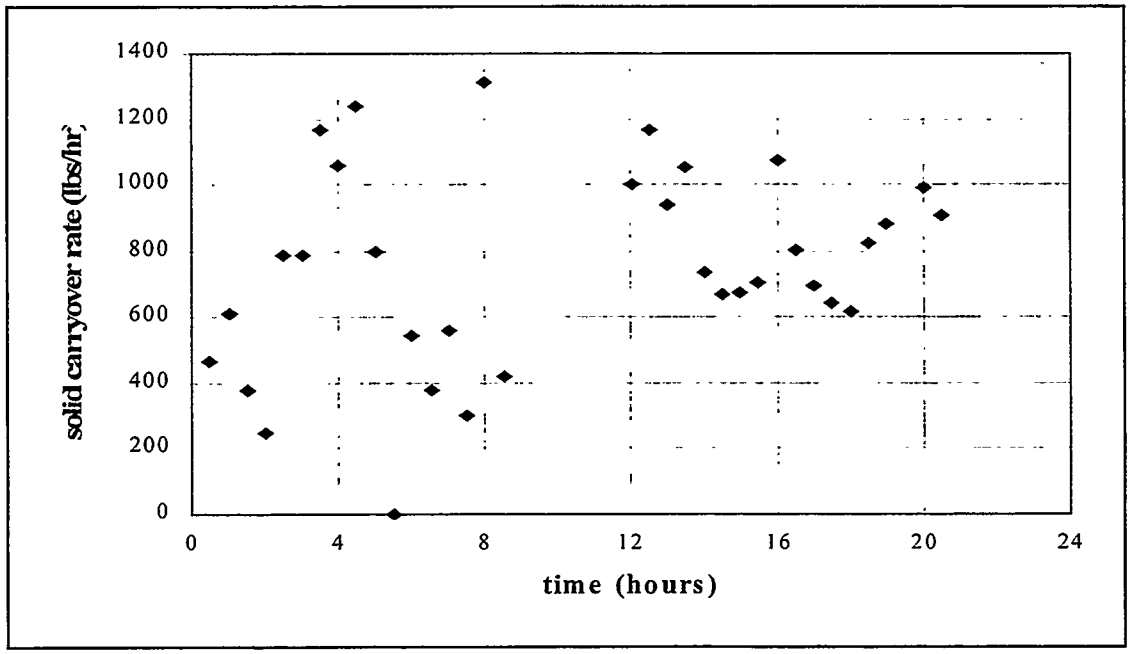

Figure 5.2-18 Estimated Solid Carryover Rate With Time for Operation Period of November 19 to 20, 1996

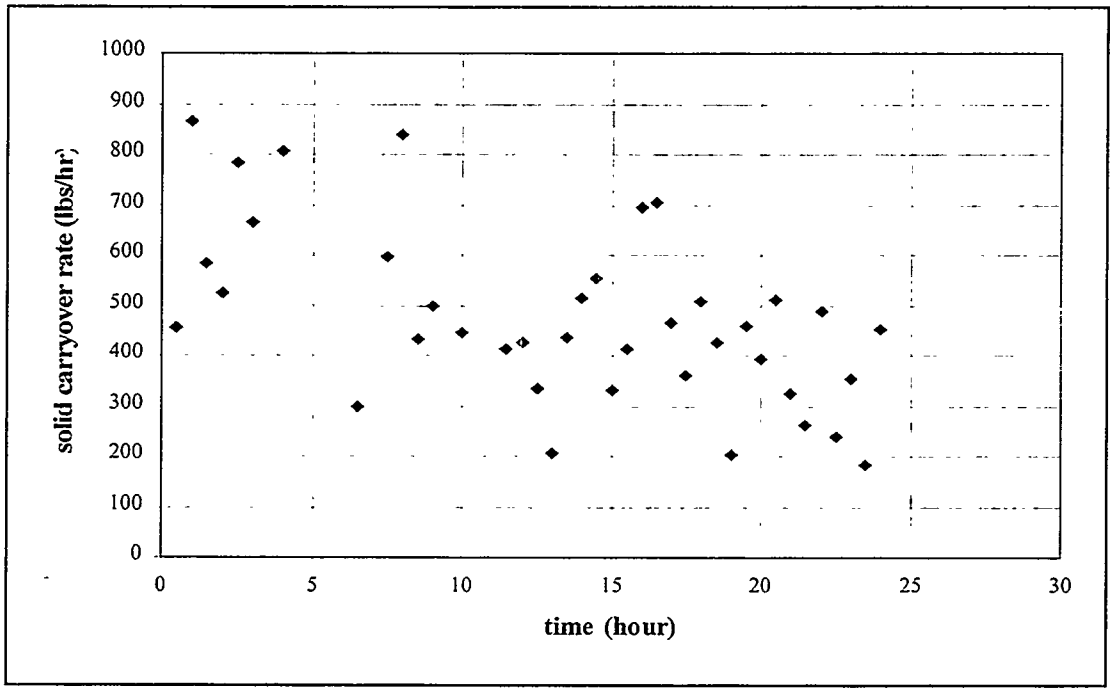

Figure 5.2-19 Estimated Solid Circulation Rate With Time for Test Period November 20 to 21, 1996

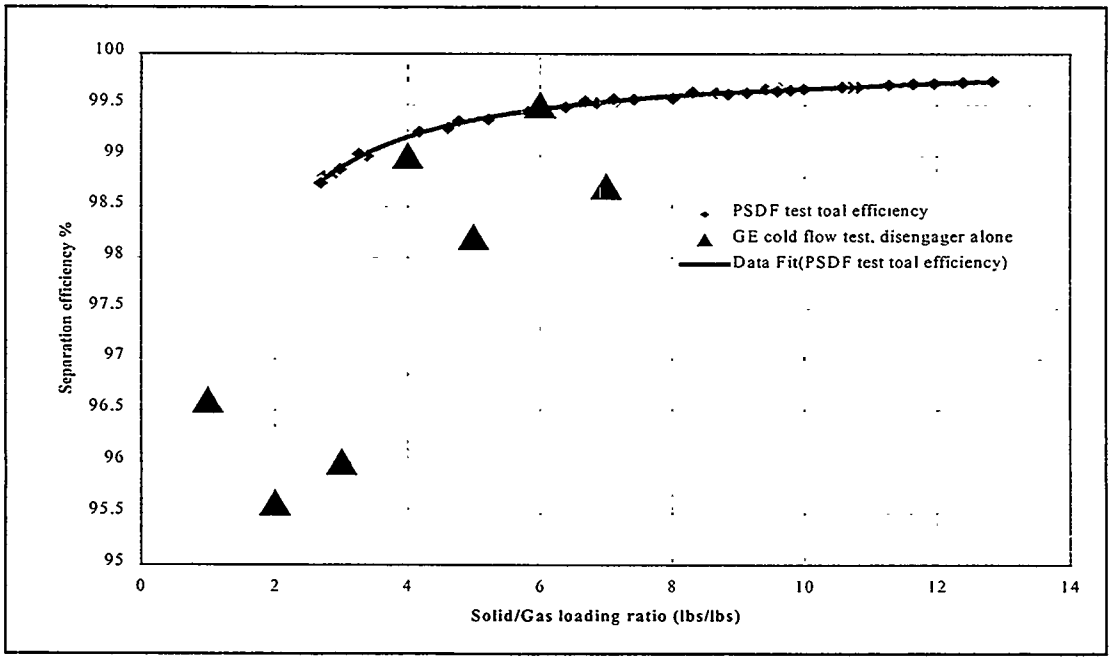

Figure 5.2-20 Estimated Cyclone System Collection Efficiency vs Solid/Gas Loading Ratio for Test Period November 19 and 20, 1996 (Cold Flow Test Data From GEESI is Also Provided in This Figure)

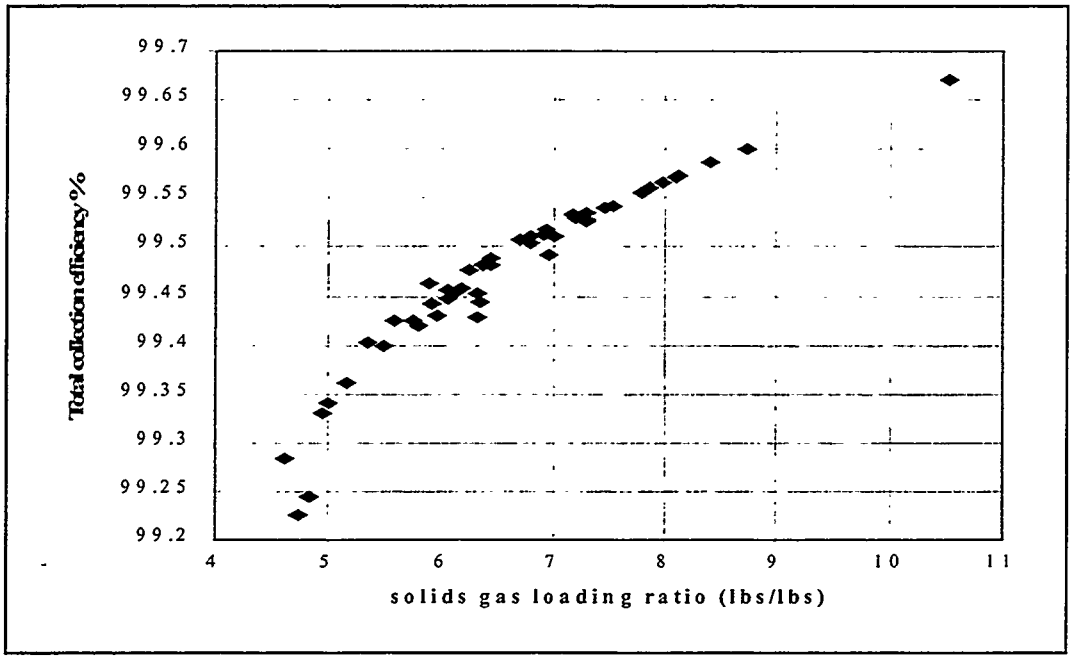

Figure 5.2-21 Estimated Cyclone System Collection Efficiency vs Solid/Gas Loading Ratio for Test Period November 20 and 21, 1996

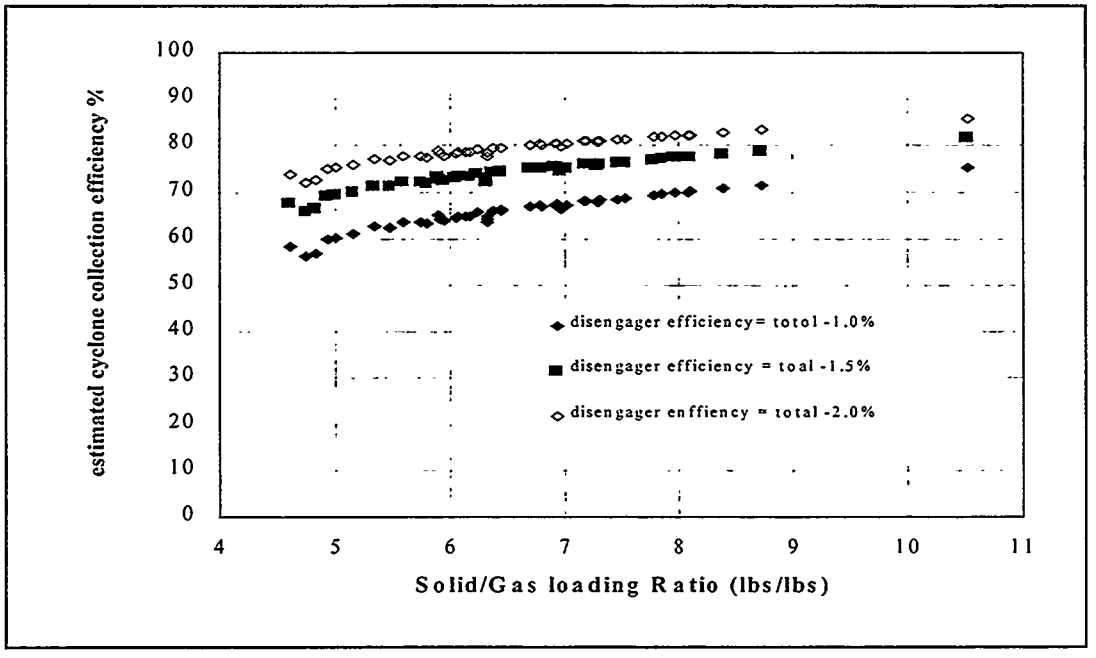

Figure 5.2-22 Estimated Cyclone Efficiency vs Solid/Gas Loading Ratio for Given Disengager Efficiency

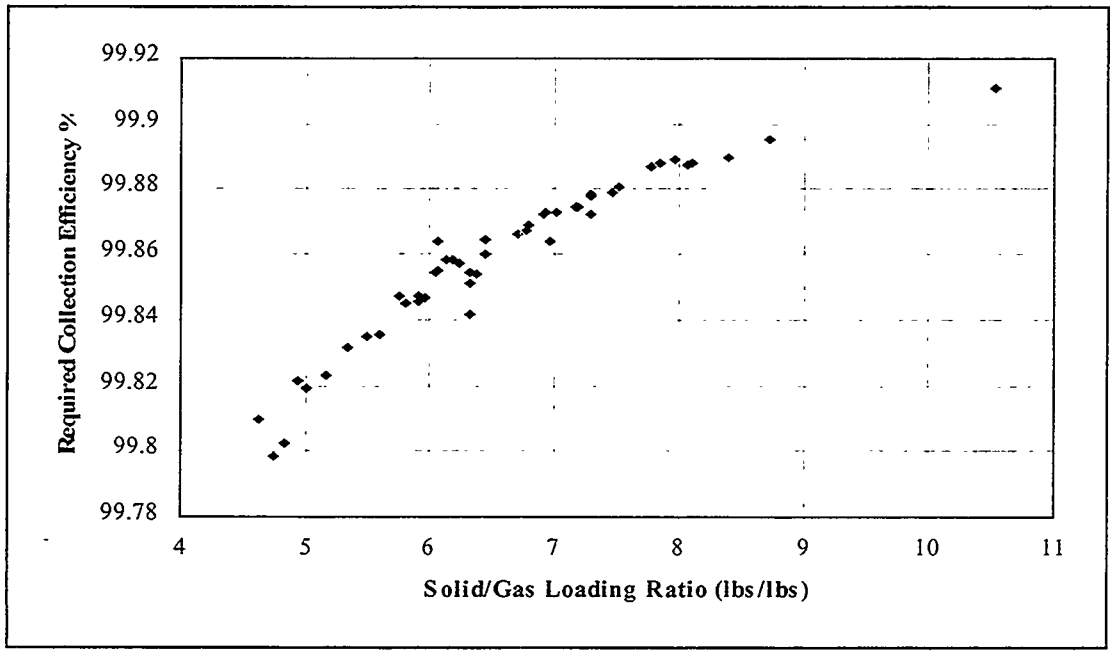

Figure 5.2-23 Required Total Collection Efficiency of Cyclone System vs Solid/Gas Loading Ratio to Balance Ash Production Rate and Solid Carryover Rate

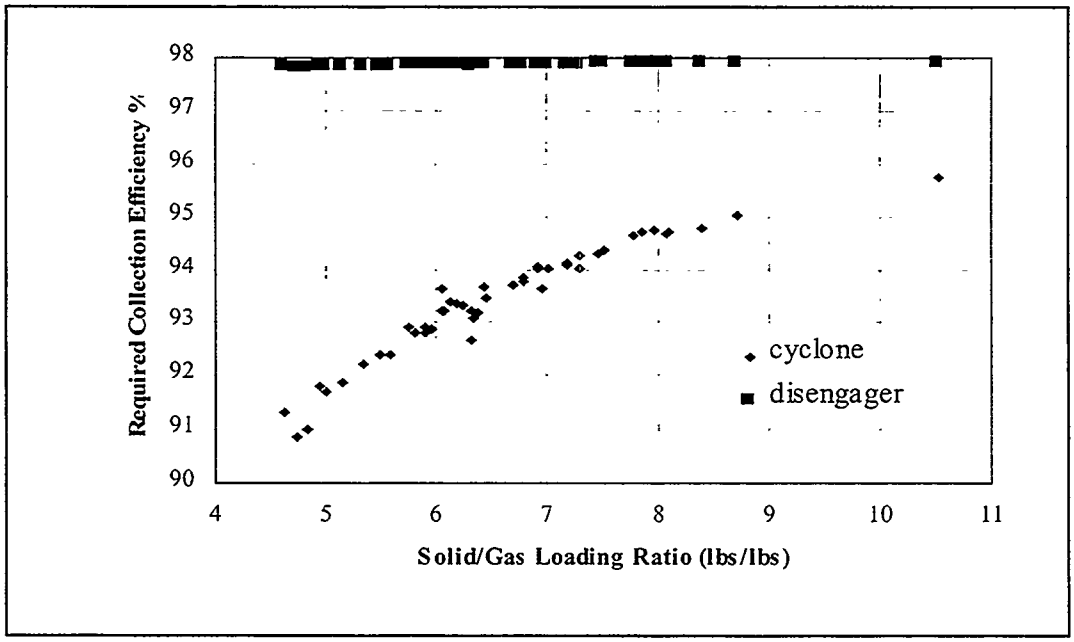

Figure 5.2-24 Estimated Collection Efficiencies for Individual Cyclone to Balance Ash Production Rate and Solid Carryover Rate

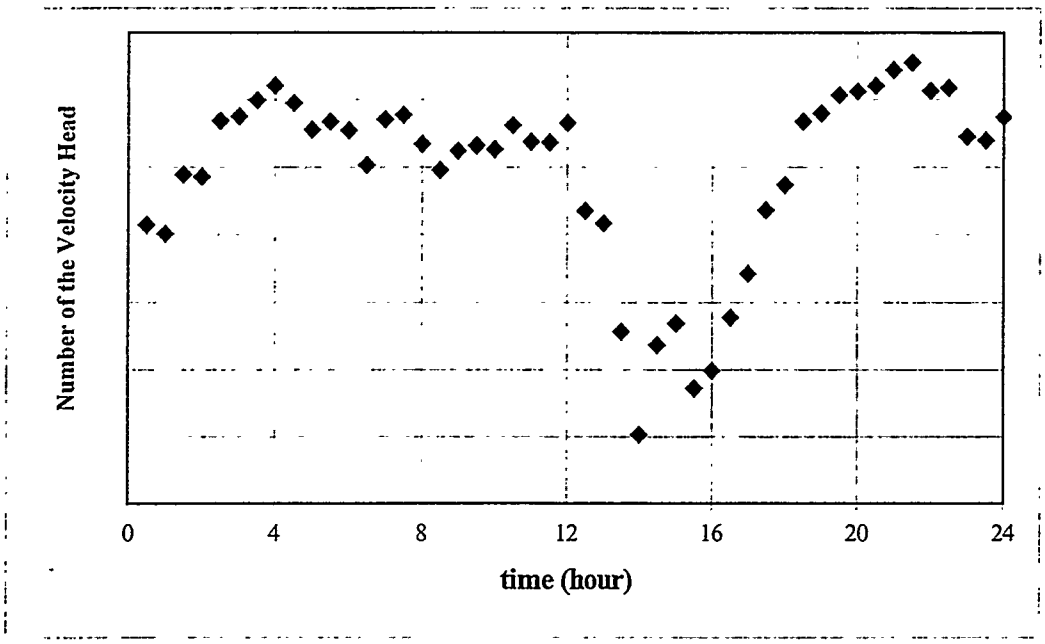

Figure 5.2-25 Pressure Drop Across Primary Cyclone for Test Period November 20 to 21, 1996.

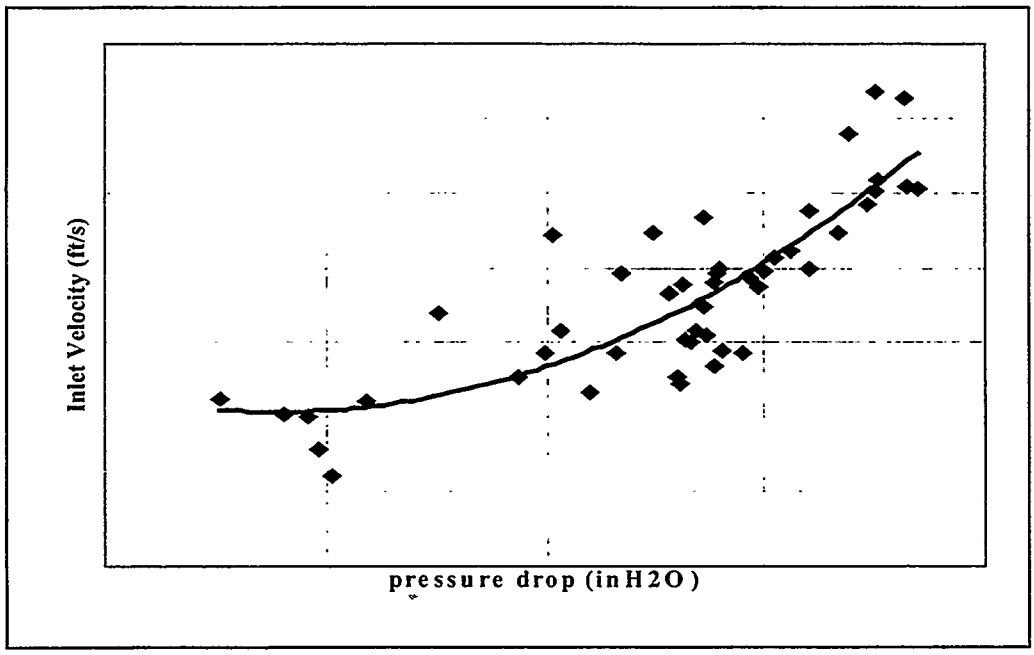

Figure 5.2-26 The Relationship Between Cyclone Inlet Gas Velocity and Cyclone Pressure Drop for Test Period November 20 to 21, 1996

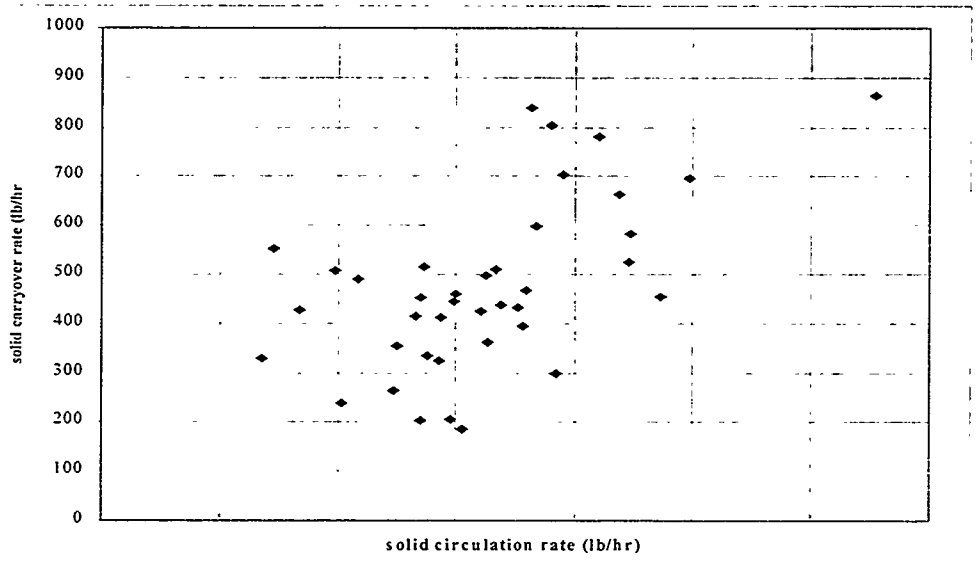

Figure 5.2-27 Estimated Solid Carryover Rate vs Solid Circulation Rate for Test Period November 20 to 21, 1996

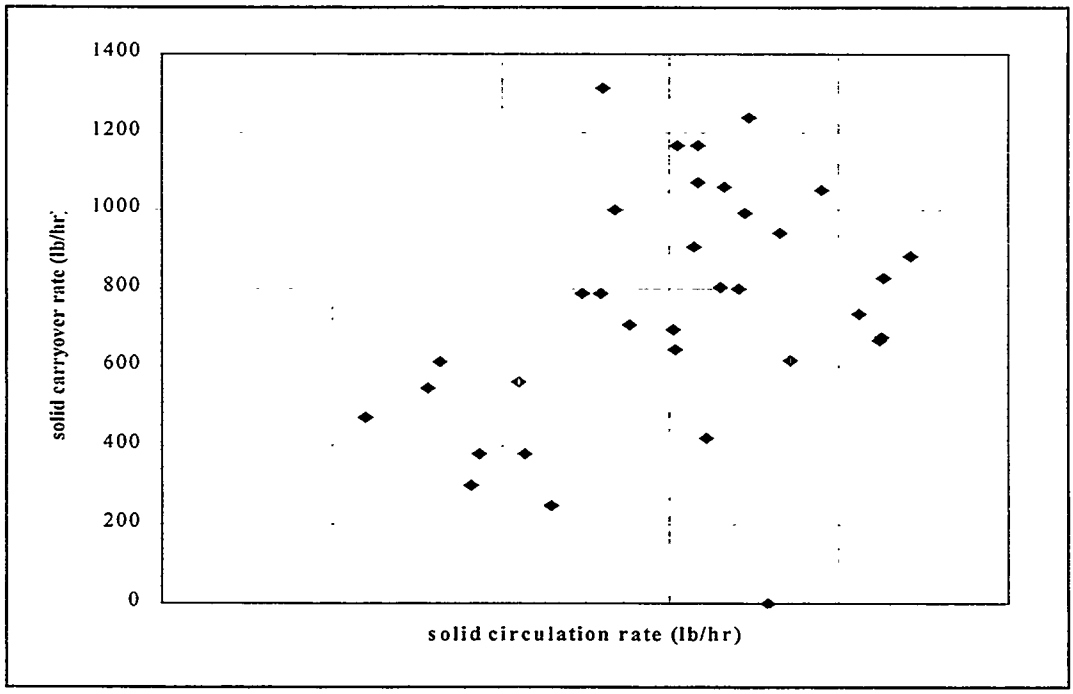

Figure 5.2-28 Estimated Solid Carryover Rate vs Solid Circulation Rate for Test Period November 19 to 20, 1996

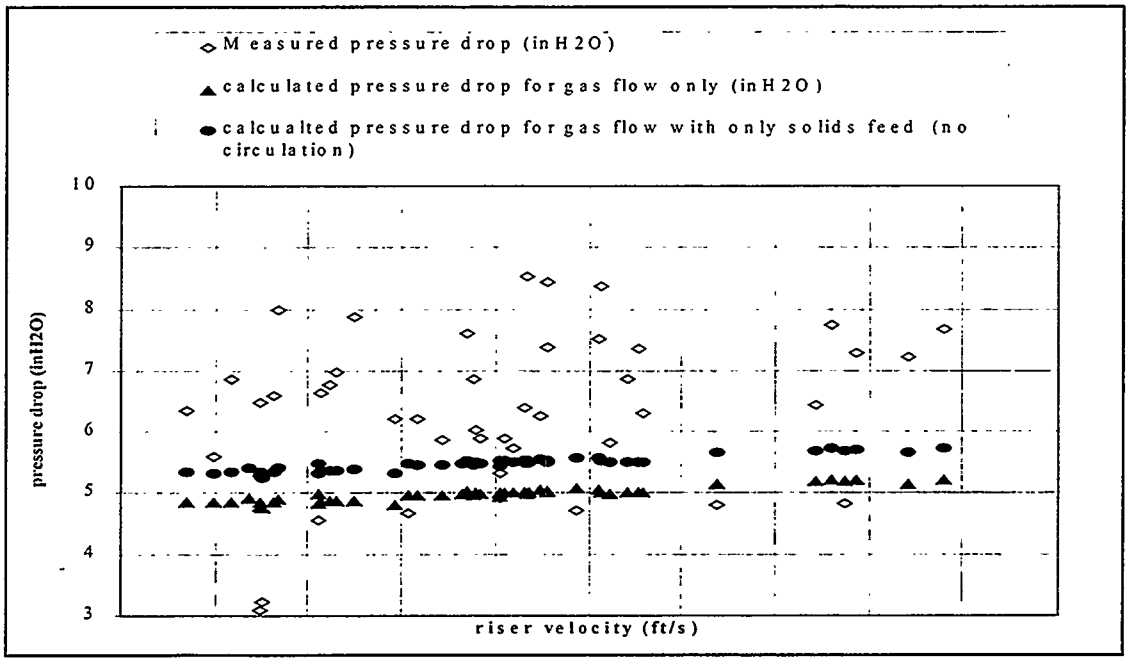

Figure 5.2-29 Comparison Between the Measured Pressure Drop Across Riser and Calculated Pressure Drop Based on Gas Phase Flow, Only, and Gas Phase With Only Solid Feed, to Show That the Measured Riser Pressure Drop is Low

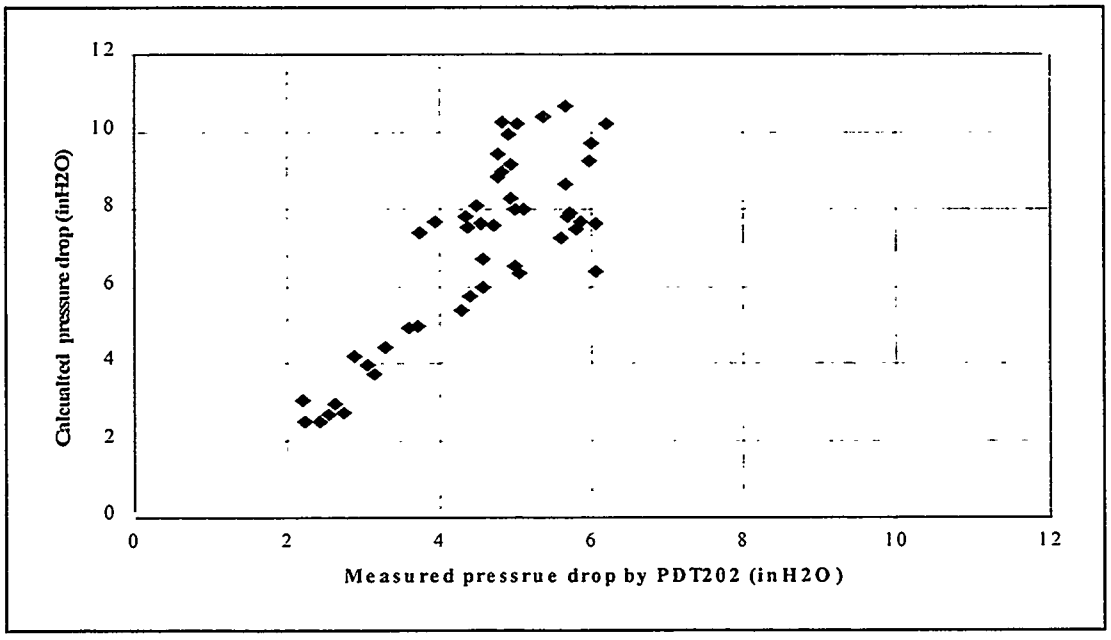

Figure 5.2-30 Comparison of the Measured Pressure Drop at Top of the Riser With Calculated Pressure Drop for Test Period November 19 to 20, 1996

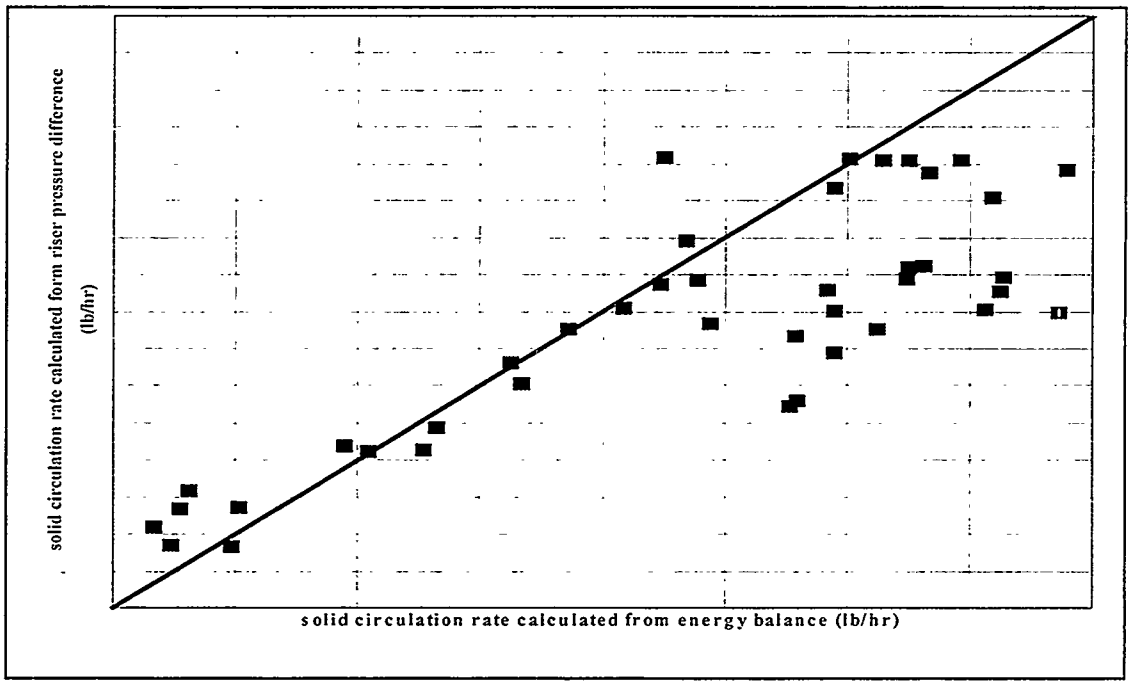

Figure 5.2-31 Comparison of Solid Circulation Rates Calculated From Energy Balance and Pressure Difference for Test Period November 19 to 20, 1996

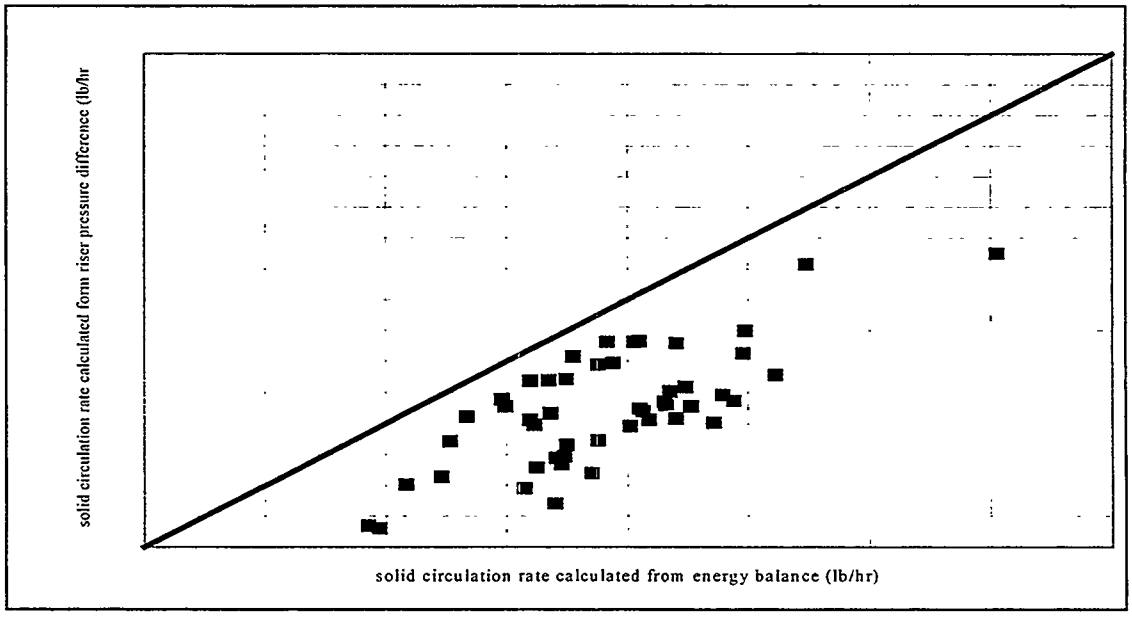

Figure 5.2-32 Comparison of Solid Circulation Rates Calculated From Energy Balance and Pressure Difference for Test Period November 20 to 21, 1996

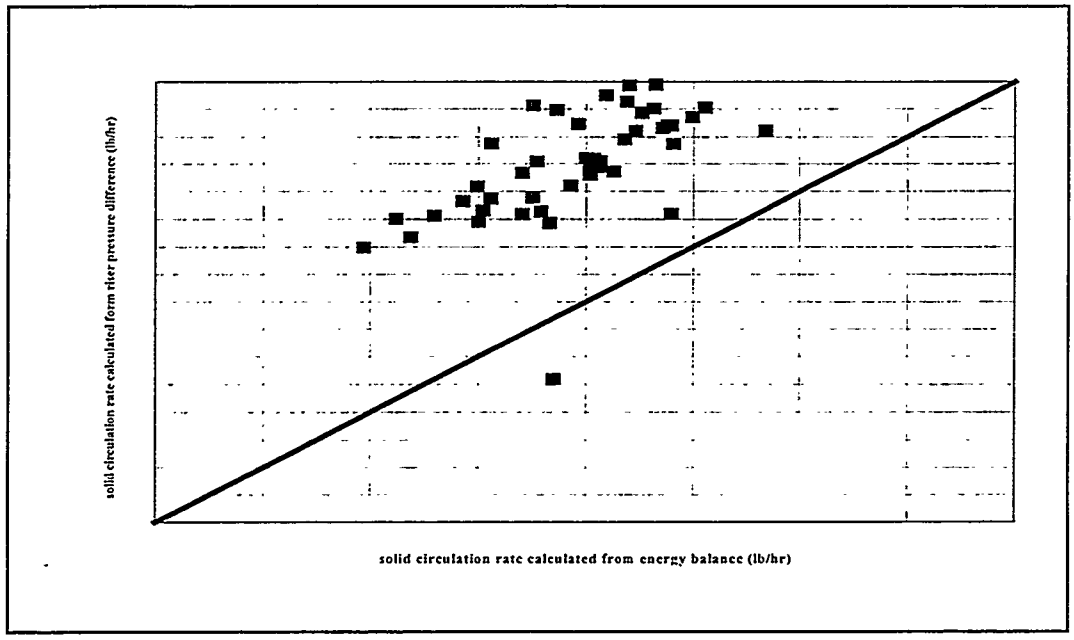

Figure 5.2-33 Comparison of Solid Circulation Rates Calculated From Energy Balance and Pressure Difference for Test Period August 20 to 21, 1996

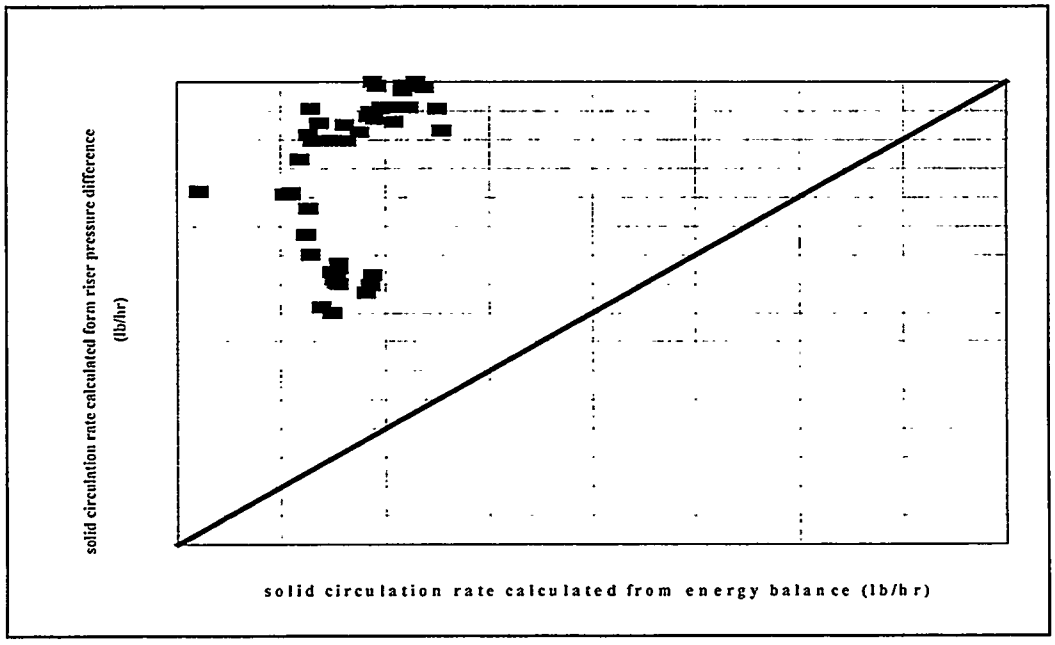

Figure 5.2-34 Comparison of Solid Circulation Rates Calculated From Energy Balance and Pressure Difference for Test Period August 19 to 20, 1996

PSDF\1996\5.2fg.

6.0 COMMISSIONING OF WESTINGHOUSE PARTICLE FILTER SYSTEM

6.1 WESTINGHOUSE FILTER SYSTEM

6.1.1 1996 PCD Overview

Since this was the start-up and commissioning of the MWK transport reactor and the Westinghouse PCD it was a very challenging year. As with most plant start-ups there were some successes as well as some fairly dramatic setbacks. However, for all involved, 1996 was a year of learning and gaining experience with the equipment at the PSDF.

Overall, the PCD operated for a total of 994 hours in 1996 (figure 6.1.1-1). For approximately 226 of those hours the PCD was filtering coal derived flue gas. The operating temperature of the PCD during 1996 was relatively cool for a combustion system. The primary reason for the low PCD temperature was the start-up of the filter in a "safe" operating regime while commissioning the transport reactor. Typically, while burning coal the PCD temperature ranged between 550 and 650°F. The maximum temperature for the PCD this year was 853°F, which occurred during a transient in the first coal fire on August 18.

By far, the biggest challenge for the PCD operating staff has been learning how to reliably estimate the level of ash in the PCD cone. During the August coal firing the PCD accumulated ash to a degree where the entire lower level of filter elements was buried in ash and the upper level was partially buried. This resulted in the breakage of 77 of the 91 filter elements. Even though these elements were "used" filters from Tidd and installed for shakedown purposes it was a painful learning experience for the PSDF staff. From this experience an operating methodology has been developed which allowed for the successful monitoring of ash level during the remaining four runs of 1996.

The performance of the PCD was substantially different during the last fours runs than for the initial test runs. This was primarily due to the use of silica sand as the start-up bed material in the transport reactor instead of alumina. Particulate samples taken from the PCD hopper when using alumina typically had a mass median diameter of 10 micrometers. Once the start-up material was changed to silica sand the mass median diameter of samples taken from the hopper rose to around 200 micrometers. In addition to the large particle size the particulate loading from the transport reactor was well above design and was measured as high as 70,000 ppm. In spite of this there have been very few operational problems with the PCD. The baseline pressure drop has remained low and relatively constant throughout the four runs.

Southern Research Institute commissioned their batch sampling system on the PCD gas inlet line during the November coal run (CCT2C). Four samples were taken that produced particulate loading data consistent with estimates derived from ash removal

system data. However, the particle size distributions from the sampling system were substantially different than samples taken from the PCD hopper. This probably is due to the geometry of the PCD, and it is theorized that there is a mechanical separation within the filter vessel which biases samples taken from the hopper. Additional information gathered in 1997 should provide insight into this phenomenon.

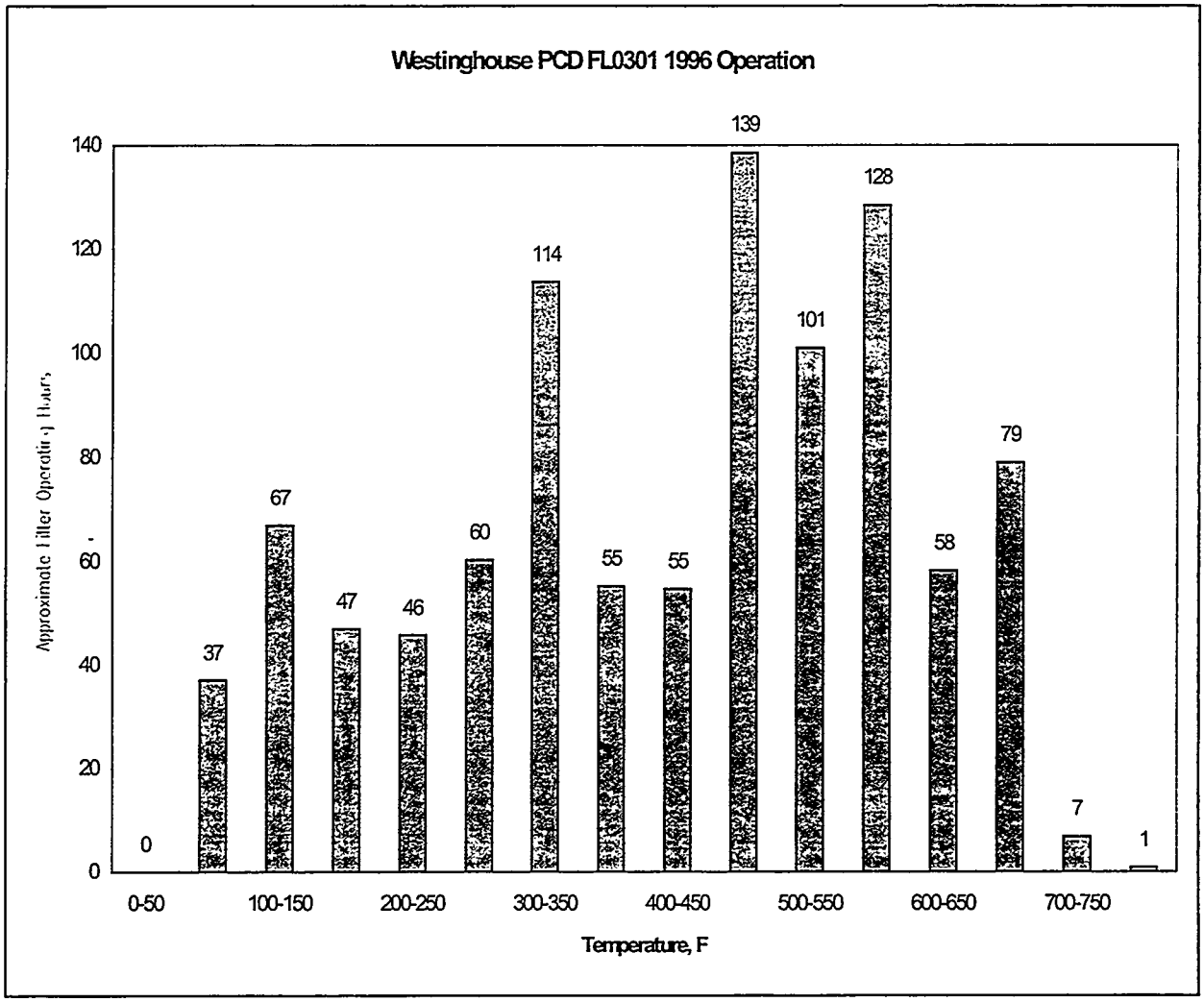

Figure 6.1.1-1 Operation Record for the PCD Over 994 Hours in 1996

S:\PSDF\6_1_1.doc

6.1.2 Westinghouse PCD FL0301 System Description

6.1.2.1 General Description

The Westinghouse PCD (FL0301) is a high-temperature, high-pressure (HTHP) gas filtration system designed to remove fine particulate at gas temperatures up to 1,800°F. The filter system can operate in either a reducing or an oxidizing environment at pressures up to 300 psig.

A process flow diagram for the filter is shown in figure 6.1.2-1. The dirty gas enters the PCD below the tubesheet via stream 1. The dirty gas flows through the elements, and the ash collects on the outside of the elements. The clean gas passes from the filter elements through the plenum pipe to the outlet pipe (stream 3).

As the ash collects on the outside surface of the filter elements, there is typically a gradual increase in the pressure drop across the filter system. The filter cake is periodically dislodged by injecting a high-pressure gas pulse (stream 2) to the clean side of the filters. The cake then falls to the discharge hopper (stream 4).

The PCD system consists of two major components:

1. Filter vessel.

   The filter vessel is a code-stamped pressure vessel which contains the filter elements as well as the support mechanism for the filter elements.

   The filter vessel is designed to operate at pressures up to 300 psig at a gas temperature of up to 1,800°F. The particulate loading design basis is from 4,000 to 20,000 ppm.

2. Back pulse system.

   The pulse system consists of the pulse tanks, pulse valves, and associated piping to deliver the high-pressure pulse required to remove the ash from the surface of the filter elements.

   The back pulse system can operate at a pressure between 400 and 1,500 psig. The pulse valves are quick acting valves capable of opening and closing in as little as 0.2 seconds.

6.1.2.2 Filter Vessel

Figure 6.1.2-2 shows the general arrangement of the PCD pressure vessel and internals. Dirty gas from the transport reactor is fed to the PCD vessel through a 30-inch diameter internally insulated pipe. Gas enters the vessel through a tangential inlet nozzle, then flows in an annulus between the vessel wall and the shroud. The gas flows both upward and downward in the annular region outside the shroud and finally flows over the top and bottom of the shroud into the central filtration zone of the vessel. Dirty gas flows through the filter elements, depositing the particulate on the filter surface.

The filter elements are attached to one of two plenums (or levels) that support filter elements, collect the clean gas, and distribute the pulse flow. There are 55 candle-type filter elements attached to the lower plenum and 36 filter elements attached to the upper plenum. Each filter element has a series of gaskets to provide a dust-tight seal and there is a Westinghouse "fail-safe" device located above each filter element. The fail-safe is designed to plug with ash in the event of a filter element failure.

The clean gas flows from the plenum to the top of the filter vessel through the support tube. This tube is also used to convey the pulse gas from the pulse pipes to the filter elements. The pulse gas is used to remove the particulate (or filter cake) from the filter surface.

From the support tube the cleaned process gas flows into the top of the PCD where it leaves the vessel through the 26-inch diameter refractory-lined outlet pipe. The support tube is attached to the vessel tubesheet. The tubesheet provides a physical barrier separating the "dirty" and "clean" sides of the PCD. The Westinghouse tubesheet is designed with a double-cone expansion joint that provides a positive seal at a variety of operating temperatures.

As the particulate accumulates on the outside of the filter surface, the differential pressure will continually rise. Periodically, the cake of particulate is removed by a pulse of high-pressure gas generated by the pulse skid. This gas flows into the filter vessel through the pulse piping and is channeled to the individual plenums via the support tube. When the filter cake is removed from the filter, the cake falls to the bottom of the vessel where it is cooled and removed by an ash removal screw cooler and a lockhopper system.

The instrumentation for the filter vessel is relatively simple and consists primarily of:

- Differential pressure, measured in two places: across the tubesheet and from the gas inlet nozzle to the gas outlet nozzle. The differential pressure is used as part of the pulse logic to determine when the filter elements need cleaning and to monitor filter system performance.

- Thermocouples (several located within the filter system) that monitor gas temperature, the temperature of the expansion joint on the tubesheet, and the temperatures inside the plenum.

- Ash Level Thermocouples used to determine the level of ash in the PCD. These thermocouples are located at several locations in the bottom cone. By monitoring changes in these thermocouples, the ash level in the cone can be approximated.

In general the filter elements are cylindrical, having an outside diameter of approximately 2.5 inches and an overall length of about 60 inches. The filter element has an internal bore of approximately 1.5 inches. This bore is used to channel the cleaned gas from the filter surface to the plenum. The bottom of the filter element is plugged and the top is flanged for attachment to the plenum.

Filter elements are constructed from a ceramic or a metal alloy. The ceramic elements may be manufactured from a variety of materials including alumina/mullite, cordierite or silicon carbide. Metal alloys typically used include stainless steel, inconel alloys, hastelloy, and iron aluminide. Metal elements have superior strength but are limited by corrosion from sulfur and/or chloride compounds in the coal ash at high temperatures. Ceramic filter elements can operate at higher temperatures and more aggressive gas chemistries but are substantially weaker mechanically than metal elements.

6.1.2.3 Pulse Skid

The pulse skid is diagrammed in figure 6.1.2-3. This diagram illustrates the pulse system that supplies pulse gas to the lower plenum. There is an identical system for the upper plenum not shown in this drawing but which is parallel to and behind the system shown.

High-pressure air or nitrogen enters the pulse skid at pressures up to 1,500 psig. The pressure is reduced to the desired pulse pressure by a regulator located between the gas inlet and the pulse tank. The pulse gas is then stored in a tank of approximately 15 ft^3. Each plenum has a completely redundant system of isolation and pulse valving. The upper line is the primary supply and the lower line is the backup.

From the pulse tank, the pulse gas flows through two isolation valves (one automatic) and then through a high-speed pulse valve. The pulse valve is a Müller coaxial valve (VSV-F80) manufactured in Germany. This valve is designed to operate from fully open to fully closed in a fraction of a second. The high-pressure pulse then flows through the pulse piping to the filter vessel.

In the event of pulse valve failure, the lower backup system is used. The pulse system is supplied with a double block-and-bleed system to allow for the pulse valves to be safely removed and replaced during operation.

The pulse sequence is started by one of three methods:

- Manual Pulse: The plant operators have the ability to pulse the filter system at any time through a "push button" located on the DCS screen.
- High Filter ΔP Trigger: When the filter ΔP exceeds the "trigger" ΔP set in the pulse logic the pulse sequence is started.
- Time Trigger: A time "trigger" in the pulse logic is typically set at 30 minutes. Once the pulse system is activated the pulse sequence is initiated every 30 minutes. If the pulse sequence is activated before 30 minutes by the manual push button or the ΔP trigger the timer is reset.

Once the pulse sequence is initiated, the following events occur:

A. The pulse logic checks to make sure that the pulse pressure is greater than the system pressure. If not, the pulse will not occur and an alarm will sound on the DCS.

B. If the pulse pressure is okay, the automatic isolation valve for the upper plenum is opened. This valve contains limit switches which are used by the pulse logic to determine if the valve is opened. If not, an alarm is sent to the DCS.

C. Once the isolation valve is opened, the pulse valve fires for the preset duration. During 1996 this setpoint was 0.2 seconds.

D. The pulse logic checks the pressure in the pulse tank.

E. If the pressure did not fall below a certain level the logic assumes the valve did not open and sends an alarm to the DCS.

F. If the pressure does not rise above a certain level within a specified time the pulse logic assumes that the valve has failed open and sends an alarm to the DCS.

G. After the pulse event the isolation valve is closed.

H. The sequence is repeated for the lower plenum.

Currently, the backup pulse system is activated manually by changing a parameter in the pulse logic. There is a plan to make this swap-over an automatic part of the pulse control logic in 1997.

The pulse system has been operated with a high reliability in 1996. The only significant problem has been with the pressure control valves upstream of the pulse tank.

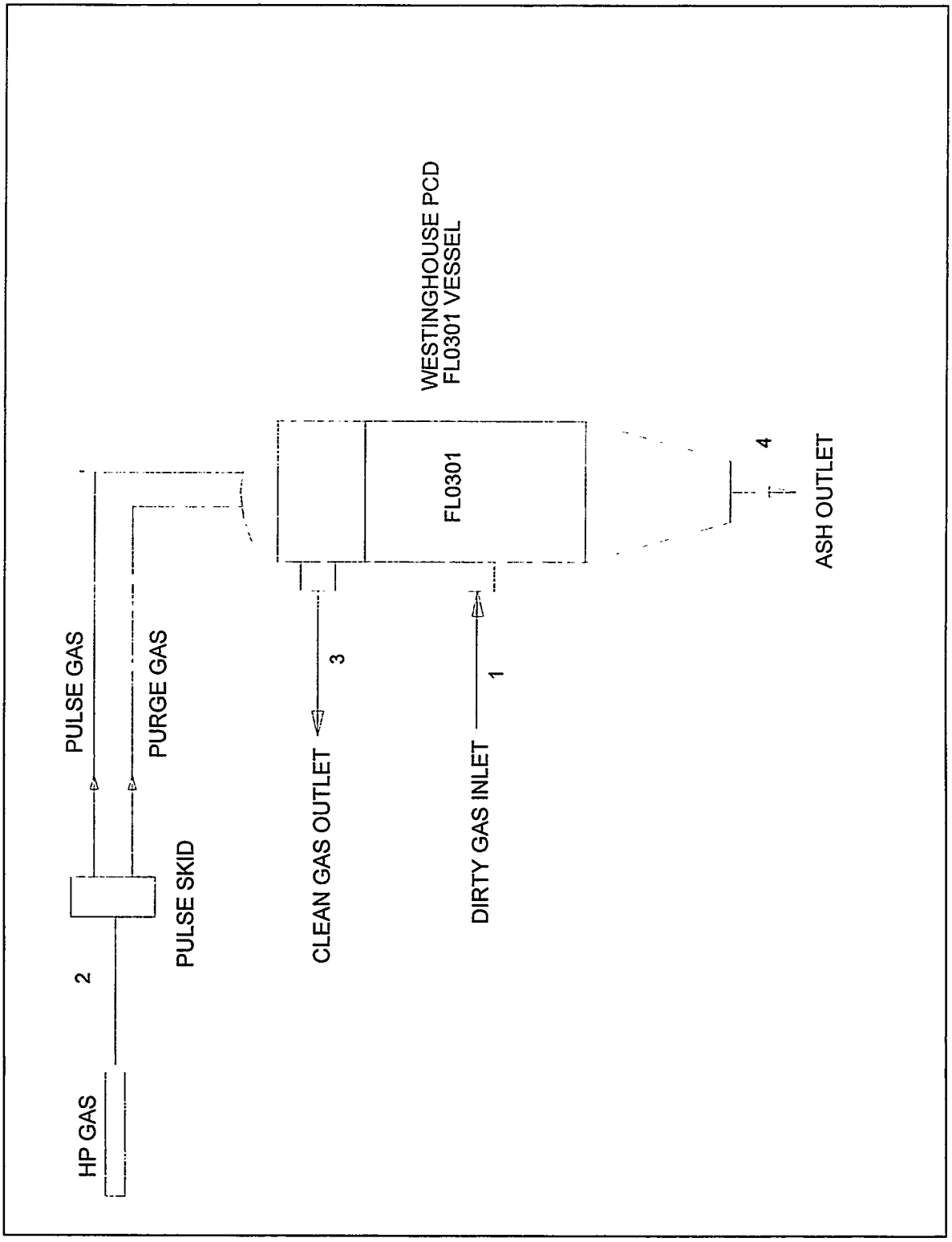

Figure 6.1.2-1 PCD Flow Diagram

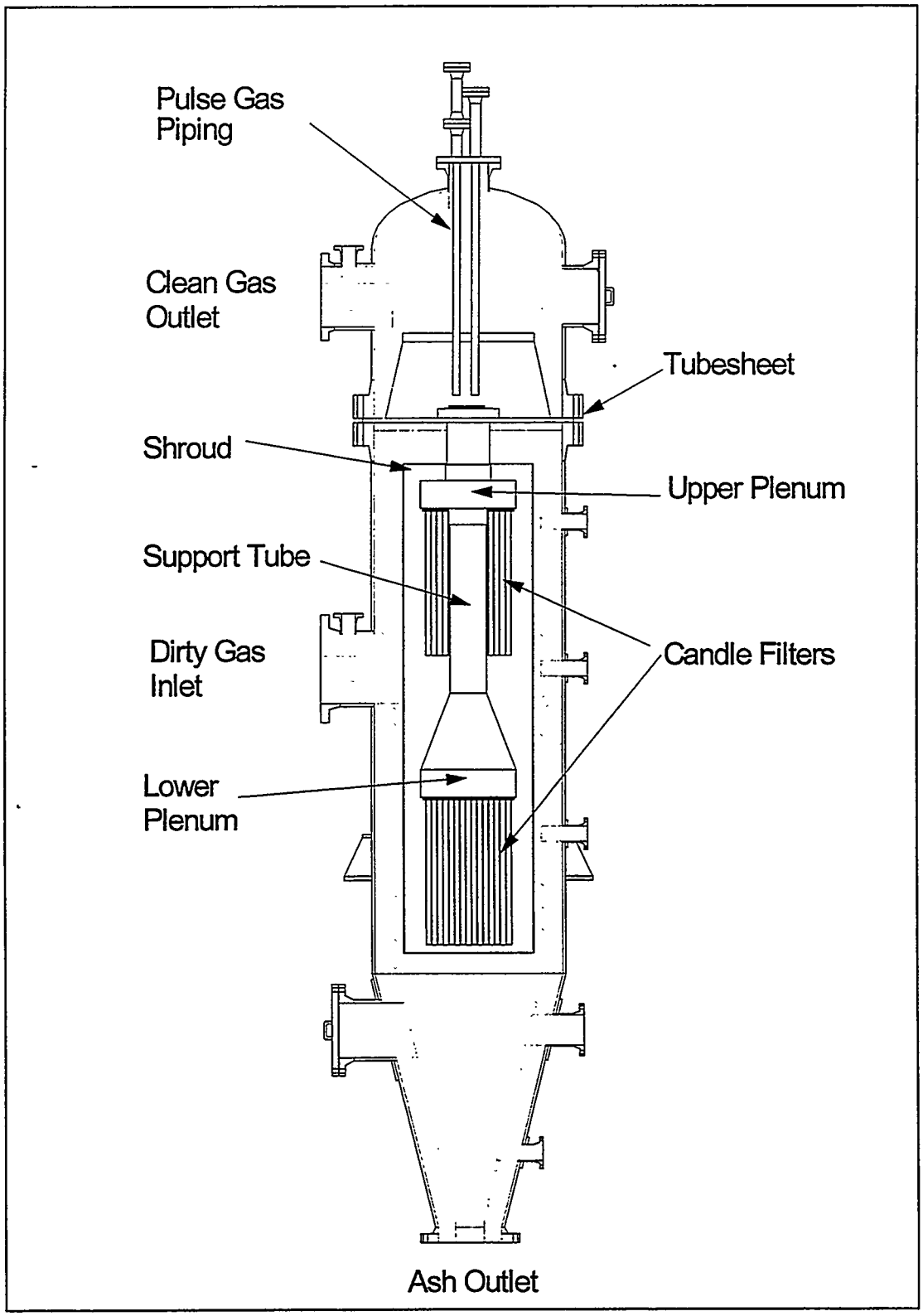

Figure 6.1.2-2 Westinghouse PCD FL0301 Filter Vessel

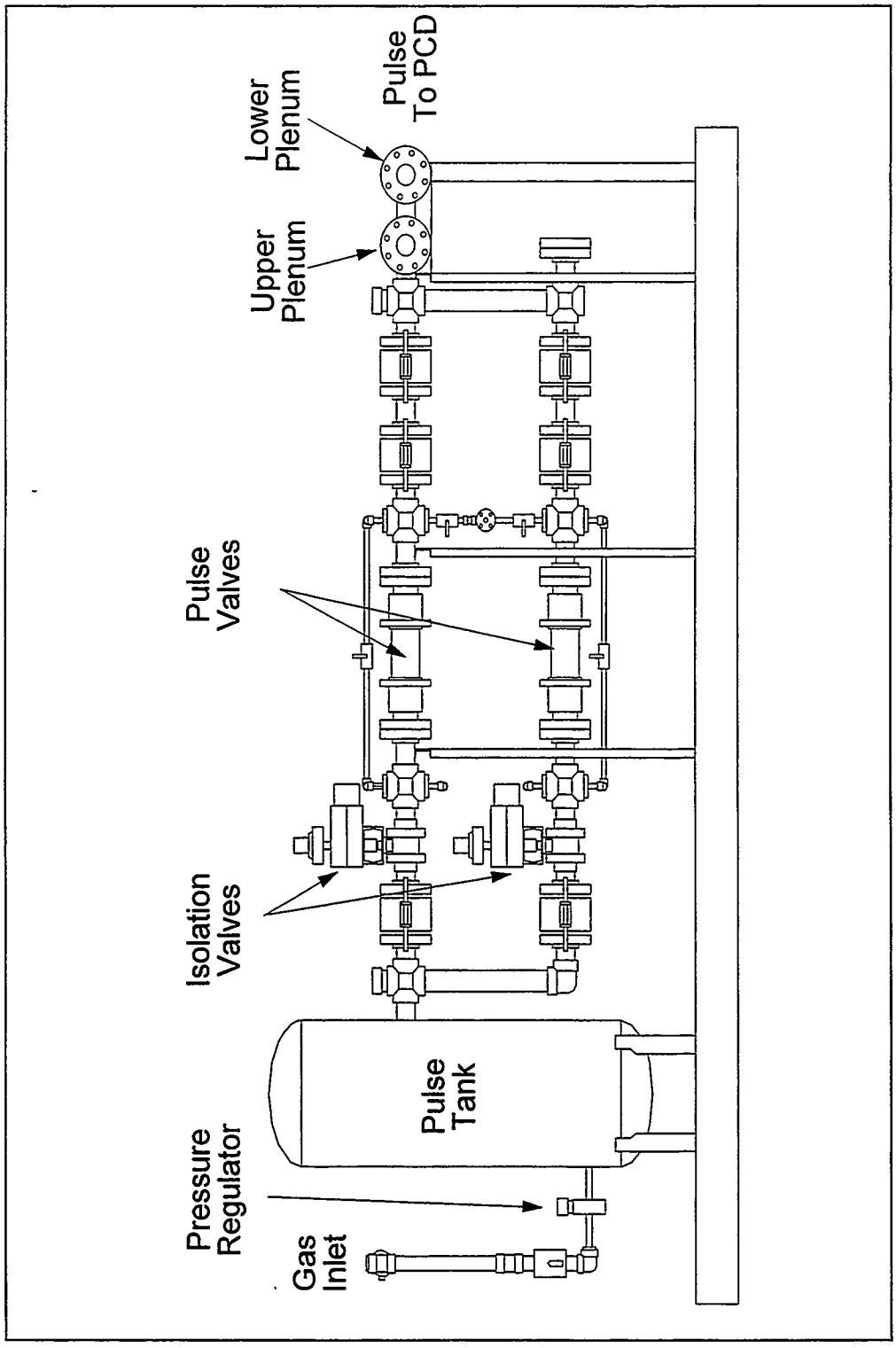

Figure 6.1.2-3 Westinghouse PCD Pulse Skid

PSDF\1996\6.1.2

6.1.3 Westinghouse PCD Installation

6.1.3.1 General

The filter vessel was installed into the structure in May 1995. Over the following 10 months the refractory lined inlet/outlet piping was installed as well as the pulse skid and its associated piping. However, the majority of installation activities occurred between March and June 1996. During that time the filter internals, filter elements, and the vessel instrumentation were installed.

Programming the pulse logic and commissioning of the pulse system occurred during the latter part of May and early June 1996. The biggest challenge was to convert the logic supplied by Westinghouse into "ladder logic" so that the Foxboro DCS could activate the pulse valves at the high speeds required.

6.1.3.2 Internals Installation

Installation of the filter internals and elements occurred the week of March 25, 1996. Westinghouse employees Zal Sanjana and John Meyers were present to assist and three employees from the Pinon Pines project were on site to watch since there are many similarities between the Westinghouse filter vessel at the PSDF and the vessel supplied by Westinghouse for Pinon Pines.

The filter cluster was attached to the tubesheet by the construction staff. Overall, the installation was straightforward and uneventful. However, due to a misinterpretation of the drawings supplied by Westinghouse, the filter cluster was installed 90° from its correct orientation. This required minor modifications to the piping connecting the pulse skid with the filter vessel. Additionally, the pulse logic had to be modified because the piping modifications required reversing the pulse sequence.

6.1.3.3 Filter Element Installation

Once the internals installation was completed, the filter elements were installed by the PSDF maintenance staff. Installation of the 91 filter elements took about a day and a half for five maintenance workers.

All maintenance work on the filter internals is performed on three temporary platforms installed in the maintenance bay (see figure 6.1.3-1). The platforms are attached to the structure with four pins. When they are not in use, two pins are removed and the other two act as a hinge so that the platforms can be "folded" out of the way to the side of the maintenance bay. This greatly reduces the amount of time required to install the platforms.

The "normal" sequence of events for installing the filter elements is as follows:

A. Lower the maintenance platforms into position and install the handrails.

B. Remove the instrumentation attached (both inside and outside of the filter head).

C. Unbolt the 26-inch refractory lined elbow at the gas outlet and lift it to the platform at elevation 218.

D. Remove the pulse piping between the pulse skid and the filter vessel. Also, remove the platform above the filter vessel at elevation 218 and store it at elevation 218.

E. Remove the 80 flange bolts holding the PCD head.

F. Once everything is disconnected, remove the PCD head and store it at elevation 218.

G. Lift the tubesheet and filter cluster from the PCD vessel and set it down on the maintenance platforms.

H. Once work required is completed, the process is reversed for installation.

The entire process, from the initial lifting of the maintenance platforms to lowering them at the end of the job, requires all five maintenance workers for about five 8-hour days.

6.1.3.4 Pulse Logic Checkout

For the Foxboro DCS to operate the pulse valves at the high speeds required, the logic supplied by Westinghouse had to be converted to "ladder logic." The logic required to pulse the primary valves was relatively straightforward. However, as mentioned in the system description report, there is a backup valve for each primary pulse valve. The intention of the logic was to automatically swap over from the primary pulse valve to the secondary pulse valve if a failure of the primary valve is detected.

Implementing this detection scheme using "ladder logic" proved to be a challenge and was deferred until 1997. Currently, if the pulse logic detects a pulse valve failure it registers an alarm on the DCS. In order to swap over to the backup valve one parameter in the pulse logic must be manually changed.

Confirmation of this logic occurred during the month of June. Overall, the pulse skid worked reliably for the first year of testing. No problems were experienced with the pulse valves in 1996.

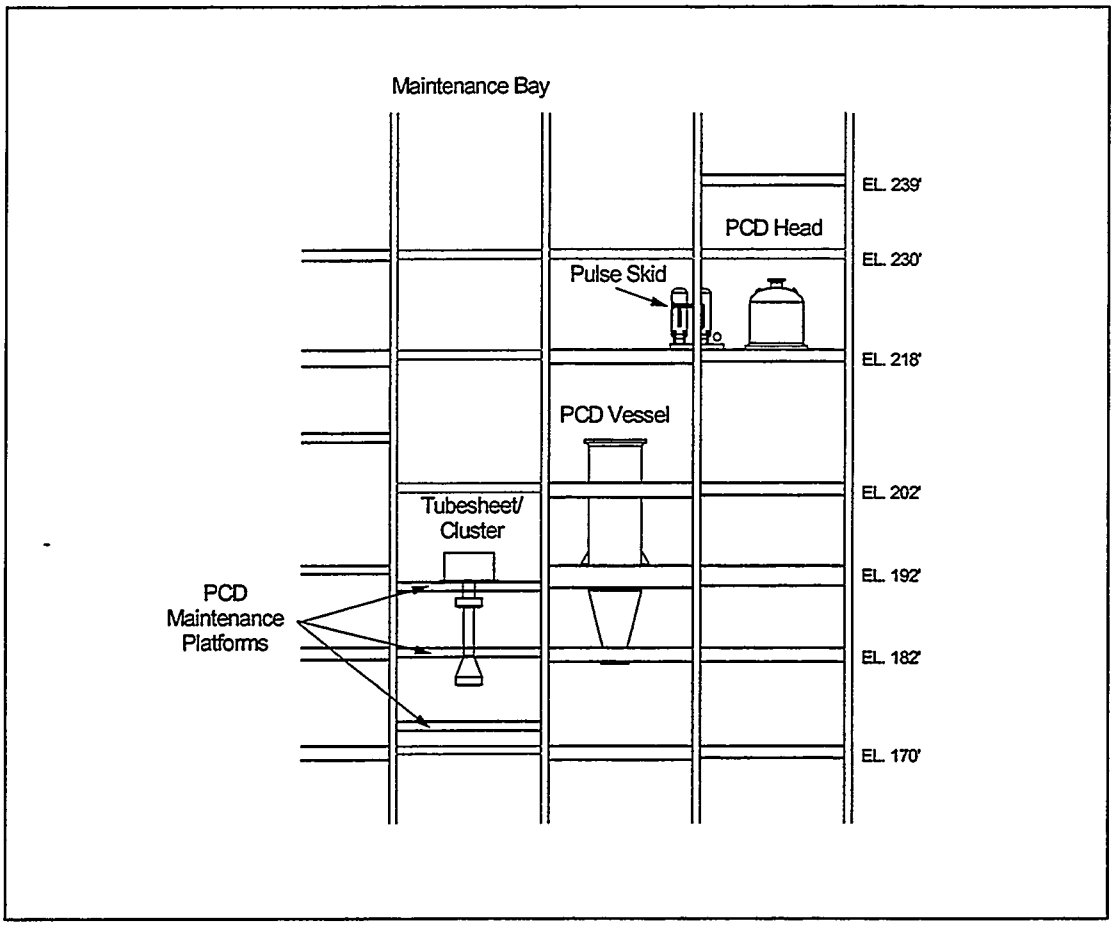

igure 6.1.3-1 PCD Maintenance Bay

6.1.4 Candle Layout #1

All of the filter elements for the initial operations of the Westinghouse PCD were used candle filters from the Tidd Project. These elements had been cleaned by Westinghouse and some qualification of the elements had occurred prior to their shipment to the PSDF. The initial installation of the filter elements occurred the week of March 25, 1996.

Of the 91 filter elements installed, 90 were Pall 442T elements and one was a Schumacher F40. It was installed on the bottom level of elements, at tubesheet ID #32 (figure 6.1.4-1, bottom plenum). Four elements were shipped to the PSDF by DOE to support an ongoing project with Dr. Roger Chen at West Virginia University. Due to poor packaging, two of these elements arrived broken. The decision was made to not install the other two elements since they were possibly also damaged during shipping.

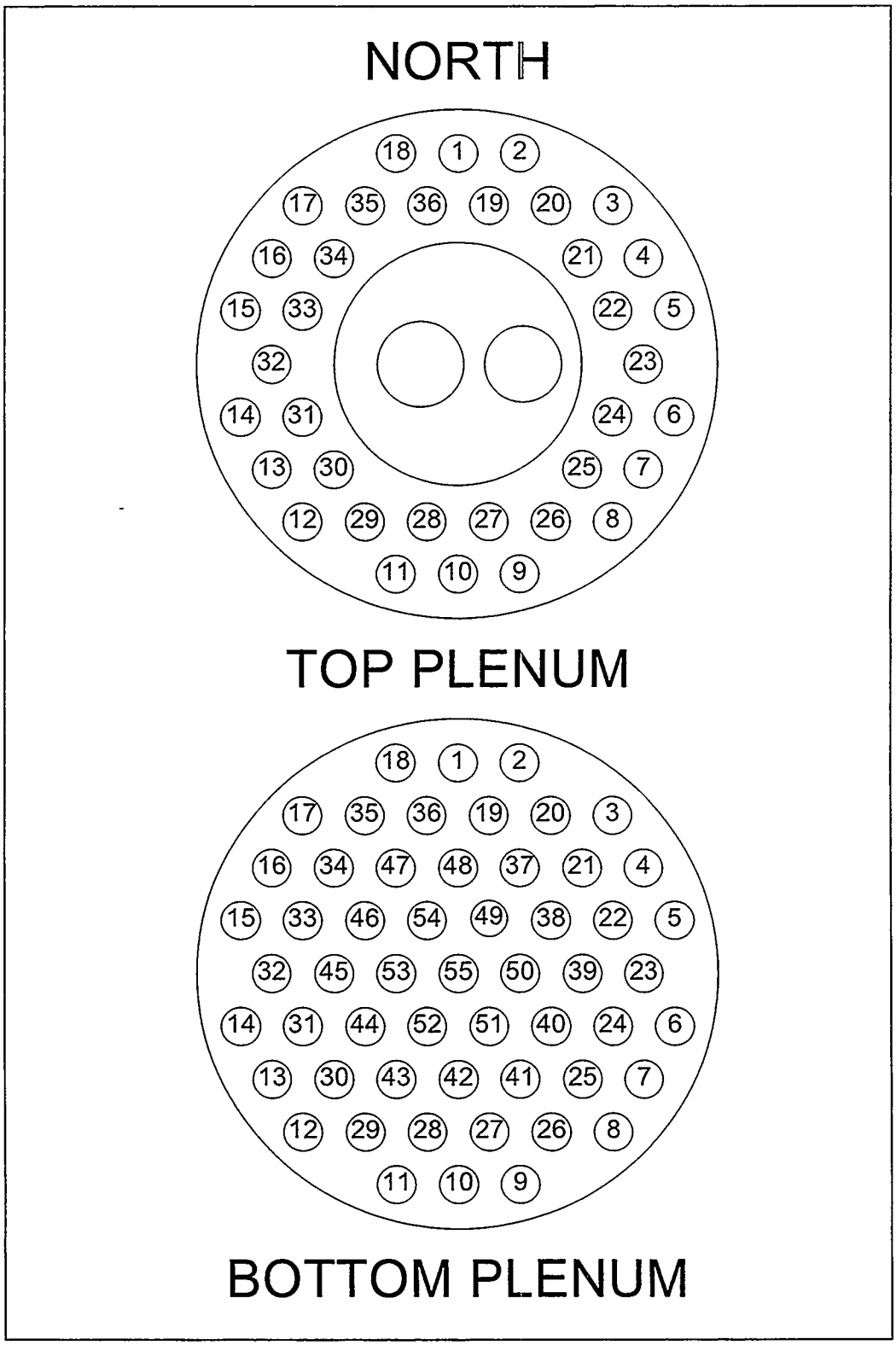

Figure 6.1.4-1 FL0301 Tubesheet Map

PSDF\1996\6.1.4

6.1.5 Westinghouse PCD Gasket

Most filter systems (whether gas or liquid) contain some type of tubesheet which supports the filter elements and separates the "dirty" side from the "clean" side. The Westinghouse PCD is no exception. The filter elements are arranged in two levels as shown in figure 6.1.5-1. The elements are attached to a tubesheet at each level, with a plenum above each tubesheet to collect the cleaned gas from the individual filter elements. The tubesheets are supported by a central pipe which provides mechanical support and is a conduit for the cleaned gas to ultimately flow out of the filter vessel. This central pipe is in turn supported by a tubesheet which is "clamped" between two 84-inch flanges welded to the cylindrical body of the filter vessel.

The mating surfaces between the tubesheet and the 84-inch flanges are part of the filter system pressure boundary and have proven to be challenging to seal. The pressure boundary consists of five components; the two 84-inch vessel flanges, the tubesheet, and two gaskets as shown in figure 6.1.5-2.

The original gaskets installed during the assembly of the vessel in March 1996 were Flexitallic spiral wound gaskets. Flexitallic gaskets are fabricated of two major components, the spiral wound gasketing material, and an integral metal gauge ring. The gauge ring is primarily for support of the gasketing material. Since it is thinner than the gasket, it also serves as a maximum compression limit. Based on the size of the flange and the operating pressure and temperature, the gasket had an inside diameter (ID) of $88^{3}/_{8}$ inches and an outside diameter (OD) of $90^{1}/_{8}$ inches. The metal gauge ring OD was 91½ inches. Due to its large size, the gasket was stored upright.

The 84-inch flange is sealed with 80 studs which each have a diameter of $1^{5}/_{8}$ inches. Maintenance personnel initially torqued the bolts to 1,100 ft-lb, as specified by the manufacturer. The bolts were torqued with a single Hytorq hydraulic wrench. A pattern for torquing the bolts was used so that the load could be applied uniformly. The load was applied in multiple passes so that on the last pass the full load was applied.

The initial pressure test for the filter vessel was on July 14, 1996. The pressure inside the filter was 50 psig when the flange was tested for leaks. When checked, it leaked profusely, especially on the northwest side. (See figure 6.1.5-3 for vessel orientation.) Maintenance increased the torque on the bolts to 1,600 ft/lb, and ultimately to 2,200 ft/lb, but still the vessel would not seal. At 2,200 ft/lb torque, the gasket had collapsed against the metal gauge ring, so it was not possible to apply a higher load to the gasket. Also, the final load was near the maximum tensile strength for the bolts, so it was decided to shutdown to inspect the vessel.

Westinghouse employees Zal Sanjana and John Meyers visited the job site for inspection. Several discussions were held and the following was learned:

- When the vessel was fabricated and hydrotested as part of its ASME Section VIII certification, the tubesheet was not in place. This was the first time the entire pressure boundary had been tested. This was a normal Westinghouse procedure and had not presented problems on other jobs.

- Unlike the pressure vessel supplied for the Tidd project (and the large Westinghouse vessel supplied for the PSDF Foster Wheeler unit) no provisions had been made for seal welding this filter vessel to provide a pressure boundary.

- Laser-based measurements of the flanges to determine flatness was suggested. However, this was impractical because it would be impossible to check the tubesheet due to its construction. Also, the vessel head would have to be lowered to the ground and flipped over so that the flange was at the top. Since the vessel head weighs over 11 tons, it was decided to inspect the vessel first for obvious problems.

- Flexitallic was consulted to provide information about flange flatness requirements, surfacing, etc. Arrangements were made to bring a Flexitallic engineer from Houston to look at the vessel but schedule conflicts prevented his visit. Flexitallic recommended using 40-bolt tensioners instead of the Hytorq to apply the sealing load. It was decided to consider this only as a last resort due to the very high cost of purchasing the equipment or having a company provide the service.

The bolts were removed on July 16; a gap was visible at the top of the tubesheet on the northwest side. This gap was near one-eighth of an inch in places. Also, the metal gauge ring on the gasket was found "notched" in several places where it had been sheared by the bolts as the load was being applied. The OD of the backing ring was essentially the same as the ID of the bolt circle, meaning that if the gasket was perfectly round, it would just touch the bolts. This "notching" was not uniform around the circumference of the gasket and was more pronounced on the northwest side of the gasket. In addition, it was apparent that the gasket was elliptical and not perfectly round. As mentioned previously, this gasket had been stored upright in the warehouse due to space restrictions and became elliptical over time.

It was discovered that the gaskets were of two different thicknesses. When the gaskets were ordered, only the inside and outside diameters of the gasket and the OD of the backing ring were specified. The OD of the gasket is $90^{1}/_{8}$ inch, and according to Flexitallic's sales literature, a gasket smaller than 90 inches would have a thickness of 0.175 inches, and a gasket larger than 90 inches would have a thickness of 0.25 inches. When the history of the gaskets was checked, it was determined that they were ordered at two different times. Apparently, when the factory received the orders different gasket thicknesses were supplied.

The vessel head and tubesheet were removed and then reassembled without the gaskets. Upon close investigation it was noticed that the refractory lining inside the vessel head protruded slightly (less than one-eighth of an inch) beyond the flange and prevented the head from sitting flat on the tubesheet. The head was removed and the refractory ground flush.

The local Flexitallic representative visited the job site and recommended trying a Garlok 3125SS gasket. This was considered for a while, but it could not be supplied in a one-quarter inch thickness within 2 weeks. Because there was another set of Flexitallic gaskets in the warehouse, it was decided to use them again. Several of the mechanics had successfully used a high temperature silicone caulk in the past on large flanges in steam turbines, so it was decided to place a bead of the caulk on all four gasket surfaces. The vessel was put back together and a load of 1,600 ft lb torque was applied in five passes (20 percent of the load on each pass) with a single head Hytorq wrench. The vessel was pressure tested on July 21 and the flange slightly leaked at 180 psig. It was decided to proceed with test run CCT1A and limit the operating pressure to 160 psig.

During the CCT1 test series, a set of gaskets (Garlok 3125SS) was ordered for the next installation. The gaskets had an OD which matched the OD of the tubesheet (so it would not engage the vessel bolts) and was 2 inches wide. Garlok 3125SS is a very soft graphite material and it was believed that it would "flow" into any imperfections in the flange surface and seal better than the Flexitallic. Because of the size of the gasket and the nature of the material it was supplied in five segments with the individual segments joined by a dovetail.

Maintenance lead the effort in determining the advantages/disadvantages of Hytorq vs. multitensioners. Apparently, Phillips Petroleum had performed a study which found no apparent advantage of one system over another. Therefore, it was decided to modify the Hytorq system currently owned by the PSDF so that four torque heads could be used simultaneously.

During CCT1C the filter vessel was filled with ash and 77 of the 91 filter elements were broken. When the head was removed from the vessel, there was significant corrosion on the tubesheet surfaces and on the upper manway door. The corrosion was removed with wire brushes, treated, and the Garlok gasket installed. The manufacturer recommended strongly against using a silicone caulk so none was used. The Garlok gasket was much simpler to install than the Flexitallic gasket. Because of the large diameter and thinness of the Flexitallic gasket it took eight people to place it without bending. Since the Garlok gasket is installed in five segments and joined by dovetails, it could be installed by two employees.

The manufacturer recommended a torque of 900 ft/lb (which was used) even though based on the Flexitallic experience there was skepticism that it would seal. There was also some

concern about whether or not the dovetailed joints would leak. The bolts were torqued with the four-head Hytorq in multiple passes to the manufacturer's recommendations. The vessel was pressure tested; there was a small leak at one of the dovetailed joints at 300 psi. The torque was increased to 1,100 ft/lb and the vessel joint held to 330 psi.

To minimize the corrosion on the manway doors, the maintenance crew installed a solid disc of Garlok 3125SS. This has worked extremely well, and during an inspection in December 1996 there was no corrosion found on the doors. For the tubesheet, the next set of Garlok gaskets ordered were $4^1/_2$ inches wide. This is much wider than required for the pressure rating, but it will entirely cover the exposed metal surfaces and help prevent corrosion.

It is unknown why the Flexitallic gasket was unable to seal the filter vessel. Both maintenance and the PCD team have considered attempting once more to use the Flexitallic gaskets with the four-head Hytorq wrench to see if it will successfully seal. However, this is difficult to justify because the Garlok gasket has the following advantages over the Flexitallic:

- At least in this application, the Garlok gasket sealed successfully and the Flexitallic did not.
- As mentioned, the Garlok gasket is much easier to handle and install.
- Because it is segmented, the Garlok gasket can be stored in a fraction of the space. (A separate storage facility for the gaskets for this vessel and the FL0352 vessel (120-inch flange) had been designed and was about to be constructed, which would have allowed for horizontal storage of the gaskets to prevent them from becoming elliptical. Construction of this facility has been canceled, which saved the project several thousand dollars.)
- A 4 1/2-inch wide Garlok gasket 1/4-inch thick costs less.

At least for the near term, there are no plans to use Flexitallic gaskets on any of the large (>60-inch) flanges for the PCDs. The largest flange on the Foster-Wheeler combustor PCD (FL0352) is 120 inches in diameter. This vessel is designed to be seal welded to provide a pressure boundary, but at this time it is believed that this vessel can be adequately sealed using only the Garlok gaskets.

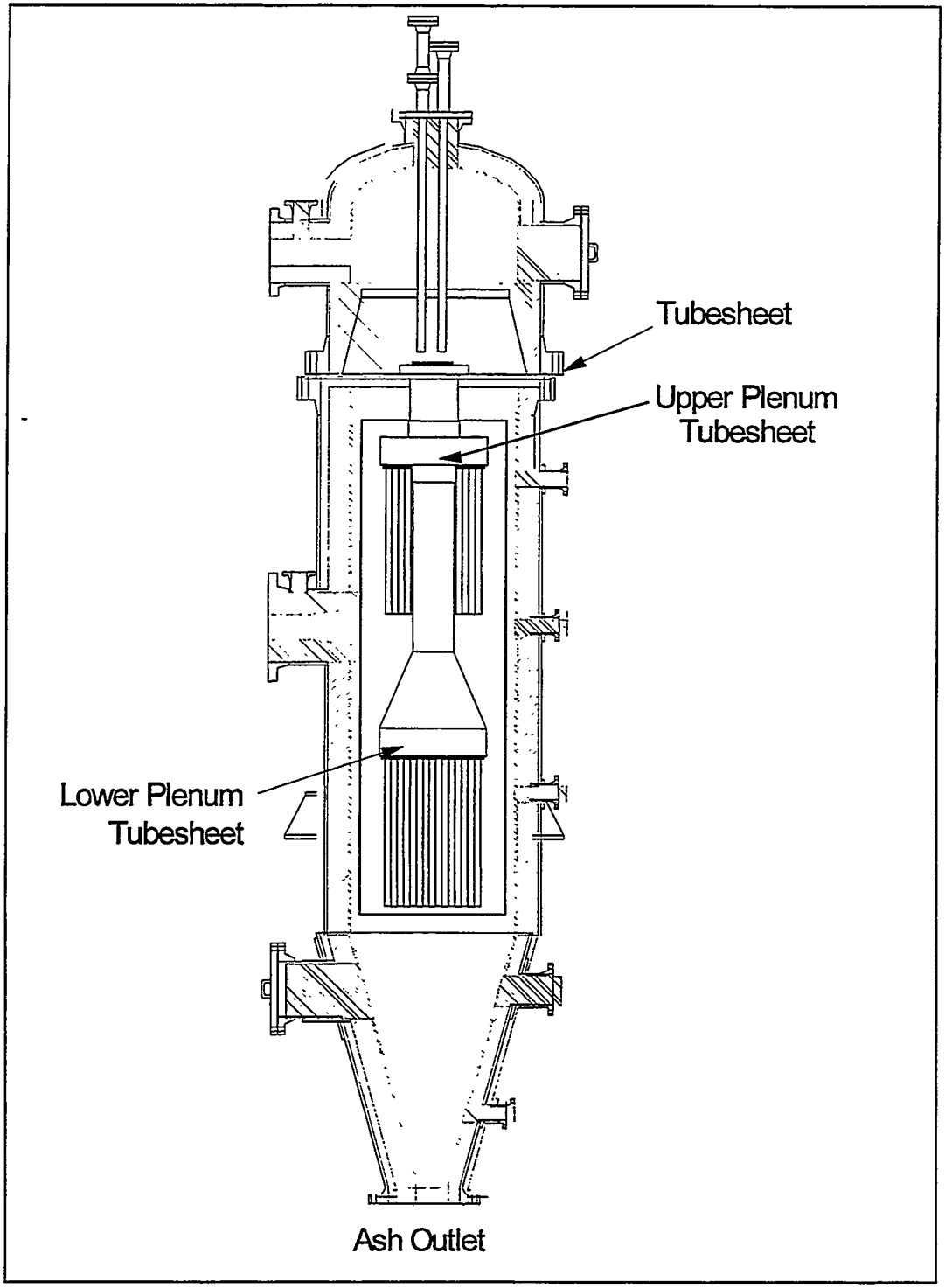

Figure 6.1.5-1 Westinghouse PCD FL0301

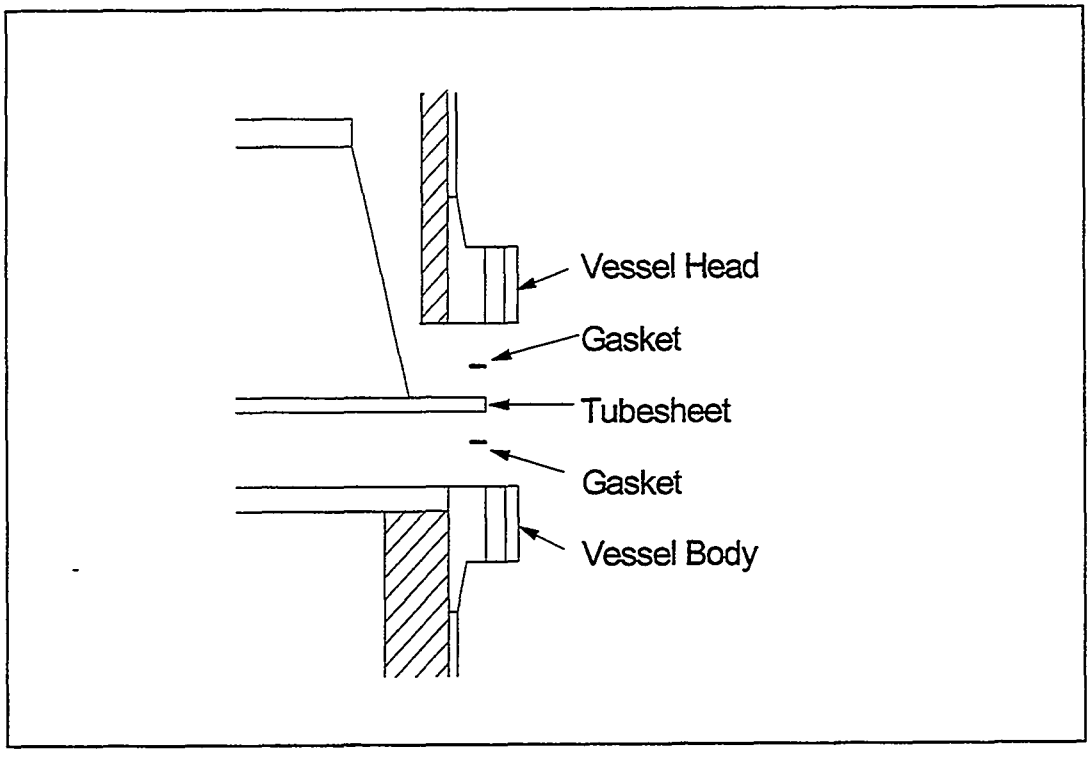

Figure 6.1.5-2 Westinghouse PCD FL0301 Gasket Details

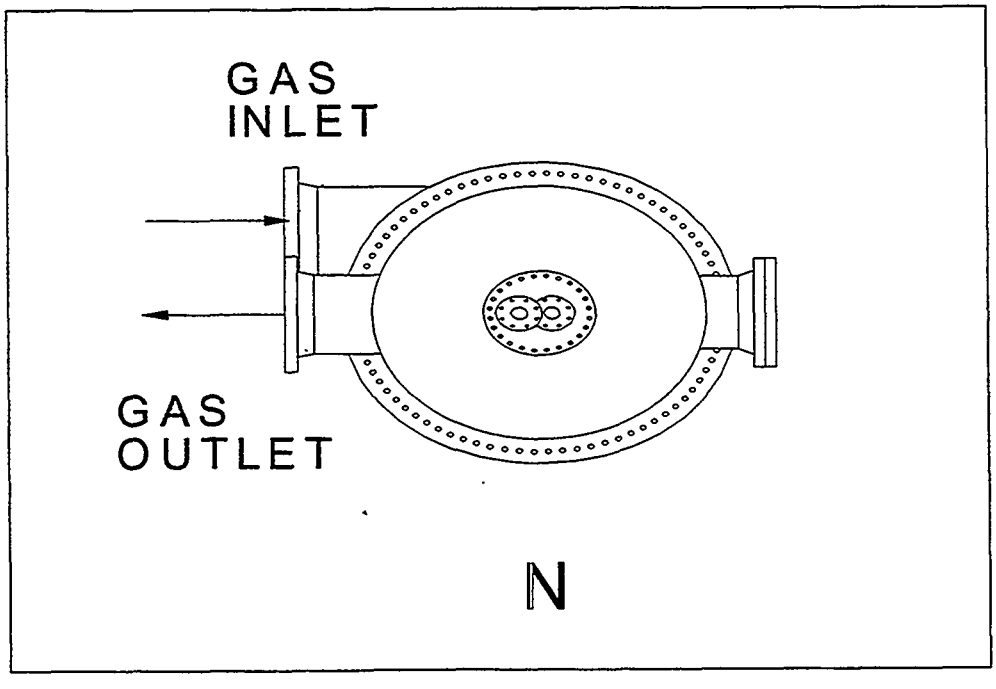

Figure 6.1.5-3 Westinghouse PCD FL0301 Orientation

PSDF\1996\6.1.5

6.1.6 Test Run CCT1A

6.1.6.1 Summary

CCT1A was the initial run for the Westinghouse PCD (FL0301.) The test lasted from July 22 to July 26, 1996. Because this was the initial test run with both the PCD and the transport reactor (TR) connected, the first part of the test concentrated on circulation of alumina within the TR to evaluate the interactions of the two systems. On July 24 coke breeze was added to the TR in an attempt to begin combusting solid fuel. However, due to low thermal input from the start-up burner the temperature in the TR was too low to burn the coke breeze. Ultimately, the test ended for two reasons: the ash removal screw conveyor for the TR jammed and the start-up burner plugged (due to the formation of deposits).

Overall, the performance of the PCD was fairly stable. The maximum temperature reached was 550°F and the operating pressure throughout the run was approximately 60 psig. The filter face velocity during the run was about 6 ft/min, and the filter baseline pressure drop was typically 40 inWG. The pulse pressure for the run was set at 450 psig and the pulse ΔP trigger varied from 50 to 100 inWG. In addition to the ΔP trigger, the pulse system automatically pulsed every 30 minutes. The rate of increase in the filter ΔP was typically a function of circulation rate in the TR. If the circulation rate was low (or stopped) the ΔP rise between pulses was small. However, at high circulation rates, the filter ΔP would rise from the baseline pressure drop to the trigger pressure drop within the 30-minute interval between pulses.

On July 25 and 26 the atmospheric baghouse ΔP increased to the point where it pulsed three times. Ash samples removed from the baghouse appeared to be fine and gray in color and became progressively darker with time. At that point there was concern about a leak/breakage within the PCD. The PCD was inspected on July 30 and no problems were discovered. Ultimately, it was discovered that the majority of particulate was probably alumina remaining in the piping from previous circulation tests before the PCD was installed. The dark color was due to coke breeze from the feeder system vent.

Test conditions for this run are listed in tables 6.1.6-1 and -2. Data from this run are shown in figures 6.1.6-1 and -2.

6.1.6.2 Test Objectives

The primary test objective was to support the TR/PCD start-up activities and gain experience operating the PCD. The only PCD-related objectives were to complete typical "shakedown" activities (varying the pulse ΔP trigger, checking out the pulse logic and instrumentation, etc.); there were no PCD-specific test objectives.

6.1.6.3 Observations/Events

The following sections refer to numbers in the graphs found in figures 6.1.6-1 and –2. Refer to table 6.1.6-2 for related information on the following observations and events.

A. Start-up/PI System Restarted - July 22 at 14:00. The system was pressure tested up to 330 psig from July 19 through 21. There were two small leaks in the 84-inch PCD flange at 185 psig, so the decision was made to limit the operating pressure for the test to 150 psig.

At 07:40 the balancing of all the pressure transmitters was completed and steam flow started to the primary gas cooler to begin warming the PCD. The PCD backpulse system was started at 16:40 with a pulse ΔP trigger of 50 inWG.

The PI system had been "down" most of this time period. The system began recording data at 14:00 on July 22.

B. PCD Ash Removal System Plugged - July 23 at 05:30. At 05:30 on July 23 the PCD ash removal dense-phase system (FD0520) tripped due to a piece of refractory plugging the outlet conveying line. The reactor was depressurized so that maintenance could safely remove the pluggage. The ash removal system was operational by 15:30.

Even though the TR was depressurized, there was a slight flow of air into the system to keep the nozzles and instrumentation from plugging. This air flow was sufficient to carryover enough particulate to the PCD to cause a rise in the filter ΔP. Because of plant safety procedures, the pulse system was also depressurized while maintenance was working on the FD0520 system. By 13:00 the ΔP had reached about 70 inWG, so the air flow to the TR was reduced.

C. Pulse System Restarted - July 23 at 15:50. Once maintenance had completed their work, the pulse system was repressurized and put back into operation.

D. Transport Reactor Main Burner Lit - July 23 at 21:00. The TR pilot was lit at 17:40 and the main burner lit at 21:00.

E. TR Circulation Started - July 24 at 00:30. Circulation was initiated in the TR at 00:30 on July 24. There was a rise in the filter ΔP as fine alumina was carried over to the PCD.

F. TR Circulation Stopped - July 24 at 05:20. Several times throughout the run the TR circulation rate was stopped (or reduced) and then restarted. This happened for a variety of reasons, but the response of the PCD to the change was consistent. Whenever the TR was circulating solids, the filter ΔP would typically rise from the baseline ΔP of about 40 inWG to the pulse ΔP trigger before the pulse system was activated by the 30-minute timer. If the TR was not circulating solids, the rise in filter ΔP would be very small over the 30-minute pulse interval.

G. PCD Pulse ΔP Trigger Raised to 75 inWG - July 24 at 12:30. At two occasions in the run, July 24 at 12:30 and July 25 at 18:30, the pulse ΔP trigger was changed. The primary reason for this change was to verify that the pulse logic was working correctly.

H. TR Circulation Started - July 24 at 15:20.

I. Coke Breeze Batch Fed to Transport Reactor - July 25 at 01:10 until July 26 at 04:30. From 01:10 on July 25 until 04:30 on July 26 several attempts were made to burn coke breeze in the TR. At that time, the thermal input from the start-up burner was not sufficient to heat the TR to a temperature where the coke breeze would ignite. Typically, the circulation was minimized to maximize the temperature in the TR in hopes that the coke breeze would ignite. After a period of time, the circulation was restarted to minimize temperature differentials throughout the system. Throughout this period there were several events when the circulation was minimized, stopped, or restarted for this reason.

J. TR Circulation Stopped - July 25 at 01:50.

K. TR Circulation Started - July 25 at 03:20.

L. TR Main Burner Tripped - July 25 at 05:55.

M. TR Circulation Decreased - July 25 at 09:40.

N. PCD Pulse DP Trigger Raised to 100 inWG - July 25 at 18:30.

O. TR Ash Removal Screw Jammed, Began Shutdown - July 26 at 15:30. The TR ash removal screw (FD0206) jammed and the decision was made to shut down by reducing the burner firing rate.

P. TR Main Burner Tripped, End of Test - July 26 at 18:05. While the temperature was being reduced, the burner tripped. The burner was difficult to restart, so the run was ended.

6.1.6.4 Analysis of Solid Samples

Only three samples were taken during the run. The first sample, taken on July 25 at 01:50, was very fine and almost pure white. When analyzed by the Microtrak, the sample had a mass mean particle diameter of about one micron. No chemical analysis was performed on the sample as it was assumed that the sample was fine alumina.

Two samples were taken on July 26, one at 01:00, and one at 06:25. The color of the samples became progressively darker due the accumulation of unburned coke breeze within the system. The 06:25 sample was essentially black. A loss of ignition (LOI) was performed on the two samples. The sample at 01:00 had a LOI of 5.2 percent and the sample at 06:25 had a LOI of 12.7 percent.

Both of the samples had a broad distribution of particle sizes ranging from 0.2 to 270 micrometers (probably due to the addition of the unburned coke breeze). The mass mean particle size of both of these samples ranged from 8 to 10 micrometers. Figure 6.1.6-3 indicates the mass mean particle size and the time the samples were taken. Figure 6.1.6-4 shows the particle size distributions (PSDs) for the three samples.

A chemical analysis was performed on the sample taken at 01:00 on July 26. The analysis of the ashed sample indicated that it was 95-percent alumina oxide with traces of calcium, iron, phosphorous, potassium, and silicon.

6.1.6.5 Run Outcome

Starting on July 25 the differential pressure in the process baghouse began rising, indicating the presence of solids. From July 25 to 26 the baghouse back-pulsed three times as shown in figure 6.1.6-5. (The "spikes" above the ΔP curve are due to an improperly tuned temperature control loop for the dilution air blower upstream of the baghouse. The controller would cause the fan inlet vanes to oscillate, causing an increase in flow to the baghouse and therefore an increase in ΔP.) There was a significant quantity of ash removed from the baghouse. The ash was dark gray in appearance and the LOI for the ash was about 1.0 percent. However, the PSD of the ash was significantly different that than of the ash removed from the PCD. As shown in figure 6.1.6-6, the mass mean particle diameter of the ash from the baghouse was approximately 25 micrometers, while the mass mean diameter of the PCD ash was 8 to 10 micrometers.

Initially it was assumed that there was a breech in the PCD. The upper manway door was opened on July 30 to inspect the clean (upper) side of the tubesheet. There was no dust present on any part of the tubesheet.

Due to the large PSD of the material in the baghouse, it is speculated that the "ash" was actually alumina which was left in the system from circulation tests conducted prior to the Westinghouse PCD commissioning. The gray color and the LOI of the material probably came from coke breeze that was carried over from the vent system on the coal feeder. This vent line discharged upstream of the system pressure letdown valve and the carryover of material through this line caused the failure of the pressure letdown valve during the next run (CCT1B).

Table 6.1.6-1

CCT1A Run Statistics

Start time	7/22/96 at 07:40
End time	7/26/96 at 18:05
Coal type	Coke breeze
Hours on coal	No sustained combustion
Sorbent type	No sorbent feed
TR bed material	Alumina
Number of candles	91
Candle layout no.	1
Filtration area	~265 ft²
Pulse valve open time	0.2 seconds
Pulse time trigger	30 minutes
Pulse pressure	450 ± 50 psi
Pulse DP trigger	Variable (50 inWG initially)

Table 6.1.6-2

CCT1A Major Events (Refer to Figures 6.1.6-1 and –2)

Event	Description	Date at Time
1	Start-up/PI system restarted	7/22 at 14:00
2	PCD ash removal system plugged	7/23 at 05:30
3	Pulse system restarted	7/23 at 15:50
4	Transport reactor (TR) main burner lit	7/23 at 21:00
5	TR circulation started	7/24 at 00:30
6	TR circulation stopped	7/24 at 05:20
7	PCD pulse DP trigger raised to 75 inWG	7/24 at 12:30
8	TR circulation started	7/24 at 15:30
9	Coke breeze batch fed to transport reactor	7/25 at 01:10 to 7/26 at 04:30
10	TR circulation stopped	7/25 at 01:50
11	TR circulation started	7/25 at 03:20
12	TR main burner tripped	7/25 at 05:55
13	TR circulation decreased	7/25 at 09:40
14	PCD pulse DP trigger raised to 100 inWG	7/25 at 18:30
15	TR ash screw jammed, began shutdown	7/26 at 15:30
16	TR main burner tripped, end of test	7/26 at 18:05

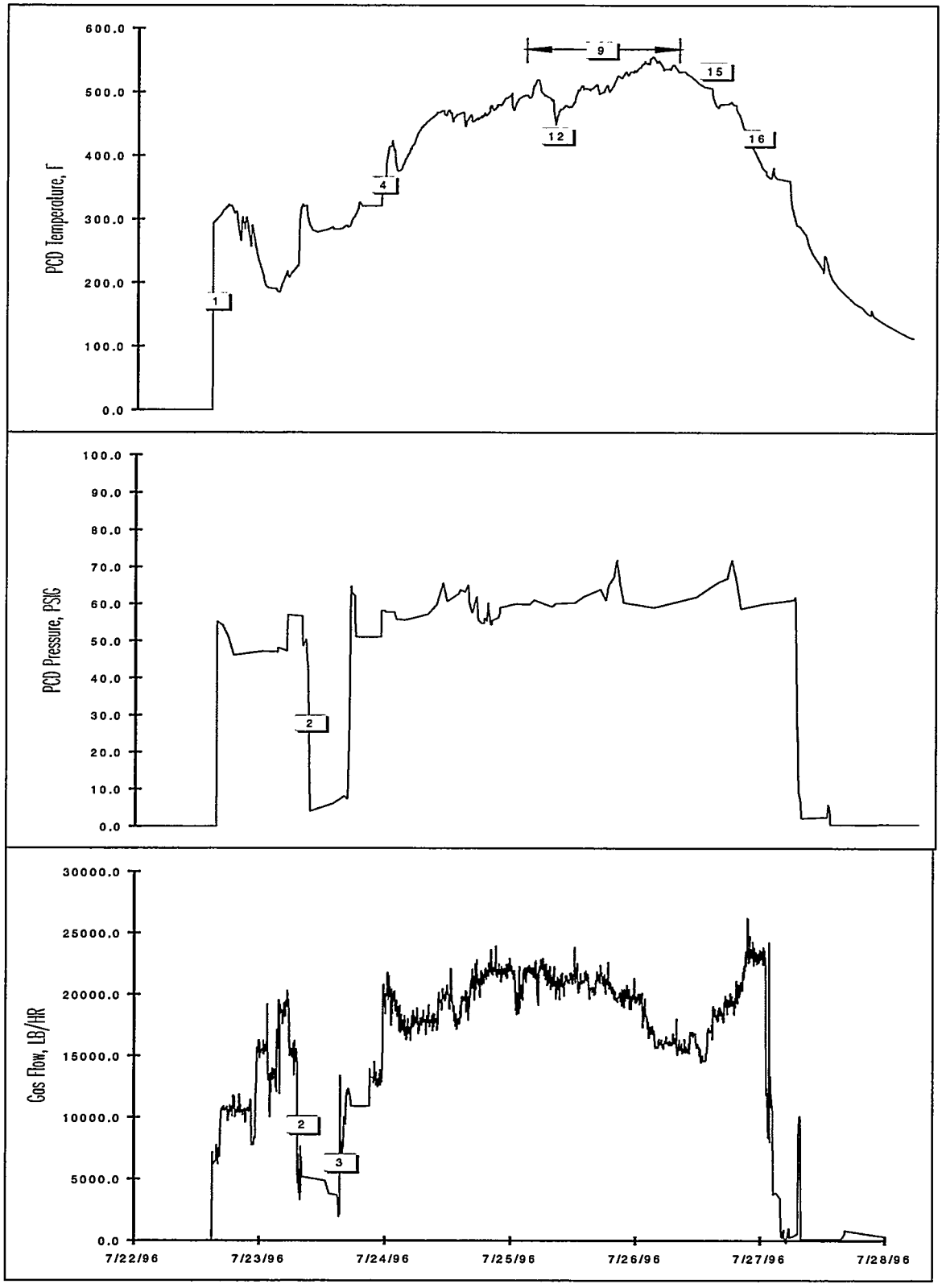

Figure 6.1.6-1 CCT1A Summary Information

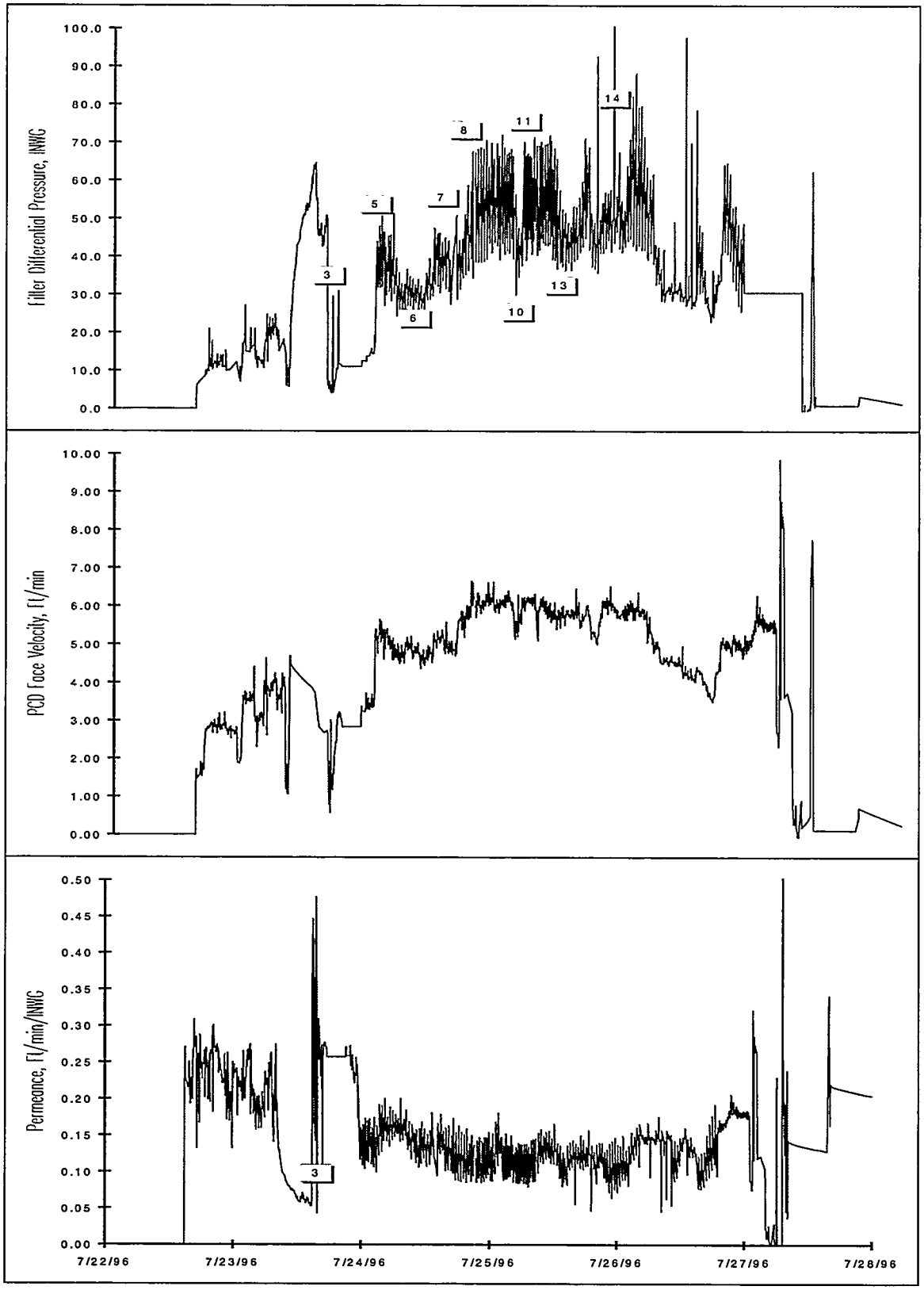

Figure 6.1.6-2 CCT1A Summary Information

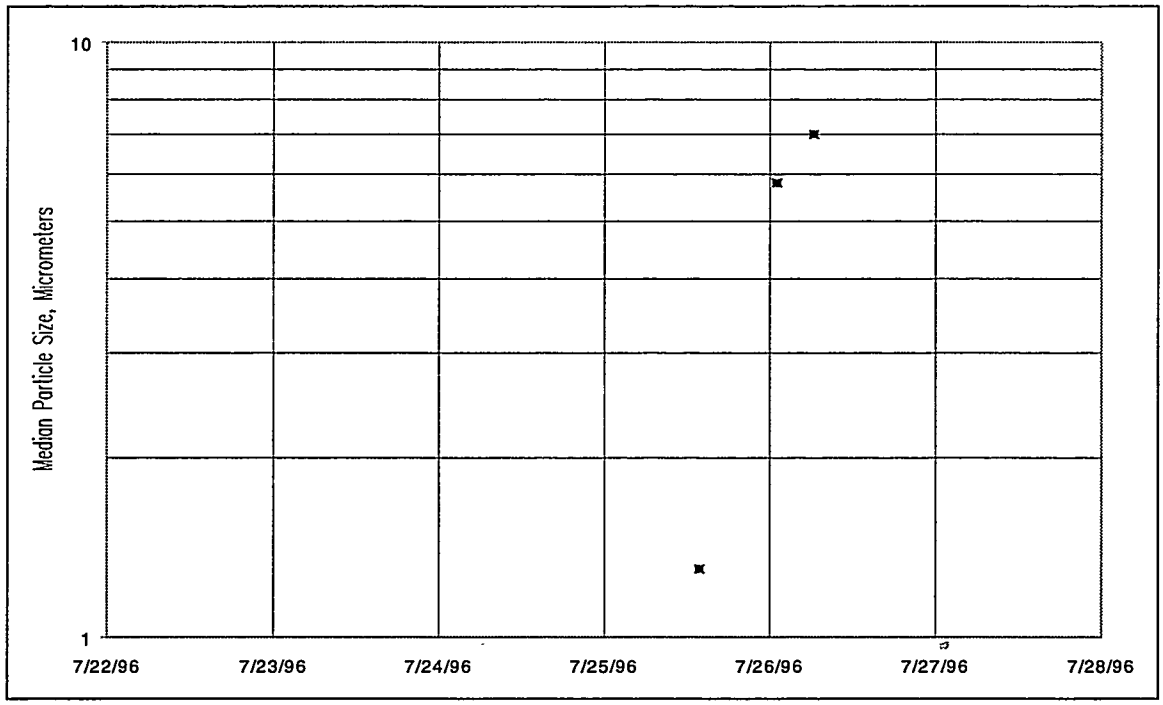

Figure 6.1.6-3 CCT1A PCD Hopper Samples

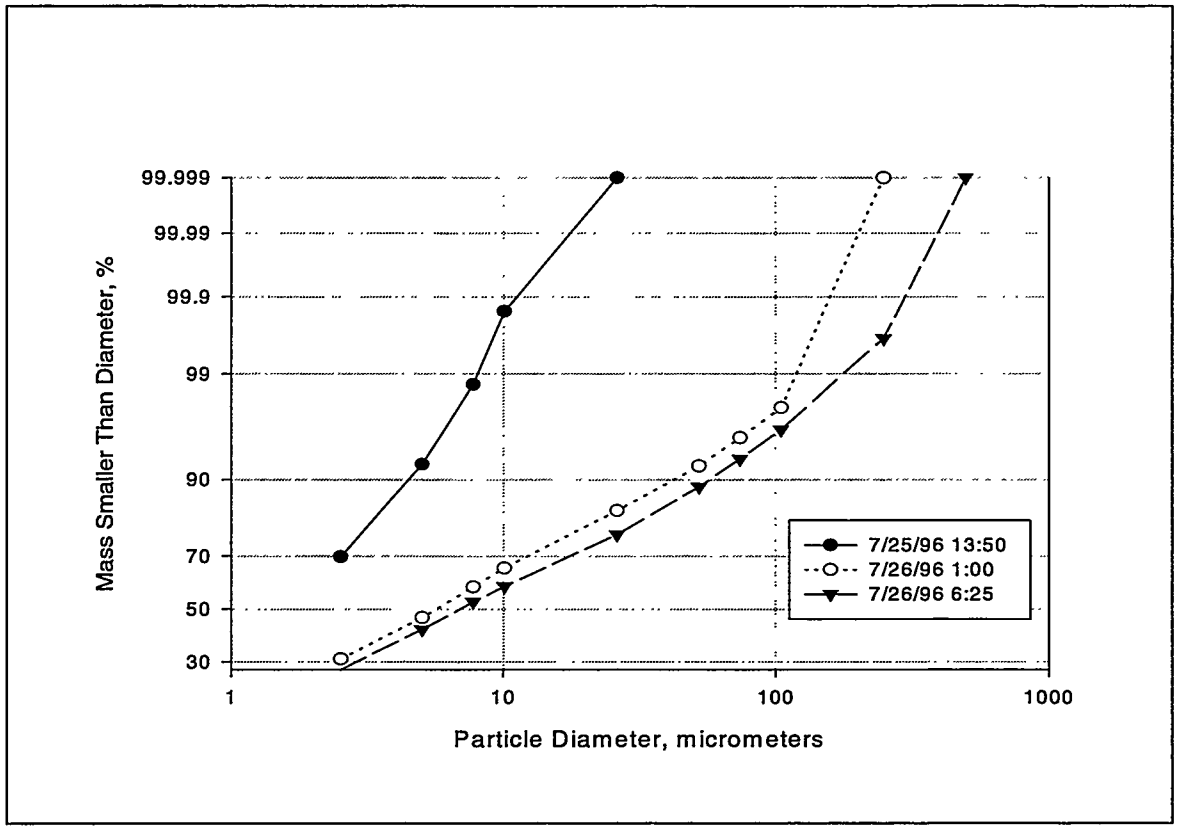

Figure 6.1.6-4 CCT1A PCD Hopper Particle Size Distribution